JUSTUS-LIEBIG-UNIVERSITÄT GIESSEN
FACHBEREICH 08: BIOLOGIE UND CHEMIE
INSTITUT FÜR ANORGANISCHE UND ANALYTISCHE CHEMIE

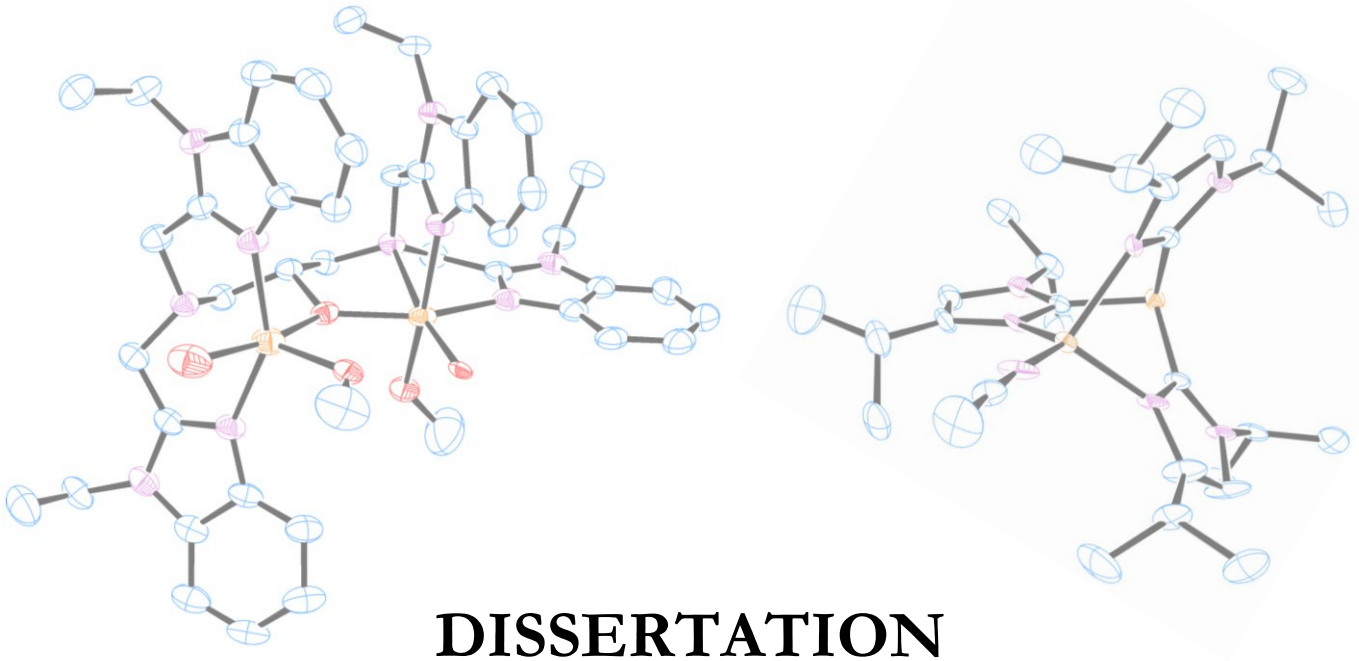

DISSERTATION

Kinetische und mechanistische Untersuchungen zur Bildung von Kupfer(II)- und Eisen(III)-peroxido-Komplexen

Kumulativ-Dissertation zur Erlangung des
Doktorgrades der Naturwissenschaften
- Dr. rer. nat. -

Vorgelegt von
Markus Lerch
aus Alsfeld

Münzenberg 2021

Vorwort

Die vorliegende Arbeit wurde von Juli 2017 bis November 2021 am Institut für Anorganische und Analytische Chemie der Justus-Liebig-Universität Gießen unter der Betreuung von Prof. Dr. Siegfried Schindler angefertigt.

Im Wesentlichen baut diese Arbeit auf zwei von mir als Erstautor veröffentlichten Publikationen auf.

Justus-Liebig-Universität Gießen

Fachbereich 08: Biologie und Chemie

Institut für Anorganische und Analytische Chemie

Erstgutachter:	**Prof. Dr. Siegfried Schindler**
Zweitgutachter:	**Prof. Dr. Richard Göttlich**
Vorgelegt von:	**Markus Lerch**
Abgabe der Dissertation:	**09.11.2021**
Termin der Disputation:	**15.12.2021**

Selbstständigkeitserklärung

Ich erkläre: Ich habe die vorgelegte Dissertation selbstständig und ohne unerlaubte fremde Hilfe und nur mit den Hilfen angefertigt, die ich in der Dissertation angegeben habe. Alle Textstellen, die wörtlich oder sinngemäß aus veröffentlichten Schriften entnommen sind, und alle Angaben, die auf mündlichen Auskünften beruhen, sind als solche kenntlich gemacht. Ich stimme einer evtl. Überprüfung meiner Dissertation durch eine Antiplagiat-Software zu. Bei den von mir durchgeführten und in der Dissertation erwähnten Untersuchungen habe ich die Grundsätze guter wissenschaftlicher Praxis, wie sie in der „Satzung der Justus-Liebig-Universität Gießen zur Sicherung guter wissenschaftlicher Praxis“ niedergelegt sind, eingehalten.

Münzenberg, den 09.11.2021

Markus Lerch

„Ohne ein genaues Studium der Chemie und Physik

werden die Physiologie und Medizin in ihren wichtigsten Aufgaben

kein Licht erhalten“

— Justus von Liebig —

Danksagung

An erster Stelle möchte ich Herrn Prof. Dr. Siegfried Schindler danken, für die Vergabe des Themenbereichs an dem ich forschen durfte, die vielseitige wissenschaftliche Anregung und die stets gewährte Unterstützung meiner Arbeit. Auch Herrn Prof. Dr. Richard Göttlich danke ich für sein Zweitgutachten meiner Dissertation.

Der ganzen Arbeitsgruppe um Herrn Prof. Dr. Siegfried Schindler danke ich für die Zusammenarbeit und die angenehme Zeit: Thomas Rotärmel, Alexander Petrillo, Stefan Schaub, Frank Mehlich, Lars Schneider und Florian Ritz. Besonderer Dank gilt hierbei Dr. Pascal Specht für das Korrekturlesen dieser Arbeit.

Auch den ehemaligen Mitarbeitern und damaligen Betreuern danke ich für das angenehme Arbeitsklima: Dr. Melanie Jopp, Dr. Tim-Daniel Stumpf, Dr. Andreas Karl Maximilian Miska, Dr. Miriam Wern und Dr. Tim Brückmann.

Weiterhin bedanke ich mich bei all meinen Kommilitonen welche mich durch das Studium begleitet und mich freundschaftlich unterstützt haben.

Ich bedanke mich bei dem gesamten Fachbereich 08, für das allgemein gute Arbeitsklima zwischen allen wissenschaftlichen Arbeitsgruppen und Mitarbeitern. Besonders hervorzuheben ist hierbei die Arbeitsgruppe um Herrn Prof. Dr. Mathias Wickleder (aktuell wieder zurück nach Köln gezogen) und Herrn Prof. Dr. Klaus Müller Buschbaum welche als direkte Nachbararbeitsgruppen stets reibungslos mit unserer Arbeitsgruppe zusammenarbeiten konnten.

Auch den Mitarbeiter der Chemikalienausgabe, Eike Santowski und Mario Deuber, gebührt Dank.

Den Mitarbeitern der Geräteanalytik der OC (Zentralanalytik) danke ich für die zahlreichen Ratschläge, Einweisungen in Messgeräte und nicht zuletzt der Durchführung von verschiedenen Servicemessungen. Namentlich zu erwähnen sind Dr. Heike Hausmann (NMR-Messung und -Expertise), Steffen Wagner (ESI-MS & GC/GC-MS), Stefan Bernhardt (Elementaranalyse).

Zuletzt, jedoch mit dem größtmöglichen Dank, möchte ich mich an dieser Stelle bei meiner gesamten Familie und meiner Freundin Jenni bedanken. In all den Jahren wurde ich in verschiedenster Weise von euch unterstützt und ihr gabt mir Halt auf dem manchmal anstrengenden Weg der Promotion!

Abkürzungsverzeichnis

Bn	-	Benzyl-Rest
Bu	-	Butyl-Rest
Bz	-	Benzoyl-Rest
d	-	Dublett (NMR)
DCM	-	Dichlormethan
DFT	-	Dichtefunktionaltheorie
DMSO	-	Dimethylsulfoxid
ESI	-	Electrospray-Ionisation
Et	-	Ethyl-Rest
et al.	-	et alii (lat. für "und andere")
GC	-	Gas-Chromatographie
iPr	-	*iso*-Propyl-Rest
LMCT	-	Ligand-to-metal charge-transfer
***m*CPBA**	-	*meta*-Chloroperoxybenzoesäure
Me	-	Methyl-Rest
MeCN	-	Acetonitril
MeOH	-	Methanol
MMO	-	Methan-Monooxygenase
MS	-	Massenspektrometrie
NMR	-	Kernspinresonanz
OAc	-	Acetat-Rest
ORTEP	-	Oak Ridge thermal ellipsoid plot
OTf	-	Trifluormethansulfonat-Rest
PAA	-	Peressigsäure

~Für Jenni~

Inhaltsverzeichnis

1 | Kurzfassung

Die Menschheit hat sich seit jeher für viele technische Anwendungen ein Beispiel an der Natur genommen, um deren hocheffiziente Vorgänge nachzuempfinden. So auch in der Untersuchung der Sauerstoff-Intermediate von Cu- und Fe-Komplexen, welche den aktiven Zentren von Metalloenzymen nachempfunden sind, um so katalytische Oxidationen an Substratmolekülen durchzuführen. Das Studium solcher Modellkomplexe kann im Umkehrschluss auch nützliche Informationen über die Mechanismen natürlicher Enzymreaktionen liefern. In der vorliegenden Arbeit wurden im Wesentlichen die Bildung und die Reaktivität von Kupfer(II)-*side-on*-peroxido-Komplexen sowie Eisen(III)-*cis-end-on*-peroxido-Komplexen untersucht. Dabei lag das Hauptaugenmerk auf der Formulierung und Diskussion möglicher Reaktionsmechanismen auf der Grundlage kinetischer Daten, welche mit Hilfe einer Tieftemperatur-*stopped-flow*-Technik (Aufnahme zeitaufgelöster UV-Vis-Spektren bei bis zu -80 °C) erhoben wurden. In Bezug auf die Kupferchemie wurde das Gleichgewicht zwischen dem Kupfer(I)-Komplex des phosphorhaltigen, tripodalen Liganden Pim^{iPr2} (Tris-[2-(1,4-diisopropylimidazolyl)]phosphin) und dem in der Reaktion mit Disauerstoff entstehenden *side-on*-peroxido-Komplex kinetisch analysiert. Dieses Gleichgewicht stellt ein ausgezeichnetes Modellsystem für den Sauerstofftransport des in Arthropoden (Gliederfüßer) vorkommenden Hämocyanins dar, da dieses in der Lage ist mit Sauerstoff den entsprechenden *side-on*-peroxido-Komplex in protischen Lösungsmitteln (Methanol & Methanol/Wasser-Gemisch) zu stabilisieren. Die beobachtete stark negative Aktivierungsentropie deutet dabei auf einen assoziativen Mechanismus im geschwindigkeitsbestimmenden Schritt hin. Des Weiteren wurde die Reaktion des dinuklearen Eisen(III)-*cis-end-on*-peroxido-Komplexes des Liganden Et-HPTB (*N,N,N',N'*-tetrakis[(*N*-ethyl-2-benzimidazolyl)methyl]-2-hydroxy-1,3-diaminopropan) mit Benzoylchlorid kinetisch untersucht. Dabei festigte sich die Vermutung, dass es sich bei dem in der Reaktion gebildeten Chromophor um eine Eisen(IV)oxido/carboxylato-Radikalspezies handelt. Weitere auf diese Reaktionsbedingungen angewandte DFT-Rechnungen bekräftigen diese Annahme. Bemerkenswert ist dabei, dass sich diese Intermediate in dem protischen Lösungsmittel Methanol bilden, wohingegen die meisten literaturbekannten Untersuchungen solcher Spezies in aprotischen Lösungsmitteln wie Acetonitril durchgeführt wurden. Die Hammett-Auftragung ergab einen überraschenden V-förmigen Verlauf, was ein deutlicher Hinweis darauf ist, dass sich der Reaktionsmechanismus unter Verwendung von elektronenschiebenden oder -ziehenden Effekten in *para*-Position des Benzoylchlorides ändert. Eine leicht negative Aktivierungsentropie lässt dabei auf einen assoziativen *interchange*-Mechanismus im geschwindigkeitsbestimmenden Schritt schließen.

2 | Abstract

Mankind has always taken an example from nature for many technical applications in order to imitate its highly efficient processes. This also applies to the investigation of the oxygen intermediates of Cu and Fe complexes, which are modeled on the active centers of metalloenzymes in order to carry out catalytic oxidations on substrate molecules. Conversely, studying such model complexes can also provide useful information about the mechanisms of natural enzyme reactions. In the present work the formation and reactivity of copper(II) *side-on*-peroxido complexes and iron(III) *cis-end-on*-peroxido complexes were examined. The main focus was on the formulation/discussion of possible reaction mechanisms on the basis of kinetic data, which were collected with the help of a low-temperature stopped-flow technique (recording of time-resolved UV-vis spectra at up to -80 °C). In terms of copper chemistry, the equilibrium between the copper(I) complex of the phosphorus-containing, tripodal ligand Pim^{iPr2} (tris-[2-(1,4-diisopropylimidazolyl)]phosphine) and the *side-on*-peroxido complex, which is formed in the reaction with dioxygen, was analyzed kinetically. This equilibrium represents an excellent model system for the oxygen transport of the hemocyanin contained in arthropods, as this is able to stabilize the corresponding *side-on*-peroxido complex in protic solvents (methanol & methanol/water mixture) with oxygen. The strongly negative activation entropy observed indicates an associative mechanism in the rate-determining step. Furthermore, the reaction of the dinuclear iron(III)-*cis-end-on*-peroxido complex of the ligand Et-HPTB (*N,N,N′,N′*-tetrakis[(*N*-ethyl-2-benzimidazolyl)methyl]-2-hydroxy-1,3-diamino-propane) with benzoyl chloride was kinetically investigated. The assumption was confirmed that the chromophore formed in this reaction is an iron(IV)oxido/carboxylato radical species. Further DFT calculations applied to these reaction conditions confirm this assumption. It is noteworthy that these intermediates are formed in the protic solvent methanol, whereas most studies of such species known from the literature were carried out in aprotic solvents such as acetonitrile. The Hammett plot showed a surprising V-shaped course, which is a clear indication that the reaction mechanism is changed by strong electron-donating or electron-withdrawing groups in the *para* position of the benzoyl chloride. A slightly negative activation entropy suggests an associative interchange-mechanism in the rate-determining step.

3 | Theoretische Grundlagen

3.1 | Biochemische Bedeutung von Kupfer und Eisen

Kupfer und Eisen wurden bereits in vielen Enzymen von Menschen, Tieren, Pflanzen und Mikroorganismen als Teil derer aktiven Zentren nachgewiesen.[1] Beide Übergangsmetalle sind Spurenelemente, wobei im menschlichen Körper durchschnittlich 3 g Eisen und 100 mg Kupfer als gesund gelten.[2,3] Diese zwei Übergangselemente sind besonders wichtig für viele Organismen, da diese eine hohe relative Häufigkeit und hohe Bioverfügbarkeit aufweisen.[4-6] Beide Elemente kommen in Lebewesen der Flora und Fauna in Form von Metalloproteinen vor, welche essentiell für alle lebenden Organismen sind, und übernehmen unter anderem als Katalysatoren (Enzyme) in biologischen Prozessen eine Vielzahl unterschiedlicher Funktionen wie beispielsweise Atmung, Photosynthese oder Aktivierung von molekularem Sauerstoff.[4,7,8]

3.1.1 | Kupferhaltige Metalloproteine

Die biochemische Relevanz von Kupfer beruht hauptsächlich auf einem in wässrigem Medium (bzw. in den Zellen eines Organismus) leicht realisierbaren Kupfer(I)/Kupfer(II)-Redoxübergang im positiven Potentialbereich. Neben der Einteilung nach ihrer Funktion (z.B. als Oxidase oder Oxygenase) werden klassische Kupferproteine auf Grund ihrer strukturellen und spektroskopischen Eigenschaften in Typ I, Typ II und Typ III Kupferproteine eingeteilt (siehe Abb. 1).[4,6,7] Kupferhaltige Proteine, welche nicht in dieses Schema eingeordnet werden können, werden als nicht-klassische Kupferproteine bezeichnet.[9] Dazu gehören mehrkernige Kupferzentren, die aus einer Mischung von Typ I-, Typ II- und Typ III-Kupferzentren bestehen oder sogar zweikernige, durch Thiolat-Gruppen verbrückte Kupferzentren.[9]

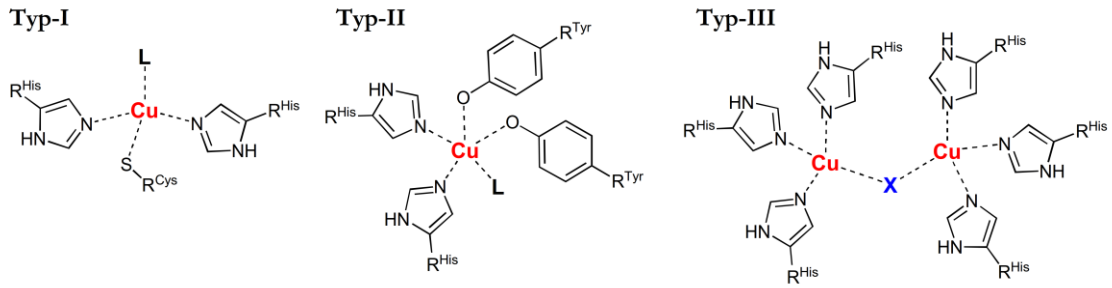

Abb. 1. Einteilung der Kupferproteine in die Klassen Typ I, Typ II und Typ III.

Aktive Zentren der Kupferproteine vom Typ I bestehen aus einem Kupfer-Ion, welches eine tetraedrisch stark verzerrte Koordinationsgeometrie aufweist. Dabei sind jeweils zwei Histidin-Reste und ein Cysteinat-Rest koordiniert und die freie Koordinationsstelle wird von einem weiteren schwach gebundenen variablen Liganden wie Methionin, Glutamin oder Leucin abgesättigt (siehe Abb. 1).[6,9] Die Bindung des Cysteinat-Restes an das Kupferzentrum und der daraus resultierende intensive Ligand-zu-Metall-Ladungsübertrag (engl. *ligand-to-metal charge-transfer*; kurz LMCT) führt zu einer intensiven Absorptionsbande im UV-Vis-Bereich bei 600 nm, wodurch diese Enzyme in einer unverwechselbaren blauen Farbe erscheinen. Die verzerrte Geometrie stellt einen Kompromiss zwischen der von Kupfer(II)-Ionen bevorzugten quadratisch-planaren (bzw. durch den Jahn-Teller-Effekt oktaedrisch-verzerrten) Anordnung und der von Kupfer(I)-Ionen bevorzugten tetraedrischen Koordinationsgeometrie dar.[10] Beispiele für Kupferproteine des Typs I sind Plastocyanin oder Azurin, welche als Elektronenüberträger an der pflanzlichen oder bakteriellen Photosynthese beteiligt sind.[11,12]

Die koordinative Umgebung in aktiven Zentren von Typ II-Kupferproteinen ist normalerweise quadratisch-planar oder tetraedrisch-verzerrt und durch vier Stickstoff- (z.B. Histidin-Rest) oder Sauerstoff-Donatoren (z.B. Tyrosinat-Rest) gegeben (siehe Abb. 1). Unter die Kategorie Typ II-Proteine fallen Oxidasen, Oxygenasen oder Superoxiddismutasen. Wichtige Beispiele sind dabei Dopamin-β-monooxygenasen, die an der Seitenkettenhydroxylierung von Dopamin zu Noradrenalin beteiligt sind.[9,13]

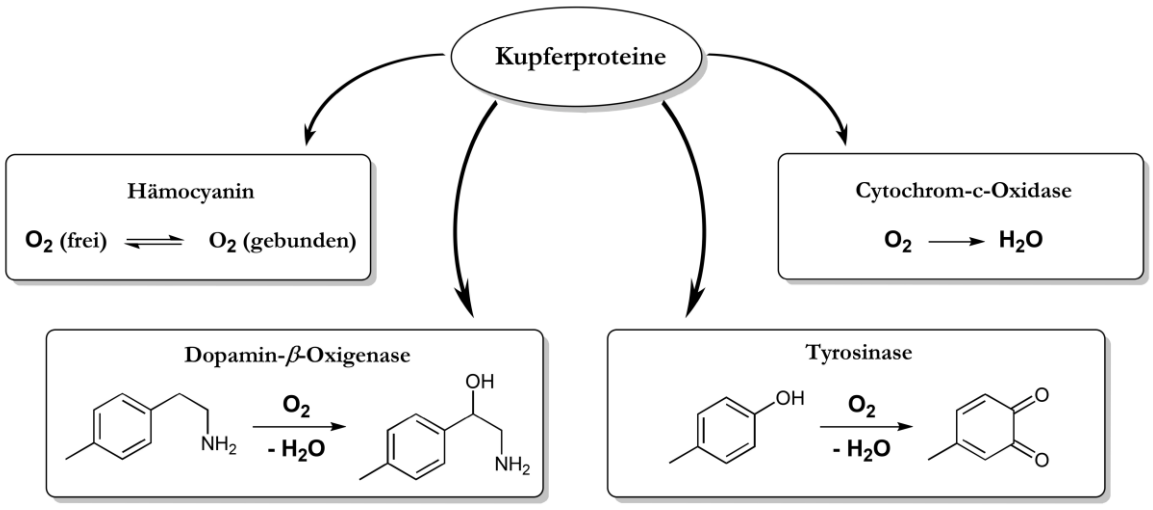

Abb. 2. Schematische Aufteilung der Kupferproteine in einige bedeutende Enzymklassen.

Typ III-Kupferproteine unterscheiden sich strukturell von Typ I und Typ II vor allem dadurch, dass diese im aktiven Zentrum zwei Kupfer-Ionen enthalten. In diesen dinuklearen Zentren sind die Kupfer-Ionen jeweils in trigonal-planarer Geometrie von drei Histidin-Resten

koordiniert (siehe Abbildung 1).[4,9,13] Diese Art von Kupferproteinen spielt eine wichtige Rolle bei der Bindung und Aktivierung von molekularem Sauerstoff. Die Anbindung von molekularem Sauerstoff kann dabei reversibel (z.B. Sauerstofftransport) oder irreversibel (z.B. Sauerstoffaktivierung) stattfinden. Die reduzierten Formen dieser aktiven Zentren weisen Kupfer-Kupfer-Abstände von ca. 4,6 Å auf und begünstigen dabei die Anbindung von molekularem Sauerstoff in Form von *side-on*-peroxido-Komplexen. Bei der Umwandlung von der Desoxy- in die Oxy-Form verringert sich dieser Kupfer-Kupfer-Abstand auf ca. 3,6 Å und die Koordinationsgeometrie ändert sich zu quadratisch-planar.[14,15] Auf Grund des Ladungsübertrages vom Liganden (*side-on*-Peroxid) zu den Metallzentren weisen diese Enzyme zwei charakteristische Banden im UV-Vis-Bereich bei 350 nm und 600 nm (LMCT-Banden) auf.[4,6,9,16] Wichtige Kupferproteine des Typs III sind z.B. die Tyrosinase (Sauerstoffaktivierung) und Hämocyanin (Sauerstofftransport).

Hämocyanin ist für den Sauerstofftransport in Weichtieren und Arthropoden verantwortlich und verursacht auch das im Gegensatz zum roten Blut des Menschen blau gefärbte Blut dieser Organismen.[17,18] In Abb. 3 ist das Sauerstoffgleichgewicht von Hämocyanin schematisch dargestellt. Die Kristallstruktur des gesamten Supermoleküls von Desoxy-Hämocyanin wurde 2015 von Gai und Mitarbeitern erstmals beschrieben.[19]

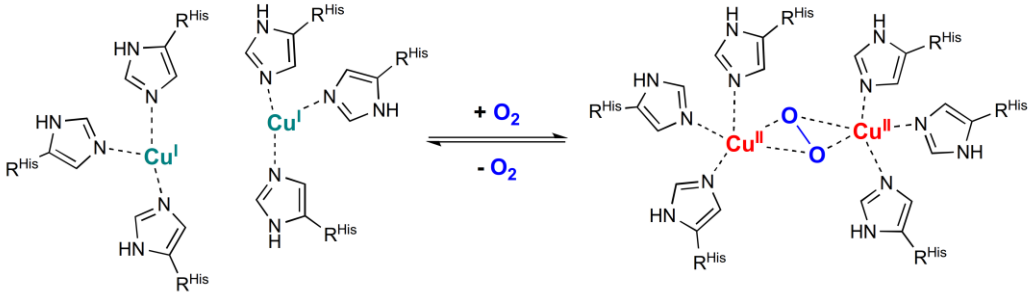

Abb. 3. Schematische Darstellung des Sauerstoffgleichgewichtes im aktiven Zentrum von Hämocyanin.

Das Enzym Tyrosinase ist eine Dioxygenase und katalysiert die Oxygenierung bzw. Hydroxylierung phenolischer Substrate zu Brenzcatechinen und die Überoxidation zu *ortho*-Chinonen.[20,21] Als Oxygenierung wird dabei der spezielle Fall einer Oxidation bezeichnet, in dem ein Sauerstoffatom durch ein Enzym (oder allgemein Oxidationsmittel) auf ein definiertes Substratmolekül übertragen wird. Als Sauerstoffaktivierung wird allgemein die Erhöhung der Reaktivität von molekularem Sauerstoff oder sauerstoffhaltigen Molekülen bezeichnet. Das Komplexzentrum des so gebildeten Sauerstoff-Addukt-Komplexes entzieht dem gebundenen

Sauerstoff einen Teil dessen Elektronendichte, woraus eine geschwächte *O*-*O*-Bindung resultiert.[22] Eine genauere Betrachtung der energetischen Zustände erlaubt das Molekülorbital-Schema (engl. molecular orbital diagram; kurz MO-Schema; siehe Abb. 4). Aus der Mischung der beiden Atomorbitale (AO) für Sauerstoff resultiert die jeweils einfache Besetzung der antibindenden Molekülorbitale 2pπ*, was zeigt, dass molekularer Sauerstoff unter normalen Bedingungen im Triplettzustand und somit als Diradikal vorliegt.[23] Wenn nun Sauerstoff mit entsprechendem Metallkomplex reagiert, so wird das Metall-Ion oxidiert und Sauerstoff zu Peroxid reduziert, wodurch die zusätzlichen Elektronen ebenfalls das antibindende Molekülorbital 2pπ* besetzen und somit die *O*-*O*-Bindung geschwächt wird.[24]

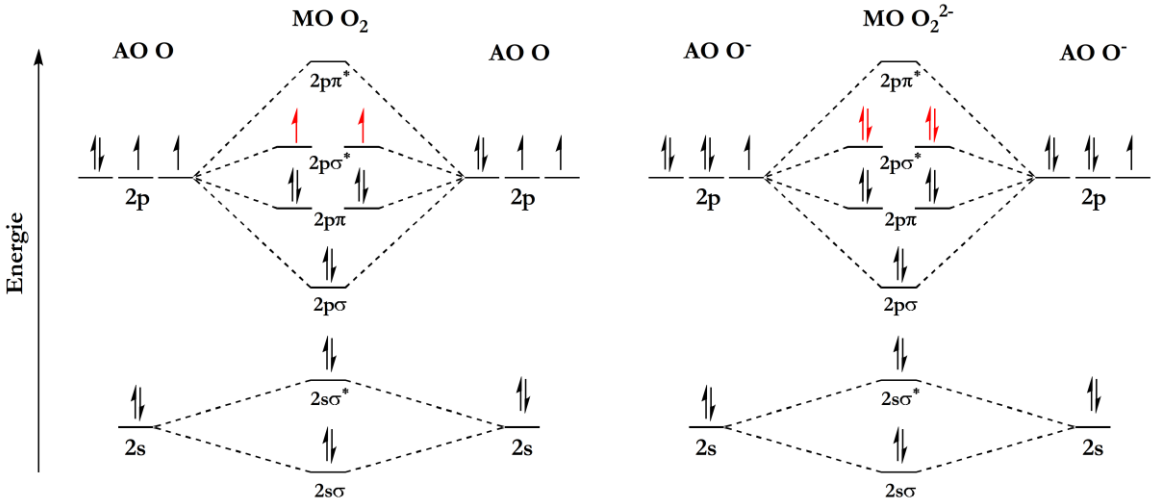

Abb. 4. Molekülorbital-Schema für molekularen Sauerstoff (links) und für das Peroxid-Ion (rechts).[24]

3.1.2 | Modellkomplexe für kupferhaltige Enzyme

Um die zugrunde liegenden Reaktionsmechanismen besser verstehen zu können, bedient man sich verschiedener Modellsysteme, welche die komplexen Mechanismen natürlicher Vorgänge vereinfachen. Als synthetische Modelle für Enzyme wurden dabei Metallkomplexe entwickelt, welche sich im Gegensatz zu ihren natürlichen Vorbildern einfacher untersuchen lassen. Ein Modellkomplex reduziert das entsprechende Enzym auf das aktive Zentrum und ahmt dabei bestmöglich die räumliche und elektrosterische Umgebung der Metallzentren nach. Die Wechselwirkung von molekularem Sauerstoff mit Kupfer(I)-Komplexen wurde in der Vergangenheit untersucht um ein besseres Verständnis der Reaktivität redoxaktiver Kupferenzyme sowie für Oxidationsreaktionen im Labor und in der Industrie zu erhalten.[21,25-30]

Die Anbindung von molekularem Sauerstoff kann in verschiedenen Formen geschehen, wodurch sich u.a. oxido-, superoxido- und peroxido-Komplexspezies ausbilden können (siehe Abb. 5). Dabei ist insbesondere das Ligandendesign (räumlicher und elektrosterischer Anspruch) ausschlaggebend für die Stabilität entsprechender Sauerstoff-Intermediate.[31,32] Die Kategorisierung dieser Sauerstoffkomplexe wird über die formale Oxidationszahl des Sauerstoffes im Komplex vorgenommen. Es wird so grundsätzlich zwischen einkernigen und mehrkernigen, bzw. verbrückten und nicht-verbrückten Sauerstoff-Komplexen unterschieden. Für mehrkernige Sauerstoff-Komplexe kann zudem eine weitere Unterteilung, über die Art der Verbrückung zwischen den Komplexzentren, in *cis*- und *trans*-Konfiguration vorgenommen werden.[28,32,33]

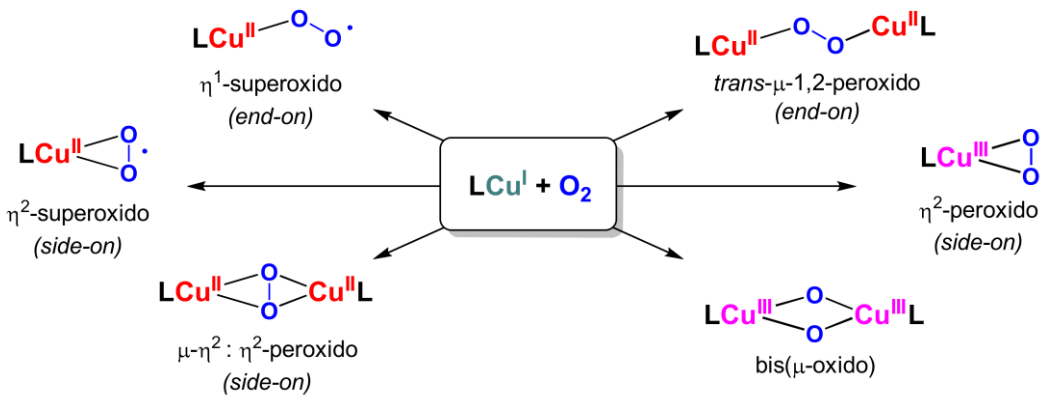

Abb. 5. Schematische Darstellung einiger Disauerstoff-Addukt-Komplexe am Beispiel eines Kupfer(I)-Komplexes mit dem Ligandenumfeld L.[26]

In den vergangenen 40 Jahren konnte eine Vielzahl dieser reaktiven Kupfer-Sauerstoff-Komplexe vollständig charakterisiert werden, welche als Intermediate für den Sauerstofftransfer verantwortlich sind.[25,27,33-43]

Die erste literaturbekannte Kristallstruktur eines synthetischen Kupfer-peroxido-Komplexes wurde bereits 1988 von Karlin und Mitarbeitern beschrieben.[34] Dieser Komplex erwies sich als *end-on*-peroxido-Komplex des vierzähnigen, tripodalen Liganden Tris(2-pyridylmethyl)amin (tmpa; siehe Abb. 7). Weitere Forschungen deuteten an, dass diese Ligandenklasse der tripodalen Liganden ausgezeichnet für die Ausbildung von Sauerstoff-Komplexen im *end-on*-Koordinationsmodus geeignet ist. Spektroskopische und kinetische Untersuchungen der Bildung dieses peroxido-Komplexes zeigten, dass als sehr reaktives Intermediat ein *end-on*-superoxido-Komplex gebildet wird.[44,45] Alle Versuche, dieses hochreaktive superoxido-Intermediat zu isolieren und zu charakterisieren waren jedoch erfolglos. 2004 beschrieben Suzuki und Mitarbeiter ein weiteres Beispiel für einen Kupfer(II)-*end-on*-peroxido-Komplex.[38] Als Ligand wurde hier die benzylierte Variante von Tren (Bz_3tren) verwendet. Zeitaufgelöste Tieftemperatur-UV-Vis-Messungen zeigten hier ebenfalls deutlich die Bildung des entsprechenden superoxido-Komplexes als Intermediat. Auch in diesem Fall blieben alle Versuche dieses Intermediat zu kristallisieren erfolglos. 2006 gelang es schließlich Schindler und Mitarbeitern den ersten *end-on*-superoxido-Komplex zu kristallisieren und die Struktur vollständig kristallografisch aufzuklären.[35] Der Kupfer(I)-Komplexes $[Cu(TMG_3tren)]SbF_6$ reagiert hierbei zu dem superoxido-Komplex $[Cu(TMG_3tren)(O_2)]SbF_6$. Bei -55 °C konnte zudem in Aceton eine reversible Reaktion mit Sauerstoff nachgewiesen werden. Die Struktur des Liganden TMG_3tren ist in Abb. 7 abgebildet. In aktiven Zentren von dinuklearen Kupfer-Monooxygenasen wie der Dopamin-β-Monooxygenase, wird den Methionin-Resten eine entscheidende Rolle zur Bildung von Kupfer(II)-superoxido-Intermediaten zugeschrieben. Die Kupfer-Schwefel-Wechselwirkung hat entscheidende Auswirkungen auf die Reaktivität dieser Intermediate und wirft immer noch Fragen über die genaue Wirkungsweise und den Mechanismus auf. Karlin und Mitarbeiter beschrieben 2021 den ersten Kupfer(II)-superoxido-Komplex mit einer experimentell nachgewiesenen Cu-S-Bindung unter Verwendung des Liganden $^{TMG}N_3S$ (siehe Abb. 7). Dabei konnte, so wie bei $[Cu(TMG_3tren)]^+$ ebenfalls, eine reversible Reaktion des Modellkomplexes mit Sauerstoff nachgewiesen werden, jedoch mussten tiefere Temperaturen (-135 °C) und somit auch ein geeignetes Lösungsmittel (2-Methyltetrahydrofuran) verwendet werden.[46]

1989 beschrieben Kitajima und Mitarbeiter den ersten synthetischen Kupfer(II)-*side-on*-peroxido-Komplex als Modellkomplex für Hämocyanin. Als Ligand wurde der dreizähnige Ligand HB(3,5-*i*Pr$_2$pz)$_3$ verwendet, welcher zu der Klasse der Tris(pyrazolyl)borate gehört.[47] Fünf Jahre später gelang es Kitajima und Mitarbeitern, mit einer kleinen Modifikation dieses Liganden, den ersten Kupfer(II)-*side-on*-superoxido-Komplex zu synthetisieren. Durch die Substitution der drei *iso*-propyl-Gruppen durch *tert*-butyl-Gruppen hat der verwendete Ligand HB(3-*t*Bu-5-iPrpz)$_3$ (siehe Abb. 7) einen wesentlich größeren sterischen Anspruch als HB(3,5-*i*Pr$_2$pz)$_3$ und ist somit in der Lage, das Superoxid zu stabilisieren.[48]

1995 gelang es Thomas N. Sorrell und Mitarbeitern einen tripodalen Liganden zu entwerfen, welcher es erlaubt, die reversible Reaktion mit Sauerstoff in dem protischen Lösungsmittel Methanol zu untersuchen (siehe Abb. 6).[49] Der Kupfer(I)-Komplex [Cu(Pim$^{i\text{Pr2}}$)(MeCN)]$^+$ des Liganden Pim$^{i\text{Pr2}}$ (Tris[2-(1,4-diisopropylimidazolyl)]phosphin; siehe Abb. 7) bildet dabei bei tiefen Temperaturen ein stabiles Gleichgewicht mit Sauerstoff und stellt somit einen ausgezeichneten Hämocyanin-Modellkomplex dar. Die Bildung des Kupfer(II)-*side-on*-peroxido-Komplexes und die Reaktivität konnte dabei erfolgreich untersucht werden.

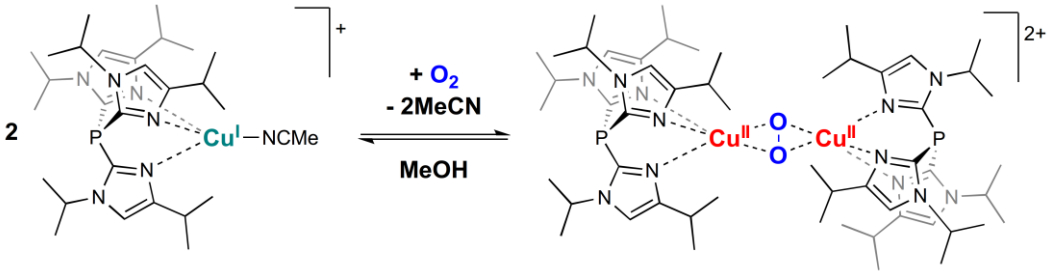

Abb. 6. Schematische Darstellung der reversiblen Reaktion des Kupfer(I)-Komplexes [Cu(Pim$^{i\text{Pr2}}$)(MeCN)]$^+$ mit molekularem Sauerstoff in Methanol.

Diese Sauerstoffintermediate sind für gewöhnlich sehr labil und können oft lediglich in aprotischen Lösungsmitteln bei tiefen Temperaturen (bis zu -140 °C) untersucht werden.[29,41,44,50-53] Protonen können dabei zur Bildung von Wasserstoffperoxid und schließlich zum entsprechenden Kupfer(II)-Komplex und Wasser führen. Normalerweise erlauben Reaktionen in protischen Lösungsmitteln keine Beobachtung von kurzweiligen, intermediären Komplexen und unterdrücken das Potenzial dieser Komplexe, Oxidationsreaktionen an organischen Substrat-Molekülen durchzuführen.[54]

Gemäß aktuellem Stand sind ausschließlich zwei Arten solcher Reaktionen in Methanol als Lösungsmittel literaturbekannt. 1994 beschrieben Lynch und Mitarbeiter ebenfalls einen

Kupfer(I)-Komplex eines Tris(imidazoylyl)phosphin-Liganden, welcher mit Sauerstoff einen *side-on*-peroxido-Komplex bildet[55] und 1997 konnten Bol und Mitarbeiter unter Verwendung eines makrocyclischen Liganden vermutlich einen *side-on*-peroxido-Komplex stabilisieren.[56] 2016 wurde ein *side-on*-peroxido-Komplex beschrieben, welcher sich in wässrigen Lösungen als relativ stabil erwies, dabei wurde das Tri-*tert*-butyl-Derivat von Triazacyclononan $^{t}Bu_3tacn$ als Ligand verwendet (siehe Abb. 7).[57] Dennoch war es technisch nicht möglich, die Bildung dieses Komplexes zu untersuchen.

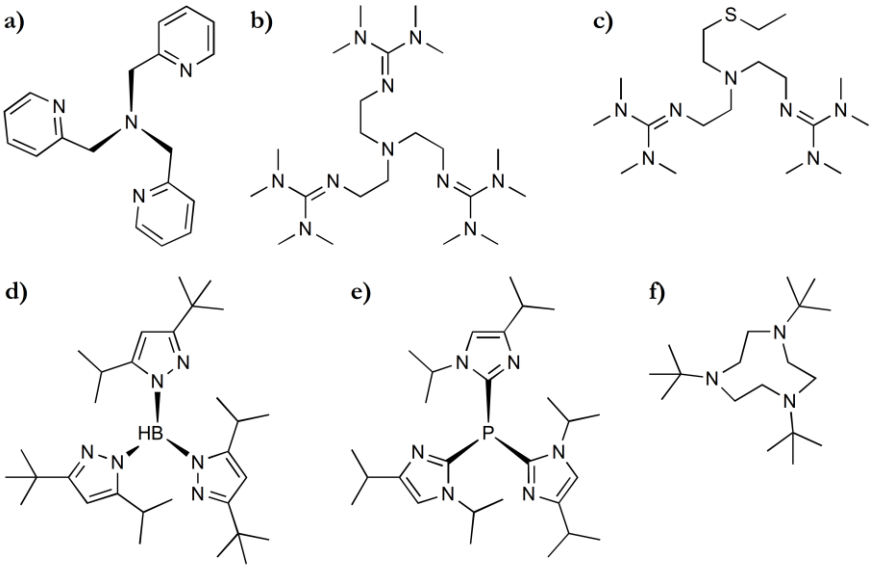

Abb. 7. Ligandenübersicht zur Verdeutlichung der Strukturen. tmpa (a), TMG_3tren (b), $^{TMG}N_3S$ (c), $HB(3,5\text{-}iPr_2pz)_3$ (d), Pim^{iPr2} (e), $^{t}Bu_3tacn$ (f).

3.1.3 | Eisenhaltige Nicht-Häm-Metalloproteine

Eisen zählt zu den wichtigsten Elementen für lebende Organismen, da es in einer Vielzahl von Proteinen und Enzymen essentielle biochemische Aufgaben übernimmt. In der Natur kommt es in den Oxidationsstufen +II und +III vor. In Organismen ist es als aktives Zentrum von Häm- oder Nicht-Häm-Eisenproteinen enthalten. Sogenanntes hochvalentes Eisen in den Oxidationsstufen +IV und +V wird zudem in reaktiven Sauerstoffintermediaten beobachtet.

Die Gruppe der Cytochrome, z.B. Cytochrom P450, das als Monooxygenase in der Lage ist aliphatische C-H-Bindungen oder vinylische C=C-Doppelbindungen zu hydroxylieren, oder die Cytochrom-c-Oxidase, vermögen es molekularen Sauerstoff in der Atmungskette zu Wasser zu reduzieren.[58-60] Bei der in Abb. 8 abgebildeten Reaktionskette kann der molekulare Sauerstoff auf unterschiedliche Weise biochemisch gebunden werden. Der gebundene Disauerstoff wird zunächst über eine Ein-Elektronen-Aufnahme zum Superoxid reduziert. Durch weiteren Elektronentransfer wird das Superoxid zu Peroxid reduziert und kann durch Protonenaufnahme zu Hydroperoxid und weiter zu Wasserstoffperoxid reagieren. Das Hydroperoxid-Addukt findet sich beispielsweise in der Atmungskette mariner Lebensformen in Hämerythrin. Im weiteren Verlauf der Reduktion des Peroxids werden zuerst Oxyl-Radikale gebildet, welche zu Oxid-Ionen reduziert werden. Unter Protonierung wird schlussendlich Wasser gebildet.[61-63]

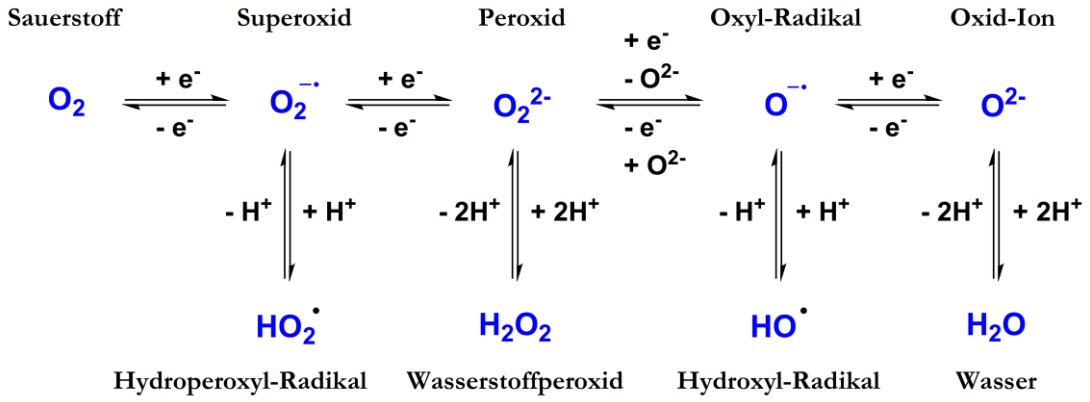

Abb. 8. Übersicht über die hochreaktiven Sauerstoff-Intermediate, welche in biologischen Organismen bei der Umwandlung von molekularem Sauerstoff zu Wasser gebildet werden.

Als eisenhaltige Nicht-Häm-Metalloproteine werden alle Eisenenzyme bezeichnet, welche keine Häm-Gruppe aufweisen, also keinen Porphyrin als koordinativen Grundkörper im aktiven Zentrum enthalten. Betrachtet man sich den Sauerstofftransport in Wirbeltieren und Mollusken (Weichtiere), so verdeutlicht sich dieser strukturelle Unterschied (siehe Abb. 9).

Beide Blutsorten enthalten einen eisenhaltigen Blutfarbstoff, das Hämoglobin (im Blut von Wirbeltieren) und das Hämerythrin (im Blut von diversen marinen Mollusken), welches für den Sauerstofftransport im jeweiligen Körper zuständig ist. Abgesehen von dem strukturellen Aufbau äußert sich der offensichtlichste Unterschied in der farblichen Erscheinung. Durch die Sauerstoffbindung im Hämerythrin färbt sich das Blut dieser marinen Lebewesen im Gegensatz zum blutroten Hämoglobin violett.

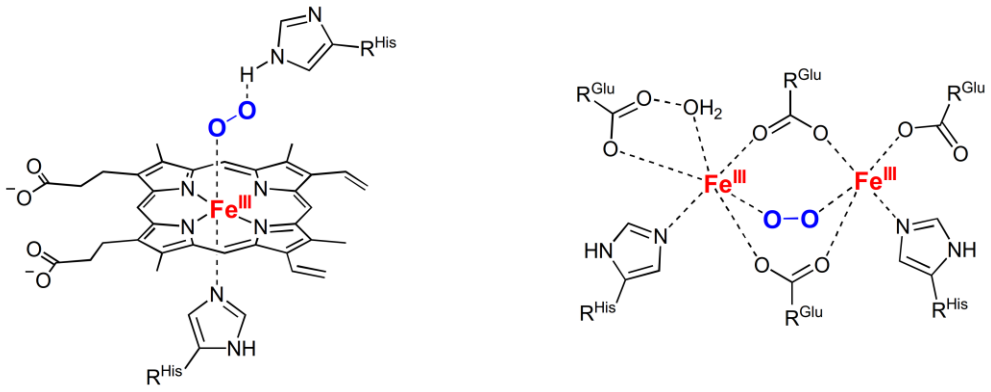

Abb. 9. Darstellungen der Oxy-Formen aktiver Zentren der Blutfarbstoffproteine Hämoglobin (links) und Hämerythrin (rechts).

Allgemein können Nicht-Häm-Eisenproteine in einkernige und mehrkernige Eisenproteine unterteilt werden, je nachdem wie viele Eisen-Ionen im aktiven Zentrum enthalten sind. Zu den mononuklearen Nicht-Häm-Proteinen zählen wichtige Mono- und Dioxygenasen, die im Fettsäurestoffwechsel, Aromatenstoffwechsel oder der Aminosäuresynthese vorkommen.[64]

Neben einkernigen Nicht-Häm-Proteinen gibt es eine Vielzahl von zweikernigen Nicht-Häm-Proteinen, die ebenfalls molekularen Sauerstoff binden/aktivieren und selektiv mit Substraten reagieren können. Wichtige Vertreter dieser dinuklearen Nicht-Häm-Eisenproteine sind das oben bereits erwähnte Hämerythrin,[65-69] die lösliche Methanmonooxygenase (sMMO)[70-83] und die Aldehyd-deformylierende Oxygenase (ADO).[84-86] Hämerythrin wurde 1969 als eine der ersten Nicht-Häm-Eisenproteine von Klotz und Mitarbeitern mit einer peroxidischen Disauerstoffbindung isoliert.[87,88] 1991 wurde die Kristallstruktur der Oxy- und Desoxy-Form dieses Proteins erstmals von Stenkamp und Mitarbeitern publiziert.[89,90]

Die Beispiele für katalysierte eisenbasierte Oxygenierungsprozesse sind sehr vielfältig, wobei die Hydroxylierung von Aromaten durch die Ribonukleotidreduktase (RNR)[91-98], die Oxidation von Aminen zu Nitroverbindungen durch die *N*-Oxygenase CmlI [99-101] oder die selektive Sauerstoffinsertion an aliphatischen Verbindungen durch die sMMO[70-83] zu nennen sind. Die

sMMO wurde erstmals im Bakterium *Methylococcus capsulatus* gefunden, welches in der Lage ist, die enorm starke C-H-Bindung in Methan (105 kcal/mol) zu brechen und dieses zu Methanol zu verstoffwechseln. Beeindruckend ist dabei, dass dieses Bakterium diese Oxidation bei Raumtemperatur mit molekularem Sauerstoff durchführt.[83] Das aktive Zentrum von sMMO enthält zwei Eisenionen, welche von Histidin- und Glutamat-Resten koordiniert und verbrückt werden (siehe Abb. 10).[71,72]

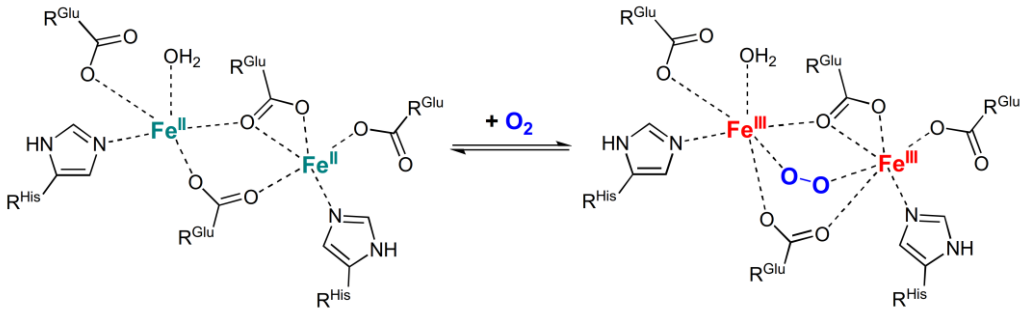

Abb. 10. Schematische Darstellung des Sauerstoffgleichgewichtes im aktiven Zentrum der sMMO.

Dinukleare Eisen(III)-peroxido-Intermediate können zwei verschiedene Rollen in natürlichen Oxidationsprozessen einnehmen. Sie können als aktive Oxidationsmittel fungieren (z.B. bei ADO) oder wirken als Vorstufe von hochvalenten Fe(IV)Fe(IV)-Intermediaten wie beispielsweise in sMMO als Eisen(IV)oxido-Spezies.[102,103]

Die ADO ist ein dinukleares Nicht-Häm-Eisenenzym, welches in Algen und Cyanobakterien zu finden ist und Fettaldehyde in Alkane umwandelt und diese in einer anschließenden Überoxidation zu Alkohol- und Aldehydprodukten abbaut.[84,85,104-108] Vorangegangene Studien deuten darauf hin, dass ADO verantwortlich für drei grundverschiedene Reaktionen ist.[86,102,103,109-111] Der Mechanismus ist in Abb. 11 beschrieben. Im ersten Schritt wird vermutet, dass das Peroxid des Sauerstoff-Intermediates den Carbonylkohlenstoff des bereits koordinierten Fettaldehyds angreift (Schritt **a**) und so die Deformylierung induziert. Darauf folgt eine Wasserstoffatomabstraktion (b) mit anschließender Rückbindung, was in einer C-H-Hydroxylierung zur Bildung eines Alkohols führt. Abschließend findet eine zwei-Elektronen-Oxidation des gebildeten Alkohols zu Aldehyd statt (c).[105] Die letzten beiden Schritte lassen auf eine reaktive Spezies mit elektrophilem Reaktionscharakter schließen, die dem von sMMO ähnelt.[71,72] Diese Beobachtungen verdeutlichen die mechanistische Vielseitigkeit der dinuklearen Eisen(III)-peroxido-Intermediate.[108]

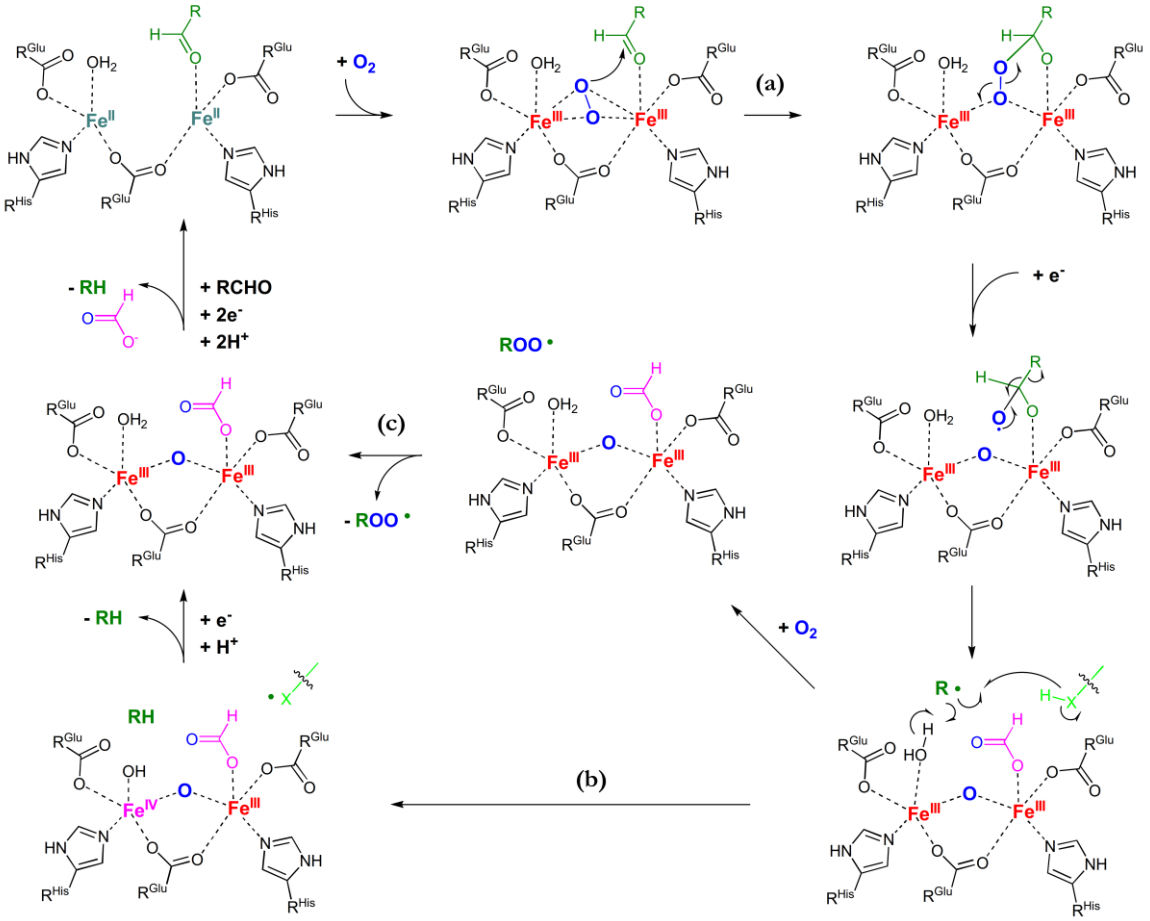

Abb. 11. Mechanismus der Aldehyd-Deformylierung im aktiven Zentrum der ADO.[109]

3.1.4 | Modellkomplexe für dinukleare Eisenenzyme

Um die zugrunde liegenden Reaktionsmechanismen besser verstehen und untersuchen zu können, wurden verschiedene Modellsysteme entwickelt, die die aktiven Zentren der oben genannten Enzyme sMMO und Hämerythrin als Nicht-Häm-Eisenproteine darstellen. Die synthetischen Modelle sind gegenüber ihren natürlichen Vorbildern spektroskopisch und kristallografisch wesentlich einfacher zu untersuchen. In den letzten 30 Jahren wurde eine Vielzahl an zweikernigen Eisen(III)-peroxido-Komplexen, welche als synthetische Strukturmodelle für Intermediate von sMMO und Hämerythrin gelten, hergestellt und ausgiebig charakterisiert.[70,102,103,112-122] Literaturbekannte typische Beispiele für Liganden, welche dinukleare Komplexe ausbilden und entwickelt wurden, um die aktiven Zentren von sMMO bzw. Hämerythrin nachzuempfinden, sind z.B. *N,N,N‘,N‘*-Tetrakis(1-methyl-2-phenyl-4-imidazolyl)methyl-1,3-diamino-2-propanolat (L^{Ph4})[123], *N,N,N′,N′*-Tetrakis(2-pyridylmethyl)-1,3-diaminopropan-2-olat) (HPTP)[116,117,124], *N,N,N‘,N‘*-Tetrakis(2-benzimidazolylmethyl)-2-hydroxo-1,3-diaminopropan (HPTB)[125,126] und *N,N,N′,N′*-Tetrakis(N-ethyl-2-benzimidazolyl-methyl)-2-hydroxy-1,3-diaminopropan (Et-HPTB).[116,118,127,128] Diese Liganden sind in Abb. 12 zur Übersicht dargestellt.

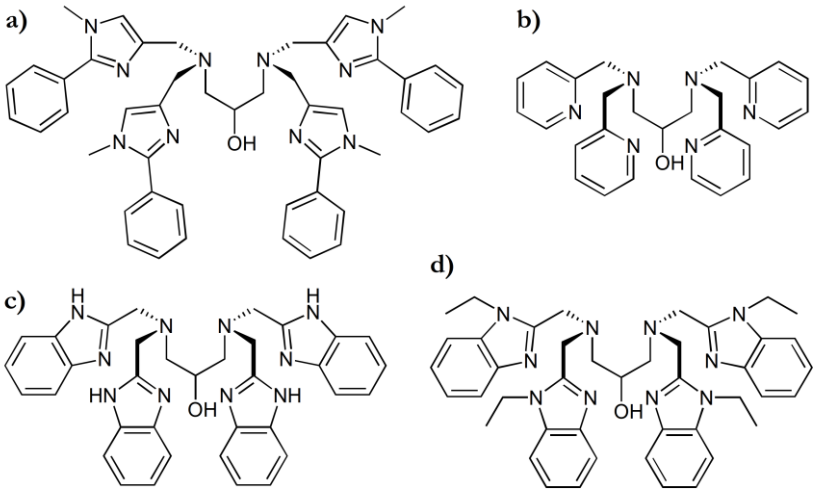

Abb. 12. Ligandenübersicht zur Verdeutlichung der Strukturen. L^{Ph4} (a) HPTP (b), HPTB (c) und Et-HPTB (d).

Durch die unmittelbare Nähe der zwei Eisen-Zentren wird die Ausbildung des peroxido-Komplexes stark begünstigt. So wurden bereits über 30 peroxido-Komplexe spektroskopisch nachgewiesen und teilweise röntgenkristallographisch charakterisiert.[115,120,127-129] Die UV-Vis-spektroskopische Untersuchung dieser basiert auf der charakteristischen

LMCT-Bande, welche ein Absorptionsmaximum in einem Wellenlängenbereich von 450 bis 730 nm zur Folge hat.[114,116-118,124,127,128,130] Die meisten Untersuchungen an dinuklearen Eisen-Disauerstoff-Addukt-Komplexen wurden in aprotischen, organischen Lösungsmitteln wie Acetonitril, Propionitril, Dichlormethan oder Tetrahydrofuran durchgeführt.[116,131-133] Die Verwendung protischer Lösungsmittel beschleunigt die Peroxid-Zersetzung, was es normalerweise schwierig macht, reaktive Intermediate wie Superoxid- oder Peroxid-Spezies zu detektieren. In aprotischen Lösungsmitteln hingegen werden die Sauerstoff-Intermediate stabilisiert, was sich in einer längeren Halbwertszeit der Zersetzungsreaktion widerspiegelt.[134-136] Die Stabilität der intermediären Komplexe kann durch externe Zugabe eines Co-Liganden wie z.B. Dimethylsulfoxid oder Triphenylphosphinoxid erhöht werden.[116,137] 1994 führten Lippard und Mitarbeiter kinetische Untersuchungen mittels Tieftemperatur-*stopped-flow*-Technik in Propionitril durch, um die Bildung des dinuklearen Eisen(III)-μ-1,2-peroxido-Komplexes weiter zu studieren.

Die Aktivierungsparameter wurden durch eine Eyring-Auftragung bestimmt, wobei eine erstaunliche Ähnlichkeit der Aktivierungsenthalpie von $\Delta H^{\neq}$ = 15,4 kJ/mol im Vergleich zum natürlichen Hämerythrin mit $\Delta H^{\neq}$ = 16,8 kJ/mol erhalten wurde. Die Bestimmung der Aktivierungsentropie ergab einen Wert von $\Delta S^{\neq}$ = -121 J/mol K, welcher auf einen assoziativen Mechanismus im geschwindigkeitsbestimmenden Schritt schließen lässt. Der Vergleich mit dem Wert von Hämerythrin von $\Delta S^{\neq}$ = -46 J/mol K zeigt eine größere Abweichung auf, welche womöglich auf Lösungsmitteleffekte zurückzuführen ist.[132,133]

1992 stellten Akamatsu und Mitarbeiter fest, dass sich der Eisen(III)-peroxido-Komplex des Liganden HPTB nicht nur über die Reaktion des Eisen(II)-Komplexes mit Sauerstoff bildet, sondern auch über eine Reaktion von Eisen(III)-Komplexen mit Wasserstoffperoxid generierbar ist.[138] Spektroskopische Untersuchungen festigten diese Vermutung der Bildung eines *cis*-1,2-peroxido-Komplexes,[139] wobei 2001 dieses System von Krebs und Mitarbeitern weiter untersucht wurde. Die schematische Darstellung dieser Reaktion ist in Abb. 13 abgebildet. Dabei wurde festgestellt, dass der peroxido-Komplex in verschiedenen Lösungsmitteln gebildet werden kann (Methanol, Acetonitril und Dimethylsulfoxid). Die Reaktionsgeschwindigkeiten unterscheiden sich dabei stark, was laut Autoren auf die Koordinationsstärke der Lösungsmittelmoleküle zurückzuführen ist. Eine weitere wichtige Beobachtung in dieser Arbeit ist die hohe Stabilität des über Wasserstoffperoxid gebildeten peroxido-Komplexes im Vergleich zu der peroxido-Spezies welche über die Reaktion des Eisen(II)-Komplexes mit Sauerstoff gebildet wird.

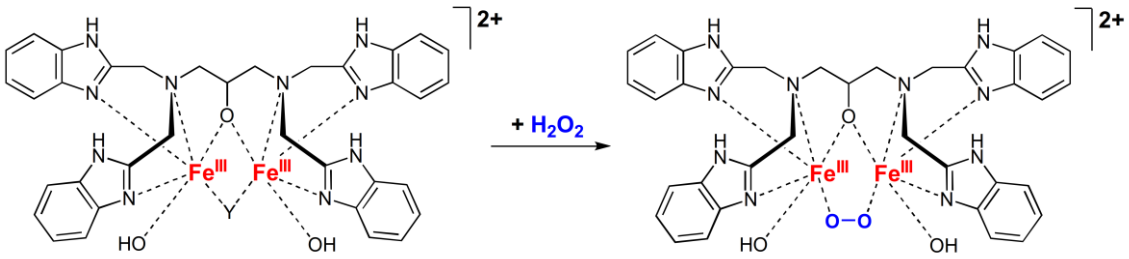

Abb. 13. Schematische Darstellung der Reaktion des Eisen(III)-Komplexes $[Fe_2(Et\text{-}HPTB)(Y)(OH)_2]^{2+}$mit Wasserstoffperoxid unter Bildung des *cis*-1,2-peroxido-Komplexes $[Fe_2(HPTB)(\eta\text{-}1,2\text{-}O_2)(OH)_2]^{2+}$. Y steht für einen benzoato- oder nitrato-Liganden in verbrückender Position.

Die Aktivierung von molekularem Sauerstoff durch zweikernige Eisenkomplexe in wässriger Lösung ist bisher kaum untersucht worden. Das liegt unter anderem am unpolaren/organischen Charakter der Modellkomplexe, aber auch an der bereits erwähnten kurzen Stabilität der Sauerstoff-Intermediate in protischen Lösungsmitteln, da darin eine Protonierung zu Hydroperoxido-Komplexen stattfinden kann und diese rasch zerfallen.[134-136] Im Gegensatz zu den am häufigsten verwendeten Modifikationen der HPTB-Liganden erhöhte die Einführung von Propansulfonat-Gruppen am Benzimidazolgerüst die Wasserlöslichkeit drastisch. Dies ermöglichte den Nachweis von peroxido-Komplexen in wässriger Lösung mittels zeitaufgelöster UV-Vis-Spektroskopie.[126] Zudem konnte erfolgreich eine katalytische Oxygenierung von Cyclohexan in wässrigem Medium realisiert werden. Für einen potentiellen Einsatz dieser Verbindungen in der Industrie in Form einer homogenen Oxidationskatalyse unter Verwendung von Luft als Oxidationsmittel ist es wünschenswert, diese Systeme in wässrige Lösungen (oder zumindest Lösungsmittel mit verringertem Gefahrenpotential) zu überführen. Diese Ergebnisse sprechen für eine mögliche zukünftige Anwendung in einem reaktiven Blasenstromsystem.[125]

2013 beschrieben Avenier und Mitarbeiter eine Photoreduktion des Komplexes $[Fe_2(N\text{-}EtHPTB)(H_2O)_2(MeOH)(OMe)](ClO_4)_4$ durch ein externes Reduktionsmittel in Acetonitril, wodurch eine Reversibilität realisiert werden konnte.[140] In ihrer Arbeit wurde eine Mischung aus dem Eisen(III)-Komplex und dem photoaktiven $[Ru(bipy)_3](PF_6)_2$-Komplex mit Licht einer Wellenlänge von 460 nm bestrahlt. Als Opfersubstanz verwendeten sie Et_3N, somit waren die Autoren in der Lage, in drei Belichtungszyklen Triphenylphosphin mit einer Ausbeute von bis zu 80 % zu oxidieren. Der Reaktionszyklus ist in Abb. 14 dargestellt.

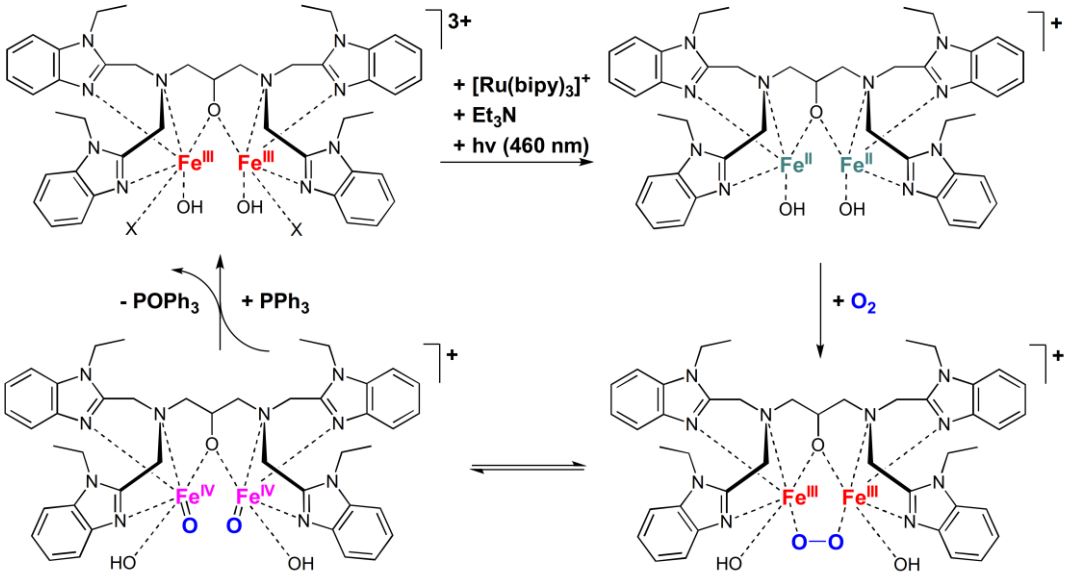

Abb. 14. Vorgeschlagener Reaktionszyklus für die photoinduzierte Sauerstoffaktivierung an dem zweikernigen Eisen(III)-Komplex des Liganden Et-HPTB und des anschließenden Oxidation von von Triphenylphosphin.[140]

Die cyanobakterielle Aldehyd-deformylierende Oxygenase (cADO) katalysiert die Umwandlung von Fettaldehyden zu Alkanen und Formiat.[141] 2019 beschrieben Kaizer und Mitarbeiter den dinuklearen Eisen(III)-μ-1,2-peroxido-Komplex $[Fe_2(\mu\text{-}O_2)(MeBzim\text{-}Py)_4(MeCN)_2]^{4+}$ als Modellkomplex für dieses Enzym. Dabei konnte der nukleophile Charakter der Deformylierung in Bezug auf verschiedene Aldehyde nachgewiesen und plausible Reaktionsmechanismen vorgestellt werden.[142] Als Ligand wurde hierbei die zweizähnige Verbindung 2-(2'-Pyridyl)-*N*-methylbenzimidazol (MeBzim-Py) verwendet. Dieser Komplex bildet sich aus der Reaktion des mononuklearen Eisen(II)-Komplexes $[Fe(MeBzim\text{-}Py)_4(MeCN)_2]^{4+}$ mit molekularem Sauerstoff (siehe Abb. 15). Obwohl die Reaktivität von diversen Eisen(IV)oxido-Intermediaten in verschiedenen elektrophilen Reaktionen detailliert untersucht wurde, konnte keine dieser Dieisen(III)-peroxido-Zwischenstufen eine direkte elektrophile oder nukleophile Reaktion durchführen. Spektroskopische Untersuchungen zu diesem zweikernigen μ-1,2-Peroxo-Eisen(III)-Komplex zeigen eine intensiv breite Absorptionsbande bei 700 nm an, welche einem Peroxido-zu-Eisen *charge-transfer* (LMCT-Bande) zuzuordnen ist.[102,103]

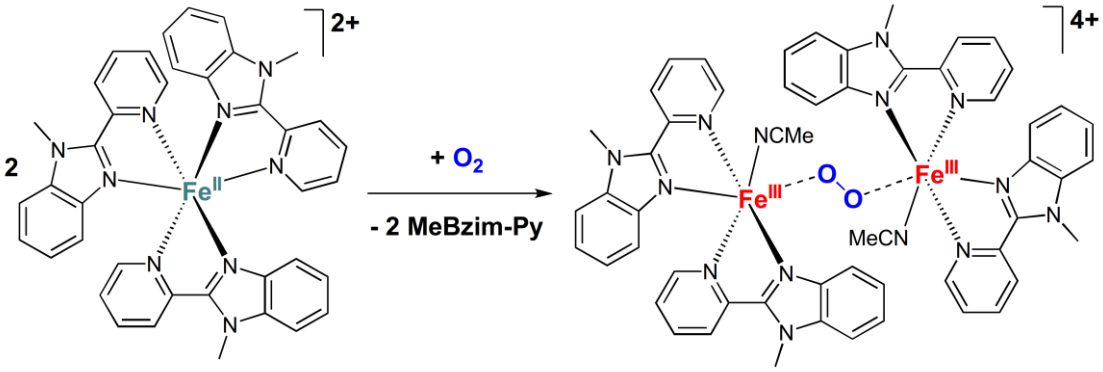

Abb. 15. Schematische Darstellung der Reaktion des Eisen(II)-Komplexes $[Fe(MeBzim\text{-}Py)_3]^{2+}$ mit Sauerstoff unter Bildung des 1,2-peroxido-Komplexes $[Fe_2(MeBzim\text{-}Py)_4(MeCN)_2]^{2+}$.

Dieser peroxido-Komplex weist, ähnlich wie der peroxido-Komplex des Liganden Et-HPTB, eine außerordentliche Stabilität bei Raumtemperatur auf. In diesem Zusammenhang wiesen die Autoren außerdem auf die mechanistische Vielseitigkeit und den ambiphilen Reaktionscharakter der dinuklearen Eisen(III)-peroxido-Intermediate hin.

3.2 | Forschungsziele

In der Einleitung dieser Arbeit wurde auf die Bedeutung der Sauerstoff-Komplexe und insbesondere der Kupfer(II)- und Eisen(III)-peroxido-Komplexe in der homogenen Oxidationskatalyse hingewiesen. Für die Etablierung neuer Katalysesysteme in Labor und Industrie ist es notwendig, den Reaktionsmechanismus der Umsetzung von Sauerstoff oder Wasserstoffperoxid mit den entsprechenden Ausgangskomplexen zu untersuchen. Daher liegt der Fokus der vorliegenden Arbeit auf der kinetischen Untersuchung der Bildung von Kupfer(II)- und Eisen(III)-peroxido-Komplexen und der weiterführenden Reaktionen dieser. Als Analysemethode wurde hierbei eine Tieftemperatur-*stopped-flow*-Apparatur verwendet, welche es ermöglicht, Reaktionen im Millisekundenbereich zu verfolgen (zeitaufgelöste UV-Vis-Spektroskopie).

3.2.1 | Kupfer(II)-peroxido-Komplexe

1995 gelang es Thomas N. Sorrell und Mitarbeitern, die reversiblen Reaktionen des Hämocyanin-Modellkomplexes $[Cu(Pim^{iPr2})(MeCN)]^+$ mit Sauerstoff zu untersuchen, und dies sogar in dem protischen Lösungsmittel Methanol (siehe Abb. 16).[49] Diese herausragende Reaktion wurde ausführlich beschrieben und charakterisiert, jedoch folgten darauf keine kinetischen und mechanistischen Untersuchungen. Daher wurden ausgiebige kinetische Untersuchungen dieser Reaktion durchgeführt, welche einen Teil der vorliegenden Arbeit ausmachen. Diese neuen wissenschaftlichen Erkenntnisse wurden 2020 in der Zeitschrift *European Journal of Inorganic Chemistry* veröffentlicht (siehe Kapitel 4).

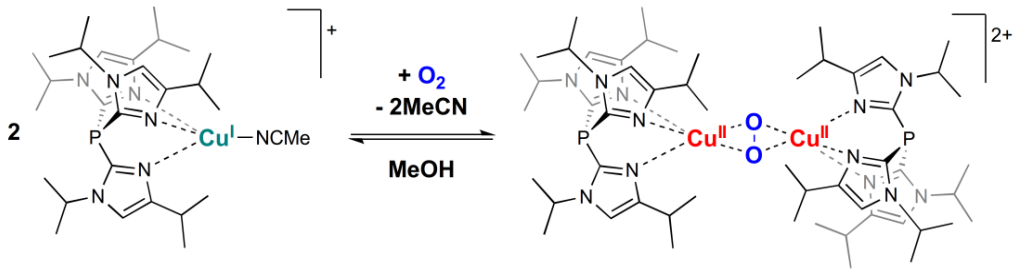

Abb. 16. Schematische Darstellung der reversiblen Reaktion des Kupfer(I)-Komplexes $[Cu(Pim^{iPr2})(MeCN)]^+$ mit molekularem Sauerstoff in Methanol.

3.2.2 | Eisen(III)-peroxido-Komplexe

Der Ligand Et-HPTB wurde bereits 1984 entwickelt[143] und 1996 konnte von Lawrence Que und Mitarbeitern die erste Kristallstruktur des Eisen(III)-*cis*-1,2-peroxido-Komplexes erhalten werden.[144] Der Fokus dieser Forschung lag dabei hauptsächlich auf der Reaktion der Eisen(II)-Komplexe des Liganden Et-HPTB mit molekularem Sauerstoff. Jedoch ist die Bildung des *cis*-peroxido-Komplexes auch ausgehend von dem entsprechenden Eisen(III)-Komplex in einer Reaktion mit Wasserstoffperoxid generierbar (siehe Abb. 17). Dies zeigten Kida und Mitarbeiter bereits 1984 mit dem Liganden HPTB, jedoch wurden keine weiteren kinetischen und mechanistischen Untersuchungen dieser Reaktion mit dem Liganden Et-HPTB durchgeführt. Dies war ausschlaggebend für die detaillierte kinetische Untersuchung der Reaktion des Eisen(III)-Komplexes $[Fe_2(Et\text{-}HPTB)(OH)_2(MeOH)_2]^{3+}$ mit Wasserstoffperoxid in Methanol

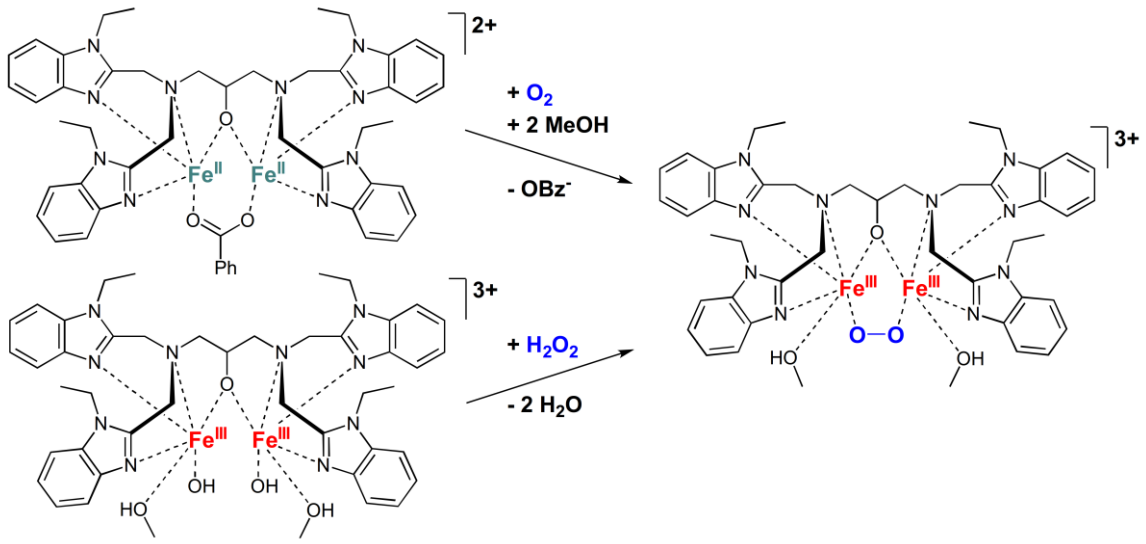

Abb. 17. Schematische Darstellung der Bildung des peroxido-Komplexes $[Fe_2(Et\text{-}HPTB)(\eta\text{-}1,2\text{-}O_2)(MeOH)_2]^{3+}$ ausgehend von der Reaktion des Eisen(II)-Komplexes mit molekularem Sauerstoff (oben) und der Reaktion des Eisen(III)-Komplexes mit Wasserstoffperoxid (unten).

Diese Daten sollten als Grundlage für die Erforschung der Reaktion des gebildeten peroxido-Komplexes $[Fe_2(Et\text{-}HPTB)(\eta\text{-}1,2\text{-}O_2)(MeOH)_2]^{3+}$ mit Benzoylchlorid dienen. Motivation der Untersuchung dieser Reaktion war die mögliche Nutzung der gebildeten Intermediate für stöchiometrische oder katalytische Oxidationsreaktionen im Labormaßstab. Diese wurden ebenfalls kinetisch untersucht und mögliche Reaktionsmechanismen vorgeschlagen und diskutiert. Diese Forschungsergebnisse wurden 2021 in der Zeitschrift *European Journal of Inorganic Chemistry* veröffentlicht und sind in Kapitel 5 detaillierter beschrieben.

4 | Veröffentlichte wissenschaftliche Artikel

4.1 | Kinetische Studie zur Bildung von Kupfer(II)-peroxido-Komplexen

Diese Arbeit wurde in der Fachzeitschrift *European Journal of Inorganic Chemistry* veröffentlicht.

Kinetic Investigation of the Reaction of Dioxygen with the Copper(I) Complex $[Cu(Pim^{iPr2})(CH_3CN)]CF_3SO_3$ {Pim^{iPr2} = Tris[2-(1,4-diisopropylimidazolyl)]phosphine}

Markus Lerch, Markus Weitzer, Tim-Daniel J. Stumpf, Larissa Laurini, Alexander Hoffmann, Jonathan Becker, Andreas Miska, Richard Göttlich, Sonja Herres-Pawlis, Siegfried Schindler, *Eur. J. Inorg. Chem.*, **2020**, 3143-3150.

doi.org/10.1002/ejic.202000462

Zudem durfte das Deckblatt der Ausgabe 33/2020 gestaltet werden.
(doi.org/10.1002/ejic.202000760)

EurJIC
European Journal of Inorganic Chemistry

Chemistry Europe
European Chemical Societies Publishing

Cover Feature:
Siegfried Schindler et al.
Kinetic Investigation of the Reaction of Dioxygen with the Copper(I) Complex $[Cu(Pim^{iPr2})(CH_3CN)]CF_3SO_3$ {Pim^{iPr2} = Tris[2-(1,4-diisopropylimidazolyl)]phosphine}

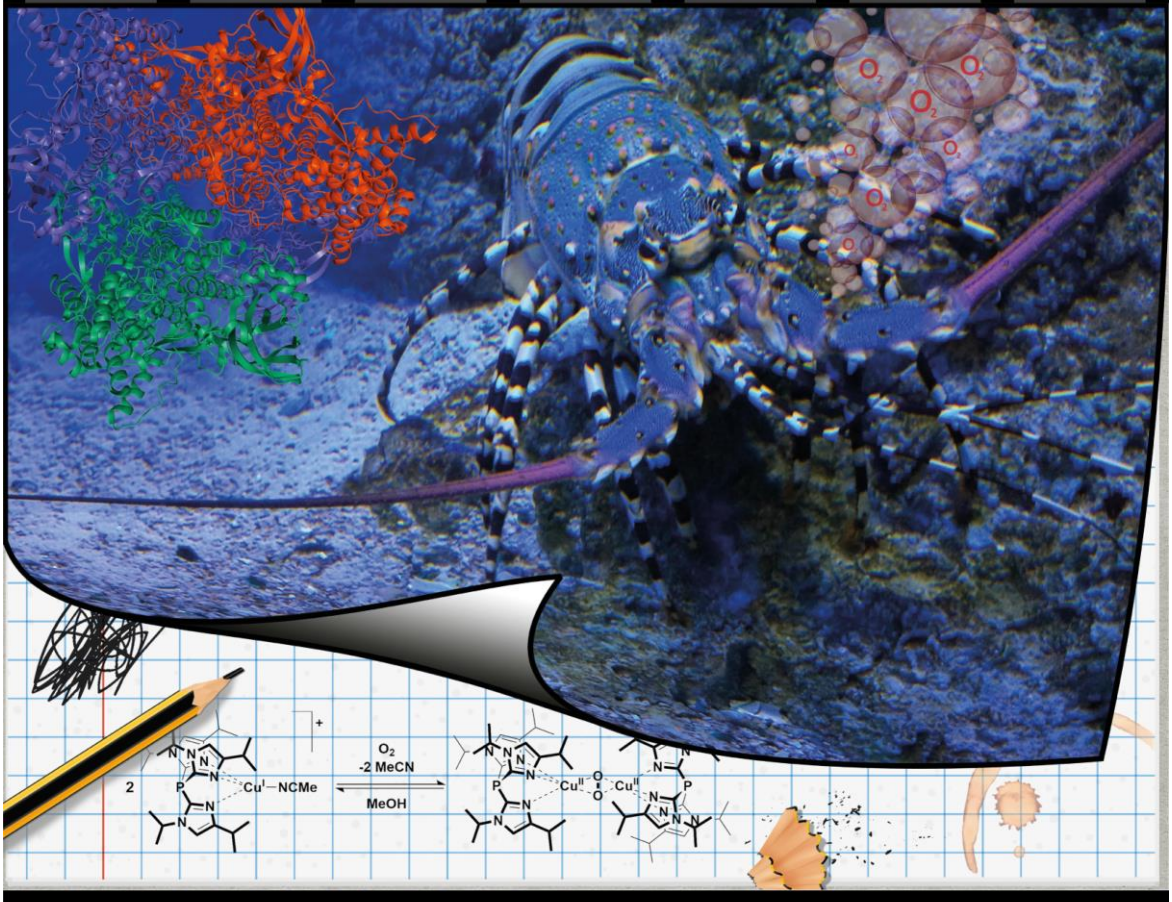

33/2020
WILEY-VCH

EurJIC
European Journal of Inorganic Chemistry

Full Paper
doi.org/10.1002/ejic.202000462

Chemistry Europe
European Chemical Societies Publishing

Dioxygen Activation

Kinetic Investigation of the Reaction of Dioxygen with the Copper(I) Complex $[Cu(Pim^{iPr2})(CH_3CN)]CF_3SO_3$ {Pim^{iPr2} = Tris[2-(1,4-diisopropylimidazolyl)]phosphine}

Markus Lerch,[a] Markus Weitzer,[a] Tim-Daniel J. Stumpf,[a,b] Larissa Laurini,[c] Alexander Hoffmann,[c] Jonathan Becker,[a] Andreas Miska,[a] Richard Göttlich,[b] Sonja Herres-Pawlis,[c] and Siegfried Schindler*[a]

Abstract: Model complexes for copper proteins such as hemocyanin or tyrosinase have been investigated in detail during the last four decades due to their potential to become valuable catalysts for selective oxidations of organic substrates. However, so far most of these compounds can only be investigated in aprotic solvents at lower temperatures. Therefore, industrial applications on a larger scale are still missing. In contrast the copper(I) complex with the ligand tris[2-(1,4-diisopropylimidazolyl)]phosphine can form a quite stable dinuclear copper peroxido complex in the protic solvent methanol at room temperature. The kinetic analysis of the reaction of $[Cu(Pim^{iPr2})(CH_3CN)]CF_3SO_3$ with dioxygen in methanol is reported. The results allowed to obtain rate constants and activation parameters ($\Delta H^{\#}$ = 25 ± 2 kJ mol^{-1} and $\Delta S^{\#}$ = −121 ± 8 J mol^{-1} K^{-1}) for the formation of the reactive intermediate, a mononuclear copper superoxido complex, prior to the consecutive reaction to a dinuclear peroxido complex.

Introduction

The interaction of dioxygen with copper(I) complexes has been studied in the past for a better understanding of the reactivity of redox active copper enzymes as well as for oxidation reactions in the lab and industry.[1] Catalytic oxidation reactions are very important, however, this is difficult to accomplish with dioxygen/air as the sole oxidant. Despite recent excellent achievements, selectivity limits still play a crucial role in aerobic oxidations of C–H bonds in more complex molecules.[2] This is in contrast to nature where enzymes such as methane monooxygenase (MMO) are capable to even oxidize unreactive substrates such as methane under ambient conditions.[3] However, during the last four decades it was possible to fully characterize a large number of intermediates of such oxidations, reactive copper "dioxygen adduct" complexes, that are responsible for the oxygen transfer.[1a,1c,4] These intermediates are usually analyzed in aprotic solvents at low temperatures (as low as −140 °C) due to the fact that most of the copper "dioxygen adduct" complexes investigated so far are not very stable, especially in the presence of protons.[1f,1h,5a–5f] Protons can lead to the formation of hydrogen peroxide and finally to the corresponding copper(II) complex and water. Usually reactions in protic solvents do not allow observation of any transient intermediate complex and suppress the potential of these complexes for oxidation reactions of organic substrates.[6]

Up to now we are only aware of two early examples (reported in 1994 and 1997) where reactions of this type were investigated in the protic solvent methanol: While Bol et al. used a macrocyclic ligand to stabilize a (most likely) dinuclear *end-on* peroxido complex,[7] Lynch et al. had based their complex on a trisimidazolate ligand system to obtain a dinuclear *side-on* peroxido unit.[8] Further studies using this ligand system have been performed by Sorrell and co-workers.[9] No crystal structures for the obtained "dioxygen adduct" complexes were reported for either system. Furthermore, quite stable dinuclear copper peroxido complexes were reported by Comba and coworkers as well as by Kodera and co-workers.[10] However, no studies in protic solvents were performed with these complexes. Most recently a *side-on* peroxido complex with a derivative of triazacyclononane (TACN) as a ligand was reported (us-

[a] M. Lerch, Dr. M. Weitzer, Dr. T.-D. J. Stumpf, Dr. J. Becker, Dr. A. Miska, Prof. Dr. S. Schindler
Institut für Anorganische und Analytische Chemie, Justus-Liebig-Universität Gießen,
Heinrich-Buff-Ring 17, 35392 Gießen, Germany
E-mail: Siegfried.Schindler@anorg.chemie.uni-giessen.de
https://www.uni-giessen.de/fbz/fb08/Inst/iaac/schindler
[b] Dr. T.-D. J. Stumpf, Prof. Dr. R. Göttlich
Institut für Organische Chemie, Justus-Liebig-Universität Gießen,
Heinrich-Buff-Ring 17, 35392 Gießen, Germany
[c] L. Laurini, Dr. A. Hoffmann, Prof. Dr. S. Herres-Pawlis
Institut für Anorganische Chemie, RWTH Aachen University,
Landoltweg 1A, 52074 Aachen, Germany
Supporting information and ORCID(s) from the author(s) for this article are available on the WWW under https://doi.org/10.1002/ejic.202000462.

EurJIC
European Journal of Inorganic Chemistry

Full Paper
doi.org/10.1002/ejic.202000462

Chemistry Europe
European Chemical Societies Publishing

ing sterically demanding *tert*-butyl groups) which turned out to be quite stable in aqueous solutions.[11] Still it was not possible to investigate its formation in protic solvents.

In industrial applications for catalytic oxidations with dioxygen it is necessary to understand the formation of the "dioxygen adduct" complexes within large bubble columns.[12] Kinetic data are necessary for the determination of the hydrodynamics and mass transport mechanisms to allow the calculation/optimization of the overall bubbly flow processes. Most organic solvents present an elevated risk under industrial conditions due to the danger of creating explosive gas mixtures. It is still a challenging task to find metal complexes that can be used as oxidation catalysts in aqueous solutions under ambient conditions.

In this context tris(imidazolyl)phosphine and its derivatives are quite interesting ligands because as discussed above they can support formation of copper peroxido complexes in the protic solvent methanol. The copper(I) complex $[Cu(Pim^{iPr2})CH_3CN]^+$ {**1**, Pim = tris[2-(1,4-diisopropylimidazolyl)]-phosphine with $R^1 = R^2 = i$Pr} reacts reversibly with dioxygen to the dinuclear *side-on* peroxido complex $[\{Cu(Pim^{iPr2})\}_2O_2]^{2+}$ (**2**) according to Scheme 1.[9]

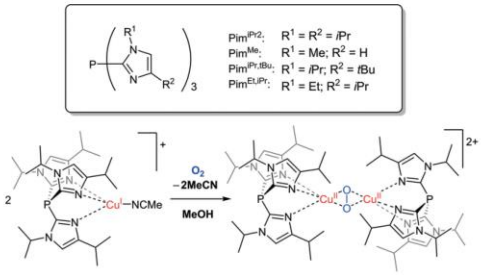

Scheme 1. Overview of the tris-(imidazolyl)phosphine ligands (top). Reaction of **1** with O_2 to form the copper peroxido complex **2** (with $R^1 = R^2 = i$Pr).

During these studies the large influence of the R^1/R^2 groups was observed e.g. the copper(I) complex $[Cu(Pim^{iPr,tBu})(CH_3CN)]BF_4$ was unreactive towards dioxygen.[8,9] Furthermore, intramolecular ligand hydroxylation occurred in good yields (35–45 %; 50 % would be quantitative for this reaction) when $[Cu(Pim^{iPr2})CH_3CN]^+$ was treated with dioxygen.[13] The oxidation of a colorless solution of **1** at low temperatures led to the intensively purple colored peroxido complex **2** easily observed in a benchtop experiment with **1** CF_3SO_3 (Figure S1, Supporting Information). Warming the solution to room temperature caused a color change to green and it was found that an oxygen atom had been inserted into the tertiary C–H bond of one of the isopropyl groups of the ligand.

Due to the fact that **1** allowed formation of a quite stable copper peroxido complex in a protic solvent it seemed worthwhile to investigate the kinetics of this reaction in more detail and to test it for its possible application in bubble columns.

Results and Discussion

Syntheses and Characterization

The ligand Pim^{iPr2} was prepared and characterized as described previously (NMR and MS data are reported in the Experimental Section and Supporting Information, Figure S2.1 and Figure S2.2).[9,13] The aqueous work-up of the reaction mixture had to be performed under inert conditions to avoid formation of a sticky solid (caused by oxidation) that makes the isolation of the ligand rather difficult. However, under inert conditions pure product could be obtained and crystals were obtained by recrystallization from methanol that could be structurally characterized (the molecular structure, Figure S2.3, and crystallographic data of Pim^{iPr2} are reported in the Supporting Information).

Furthermore, temperature control of the reaction is important due to the possible formation of an isomer of the ligand. The reason for this is the deprotonation/lithiation of the "wrong" methine-position on 1,4-diisopropylimidazole followed by further reaction with PCl_3. The poor solubility of Iso-Pim^{iPr2} (Pim^{iPr2} where one "imidazole-arm" is flipped) allowed to crystallize it (NMR data are reported in the Experimental Section and furthermore, together with crystallographic data in the Supporting Information). The corresponding copper(I) complex with Iso-Pim^{iPr2} did not form a "dioxygen" adduct complex when reacted with dioxygen and therefore was not investigated further.

Additionally we prepared the sterically less demanding known ligand tris(1-methylimidazol-2-yl)phosphane (Pim^{Me}; R^1 = Me and R^2 = H) according to the literature.[14] Efforts to obtain crystals of a copper(I) complex with Pim^{Me} as a ligand were not successful. A solution of a 1:1 mixture of $[Cu(CH_3CN)_4]CF_3SO_3$ and Pim^{Me} did not react with dioxygen under all conditions applied. We believe that here the complex $[Cu(Pim^{Me})_2]^+$ formed which is quite stable towards oxidation. This is a typical finding for copper(I) complexes that react in a ratio of 2:1 (ligand to copper ratio) and has been already discussed in the past.[9] Most of the time this can lead to a dramatic stabilization of copper(I) complexes towards dioxygen and has been observed by some of us previously when using bidentate ligands.[15] Efforts to observe/obtain a peroxido complex with this ligand by treating a solution of the copper(I) complex with hydrogen peroxide at ambient conditions were not successful either. Only the corresponding copper(II) complex, $[Cu(Pim^{Me})_2](CF_3SO_3)_2$, with a ligand to copper ratio of 2:1 was formed [supporting the proposed same stoichiometry for the corresponding copper(I) complex]. The molecular structure of $[Cu(Pim^{Me})_2](CF_3SO_3)_2$ (see Supporting Information, Figure S4) is in accordance with crystallographic data reported previously for the perchlorate analogue.[14]

In contrast the copper(I) complex $[Cu(Pim^{iPr2})CH_3CN]CF_3SO_3$ (**1** CF_3SO_3) was synthesized in good yields and characterized according to the literature.[9,13] Furthermore, it was possible to obtain crystals of **1** CF_3SO_3 and its molecular structure is presented in Figure 1 (crystallographic as well as NMR and MS data are reported in the Supporting Information). The molecular structure of this complex is quite similar to the related complex

EurJIC
European Journal of Inorganic Chemistry

Full Paper
doi.org/10.1002/ejic.202000462

Chemistry Europe
European Chemical Societies Publishing

[Cu(T1Et$_4$*i*PrIP)CH$_3$CN]PF$_6$ (T1Et$_4$*i*PrIP = Pim^{Et,iPr}) described by Kurtz and co-workers.[8] Both structures demonstrate that due to sterically demanding R groups the formation of complexes with a ligand to copper ratio of 2:1 is suppressed. Copper(II) complexes with Pim^{iPr2} have been reported previously by Sorrell et al.[9]

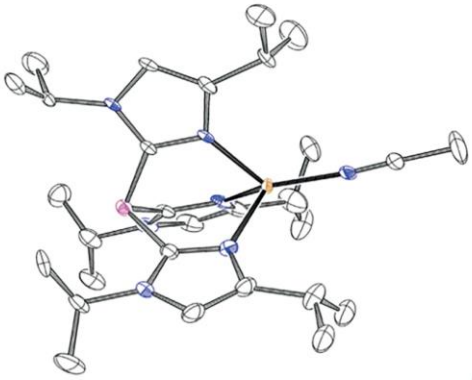

Figure 1. ORTEP plot of **1**. Hydrogen atoms are omitted for clarity, thermal ellipsoids were set to 50 % probability.

As described above copper(I) salts with the ligand Pim^{iPr2} react with dioxygen (in CH_3OH or CH_2Cl_2 as solvents) to form the corresponding dinuclear *side-on* peroxido copper complexes (Scheme 1). However, despite the fact that **2** has been thoroughly characterized by spectroscopy[9] it has not been possible so far to structurally characterize it or its derivatives.[8] All our efforts failed as well, most likely a consequence of the equilibrium between the starting material **1** and the product **2**.[9]

DFT Calculations

To further confirm the molecular structure of **2**, DFT calculations were performed. They reveal that the peroxide species is energetically stabilized against the *bis(μ-oxido)* species by 12 kcal/mol (broken-symmetry approach for peroxide species). Figure 2 depicts the optimized structure of **2**. The Cu–N(eq) bond lengths are in the range of 1.987 Å to 2.074 Å and the Cu–N(ax) bond lengths are 2.172 Å or 2.300 Å whereas the Cu···Cu distance is predicted to 3.394 Å and the O–O distance to 1.440 Å (see Supporting Information Table S22).

Stopped-Flow Measurements

To gain better understanding of the reaction of **1** CF_3SO_3 with dioxygen (Scheme 1) a low temperature stopped-flow investigation was performed. The oxidation of **1** CF_3SO_3 in methanol can be observed spectrophotometrically, and a representative plot of time-resolved UV/Vis spectra for the formation of **2** $(CF_3SO_3)_2$ at 0.0 °C is shown in Figure 3.

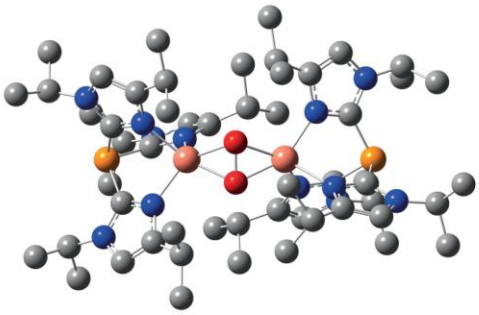

Figure 2. Optimized geometry of **2** (TPSSh/def2-TZVP, MeOH, GD3BJ, broken-symmetry; hydrogen atoms are omitted for clarity).

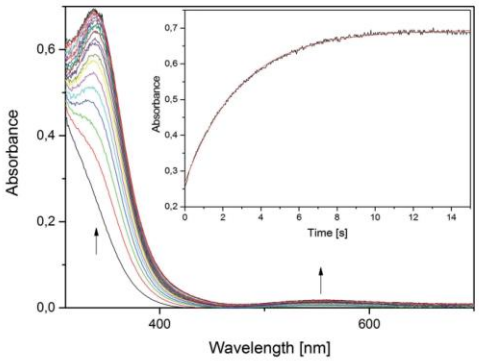

Figure 3. Time-resolved UV/Vis spectra of the reaction of **1**CF_3SO_3 with dioxygen in methanol (T = 0.0 °C, [**1**CF_3SO_3] = 0.4 mmol/L, [O_2] = 5.2 mmol/L). Inset: absorbance vs. time trace at 370 nm together with one exponential fit.

The obtained UV/Vis spectra show maxima at 343 nm and 549 nm typical for a *side-on* peroxido copper complex. Again TD-DFT calculations reproduced the measured UV/Vis spectra very well with 360 nm for the in-plane feature and 493 nm for the out-of-plane peroxide feature (Supporting Information, Figure S6).

The reaction was carried out under pseudo first order conditions ([O_2] > [**1** CF_3SO_3]). Absorbance vs. time data in the wavelength range between 340 nm and 700 nm could be fitted perfectly well to a single exponential function leading to a first order dependence of [**1**] in the rate law. At longer time scales or higher temperatures, the decomposition of the peroxido complex is detectable (Supporting Information Figure S7).

The variation of [O_2] from 0.65 to 5.2 mmol/L at different temperatures (–25.0 to +20.0 °C) leads to straight lines with an intercept in a plot of the observed rate constants k_{obs} vs. [O_2] (Figure 4). Therefore, [O_2] also will be first order in the rate law. The intercept is a consequence of the reversibility of the reaction. Turning around the pseudo first order conditions

EurJIC
European Journal of Inorganic Chemistry

Full Paper
doi.org/10.1002/ejic.202000462

Chemistry Europe
European Chemical Societies Publishing

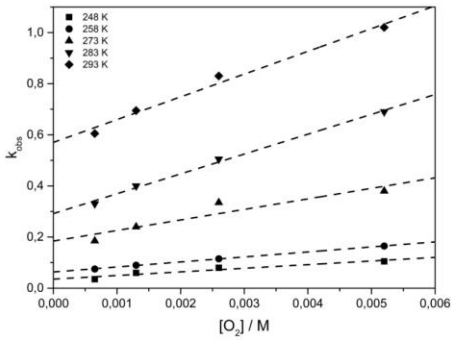

Figure 4. Plot of k_{obs} vs. $[O_2]$.

([**1** CF_3SO_3] > $[O_2]$]) did lead to the same results (Supporting Information, Figure S 8).

Regarding the mechanism of this reaction it should proceed at least in two steps. In the first step a superoxido complex must form according to Equation 1. In a consecutive reaction with a second copper(I) complex (Equation 2) the dinuclear *side-on* peroxido complex is formed.

$$\mathbf{1}^+ + O_2 \underset{k_{-1}}{\overset{k_1}{\rightleftharpoons}} [Cu(Pim^{iPr2})(O_2)]^+ + CH_3CN \qquad (1)$$

$$[Cu(Pim^{iPr2})(O_2)]^+ + \mathbf{1}^+ \underset{k_{-2}}{\overset{k_2}{\rightleftharpoons}} \mathbf{2}^{2+} + CH_3CN \qquad (2)$$

Such a reaction sequence has been observed and kinetically analyzed in detail previously for the formation of dinuclear copper *end-on* peroxido complexes.[5b,5c,5d,16] In contrast to these studies the formation of a copper superoxido complex according to Equation 1 when reacting **1** with dioxygen was not observed (even when the temperature was lowered to –90.0 °C). This is not unusual and similar findings were reported for the formation of analogous dinuclear *side-on* peroxido as well as *bis(μ-oxido)* copper complexes.[15a,15c,17] For the irreversible formation of a related *bis(μ-oxido)* copper complex it could be shown by DFT calculations that it would not be possible to observe this intermediate spectrocscopically.[15b] Here the formation of the mononuclear superoxido complex is rate-determining and the following steps are "extremely downhill without any larger transition states confirming experimental results".[15b]

This holds true for our studies as well: the reversible reaction to form the mononuclear superoxido complex is rate-determining while the formation of the dinuclear peroxido complex is much faster thus leading to a treatment of the superoxido complex as a steady state species. A detailed description of this approach has been reported in the literature for the irreversible reaction of dioxygen with the complex $[Cu(iPr_3TACN)(CH_3CN)]^+$.[4h,4k,17b]

However, in contrast to this system formation of **2** is not complete and the reversibility (Equation 1 and 2) has to be included. Applying the steady state approach, we obtained (see Supporting Information for the derivation) the following equation for k_{obs}:

$$k_{obs} = k_1 [O_2] + \frac{k_{-1} k_{-2}}{k_2 [\mathbf{1}]} \qquad (3)$$

Thus, it is possible from the slopes of the plot of k_{obs} vs. $[O_2]$ (Figure 3, $k_{obs} = k_1[O_2]$) to determine the second order rate constants for the forward reaction at different temperatures (Table 1) while the intercept is caused by the reversibility of the reaction. With an Eyring plot for k_1 (Supporting Information, Figure S9) activation parameters were calculated to $\Delta H^{\#}$ = 25 ± 2 kJ mol^{-1} and $\Delta S^{\#}$ = –121 ± 8 J mol^{-1} K^{-1}.

Table 1. Kinetic and thermodynamic parameter for the O_2-interaction with $[Cu(P(Im^{iPr2})_3)(CH_3CN)]^+$ (**1**) and $[Cu(iPr_3TACN)(CH_3CN)]^+$.

Parameter	Temperature	**1**	$[Cu(iPr_3TACN)(CH_3CN)]^+$
k_1	248 K	13.0	–
(mol^{-1} Ls^{-1})	258 K	19.5	
	273 K	41.1	243.2
	283 K	78.1	–
	293 K	87.8	–
$\Delta H^{\#}$		25 ± 2	37.2 ± 0.5
(kJ mol^{-1})			
$\Delta S^{\#}$		–121 ± 8	–62 ± 2
(J K^{-1} mol^{-1})			

While the reaction of **1** with dioxygen (similar to the reaction of $\{[Cu(HB(3,5\text{-}^{iPr2}pz)_3)]_2(O_2)\}$, Scheme 1) described previously[4f] quite nicely models the chemical reaction of the oxygen carrier protein hemocyanin there are still – as expected – huge differences in their reactivity. The preorganized active site in hemocyanin reacts much faster with dioxygen than the model compound and its oxygen uptake had to be measured using temperature jump methods.[18] Furthermore, an activation volume of close to zero had been obtained for hemocyanin (therefore indicating an activation entropy of close to zero as well) leading to an interchange mechanism (facile substitution of a water molecule by dioxygen in contrast to replacing strongly coordinated acetonitrile in the model complex).[18] While activation entropies in principle cannot be obtained with high accuracy (due to its calculation from the intercept in the Eyring plot at $T = \infty$) a quite large negative activation entropy for the reaction of **1** with dioxygen accounts for an associative mechanism.[16,19] Together with the relatively small activation enthalpy this is quite typical for the formation of a dinuclear copper peroxido complex.[4h,16–17,20] The "O_2 adduct" formation leads to a tighter metal-dioxygen bond and a species with fewer degrees of freedom.

Kinetic data compare quite well for the analogous irreversible reaction of dioxygen with the complex $[Cu(iPr_3TACN)(CH_3CN)]^+$ (Table 1)[4h,4k] and furthermore with observed copper superoxido complex formation with tripodal ligands.[5c,16,21] In contrast kinetic data for the formation of some other copper peroxido complexes are different.[17a,17c,20,22]

However, these findings should not be overinterpreted due to the fact that these reactions are extremely sensitive towards ligand modification and/or solvent. Thus the complex $[Cu(Pim^{iPr,tBu})(CH_3CN)]PF_6$ (Scheme 1: R^1 = *i*Pr, R^2 = *t*Bu) showed no reactivity towards dioxygen, obviously due to the increase of the steric hindrance in this system.[9] Furthermore, when the reaction of dioxygen with $[Cu(Pim^{iPr2})(CH_3CN)]PF_6$ was per-

EurJIC
European Journal of Inorganic Chemistry

Full Paper
doi.org/10.1002/ejic.202000462

Chemistry Europe
European Chemical Societies Publishing

formed in dichloromethane a relatively stable copper peroxido complex was observed at low temperatures as well. However, the reaction became so slow that subsequent decay started to play an important role and affected the formation of the peroxido complex. The rate-determining step in the formation of the copper superoxido complex is the breaking of the copper–nitrile bond and the consecutive reaction with dioxygen. In this case the acetonitrile molecule has a strong coordination tendency to copper(I) ions and slows down the reaction with dioxygen and acts as a competitive ligand. This effect is more recognizable when the reaction is carried out in nitrile solvents. Under these conditions no reaction of **1** with dioxygen was observed. Therefore, no kinetic analysis was carried out in dichloromethane or nitrile solvents.

To avoid the presence of acetonitrile and thus pushing the equilibrium further to the formation of **2**, Pim^{iPr2} was treated with the copper(I) triflate toluene complex in methanol. Under these conditions a dinuclear complex, $[Cu_2(Pim^{iPr2})_2](CF_3SO_3)_2$, was formed that could be structurally characterized (crystallographic data are reported in the Supporting Information). A solution of this compound in either methanol or acetone still reacted with dioxygen to form the deep purple colored complex **2**. However, without the stabilization of acetonitrile disproportionation was also observed and therefore no further experiments with this compound were performed.

Reactions in Water

Unfortunately, efforts to analyze the reaction of **1** with dioxygen in water were unsuccessful. Only oxidation to copper(II) compounds with some foam formation was observed (caused by shaking of the suspension of the complex), without any indication of the occurrence of an intermediate. However, adding an excess of a H_2O_2/Et_3N solution (1:2 in methanol) to a $Pim^{iPr2}/[Cu(H_2O)_6](ClO_4)_2$ solution (1:1 in methanol) allowed to observe the brief formation (less than one second) of **2** (deep purple solution) at room temperature. At –80 °C the purple color is persistent for a few seconds.

Continuous Flow Measurements

Previously we used a SuperFocus mixer to investigate the kinetics of fast reactions by continuous flow.[12c,23] Due to the short mixing time of this setup it was possible to analyze the formation of $[Cu_2O_2(btmgp)_2]I_2$, a temperature sensitive guanidine-stabilized *bis(μ-oxido)* species at room temperature.[23] In contrast, the reaction of **1** with O_2 at room temperature is slower with a faster decay (for decay k_{obs} = 0.06 s^{-1} at 25 °C, see below). Hence, the detection of **2** with the SuperFocus mixer was difficult. Variation of complex concentration and flow rates revealed that formation and decay of **2** already occur during mixing and thus prevent kinetic data collection (Supporting Information, Figure S10). This is supported by stopped-flow measurements under the same conditions (Supporting Information, Figure S7) indicating that reliable kinetic data for the formation of **2** only can be obtained using this instrumentation.

To gain more information on the decay of **2** it was kinetically analyzed. Decomposition of **2** (decay of the peroxido UV/Vis band at 449 nm) is a first-order reaction and time resolved UV/Vis spectra are reported in the Supporting Information (Figure S11). The Eyring plot for this reaction (Supporting Information, Figure S12) allowed to calculate the activation parameters to $\Delta H^{\#} = 43 \pm 1$ kJ mol^{-1} and $\Delta S^{\#} = -124 \pm 2$ J mol^{-1} K^{-1}. These data compare well with previous reports.[17b] No H_2O_2 formation was observed during/after the decomposition of the peroxide complex.

Conclusions

The copper(I) complex **1** with the ligand Pim^{iPr2} (Scheme 1) reversibly forms a dinuclear μ-η^2:η^2-*side-on* peroxido complex thus modeling the reactivity of the oxygen carrier protein hemocyanin in some aspects (reversible reaction with dioxygen to form a dinuclear peroxide complex in a protic solvent). In contrast to previous kinetic studies on the reaction of copper(I) complexes with dioxygen we were able to investigate this reaction of **1** in detail in the protic solvent methanol. Mechanistic studies in protic solvents so far have not been very successful. E.g. in our own work we could not detect any intermediate complex during the oxidation of a copper(I) complex with the ligand *N*,*N*′-bis[2-(dimethylamino)ethyl]*N*,*N*-dimethylethane-1,2-diamine (Me_6trien) in water in contrast to the reaction of hemocyanin with dioxygen.[6,18] However, the results of our analysis of the reaction of **1** with dioxygen together with a recent report[11] on a quite stable copper peroxido complex in water are promising for finding a copper system that can be used in aqueous solutions for industrial applications of selective oxidations in the future. While it turned out that **1** is not suitable for the investigation of its reactivity with dioxygen in bubbly flows this is different for an iron peroxido complex reported by some of us previously.[12c,24] Besides the problems with protic solvents, rates for formation and decay of reactive intermediates need to be in a time window to allow their study in an industrial setup such as a bubble flow column.

It seems to be important to point out one more time how much reactions of copper(I) complexes with dioxygen are affected by ligand design and solvents (sometimes also anions can show an effect). Especially the formation of a copper(I) complex with a ligand to copper ion ratio of 2:1 is a serious problem that can completely suppress the reactivity of these complexes.[15] At the moment the question still remains what the requirements are to stabilize a "dioxygen adduct" copper complex in a protic solvent.

Experimental Section

All reagents and solvents were purchased from commercial sources. The solvents were purified by distillation and dried by standard procedures or used from the solvent purification system SPS-800 by MBraun (Garching, Germany). Preparations under anaerobic conditions were carried out in Schlenk tubes using dry nitrogen or in a glovebox by MBraun under an argon atmosphere. ^{1}H and ^{13}C NMR spectra were recorded on a Bruker Avance II 200 spectrometer

EurJIC
European Journal of Inorganic Chemistry

Full Paper
doi.org/10.1002/ejic.202000462

Chemistry Europe
European Chemical Societies Publishing

(^{1}H at 200 MHz; ^{13}C at 50 MHz), Bruker Avance II 400 spectrometer (^{1}H at 400 MHz; ^{13}C at 100 MHz) and Bruker Avance III HD 400 spectrometer (^{1}H at 400 MHz; ^{13}C at 100 MHz; ^{31}P at 162 MHz) in $CDCl_3$ using TMS as internal standard. The ^{31}P NMR spectra were referenced to external 85 % H_3PO_4, the ^{1}H and ^{13}C NMR spectra were calibrated against the proton and carbon signals of tetramethylsilane.

Stopped-Flow Measurements: Solutions of copper(I) complexes for stopped-flow measurements were prepared in glass syringes under argon in a glove box. Saturated solutions of dioxygen were prepared by bubbling dry dioxygen (grade 5.5, Messer Griesheim, Germany) through the solvent in a syringe for about 10 min. Dioxygen concentration in a saturated methanol solution has been reported to be 10.4×10^{-3} mol/L at 25 °C.[25] Different concentrations of dioxygen were obtained by mixing a dioxygen saturated solution with an argon saturated solution using two connected syringes (thus leading to a variation of dioxygen concentration of 0.65 to 5.20×10^{-3} mol/L in the measurements) Temperature dependent stopped-flow analysis was performed in a range from −25.0 °C to +25.0 °C. All measurements were repeated about 5 times at each concentration and temperature and gave consistent results. The kinetic data were obtained using a Hi-Tech SF-61SX2 low-temperature stopped-flow unit equipped with a diode array spectrophotometer (Hi-Tech, Salisbury, UK; now TgK Scientific, Bradford-on-Avon, UK). Kinetic data were analyzed either using the integrated software Kinetic Studio (TgK Scientific) or Igor Pro (Wavemetrics, Lake Oswego, USA). Details on the setup and kinetic measurements have been described previously.[5c,16,26]

The SuperFocus mixer setup was described in detail previously including analyses of the results.[12c,23]

Deposition Numbers 1998658, 1998659, 2001562, 2001563, 2001564 contain the supplementary crystallographic data for this paper. These data are provided free of charge by the joint Cambridge Crystallographic Data Centre and Fachinformationszentrum Karlsruhe Access Structures service www.ccdc.cam.ac.uk/structures.

Density functional theory (DFT) calculations were performed with Gaussian 16, Revision B01.[27] For the calculations we used TPSSh[28] as functional and the Ahlrichs type basis set def2-TZVP[29] as implemented in Gaussian 16, Revision B01.[27] As solvent model, we used the Polarizable Continuum Model (PCM) as implemented in Gaussian 16. As empirical dispersion correction, we used the D3 dispersion with Becke–Johnson damping as implemented in Gaussian16, Revision B.01.[30]

Synthesis of Tris(1-methylimidazol-2-yl)phosphane (Pim^{Me}): The ligand was prepared according to the method reported by Tolmachev et al.[31] However, we used a modified procedure of the synthesis described in a patent by Hätzelt.[32] The product was obtained as a slightly yellow solid (1.39 g, 5.10 mmol, 48 % yield). ^{1}H-NMR (400 MHz, $CDCl_3$): δ (ppm) = 7.18 (s, 3H, 3 × Ar-CH), 7.06 (s, 3H, 3 × Ar-CH), 3.62 (s, 9H, 3 × CH_3). ^{13}C-NMR (100 MHz, $CDCl_3$): δ (ppm) = 140.2 (d, Ar-C_q), 130.6 (d, Ar-CH), 125.1 (s, Ar-CH), 34.4 (d, CH_3). ^{31}P-NMR (162 MHz, $CDCl_3$): δ (ppm) = −60.5 (s). MS (ESI): m/z = 275.12 $[M + H]^+$.

Synthesis of Tris[2-(1,4-diisopropylimidazolyl)]phosphane (Pim^{iPr2}): This Ligand was prepared in a four-step synthesis according to procedure described by Sorrell et al.[9] Because of the slow oxidation of the phosphor backbone under aerobic conditions, the workup of the ligand is quite challenging. It is important to note that the aqueous work-up should be carried out largely in the absence of air (deoxygenated solvents). The product was obtained as a fine colorless powder (4.55 g, 9.39 mmol, 39 % yield). Crystals suitable for X-ray diffraction were grown by cooling a saturated pentane solution to 0 °C. ^{1}H-NMR (400 MHz, $CDCl_3$): δ (ppm) = 6.80 (s, 3H, 3 × Ar-CH), 4.77–4.65 (m, 3H, 3 × *i*Pr-CH), 2.85 (quin, 3H, 3 × *i*Pr-CH), 1.19 (d, 18H, 6 × *i*Pr-CH_3), 1.12 (d, 18H, 6 × *i*Pr-CH_3). ^{13}C-NMR (100 MHz, $CDCl_3$): δ (ppm) = 151.4 (s, Ar-C_q), 138.4 (d, Ar-C_q),113.2 (s, Ar-CH), 49.1 (d, *i*Pr-CH), 28.3 (s, *i*Pr-CH), 23.8 (s, *i*Pr-CH_3), 22.8 (s, *i*Pr-CH_3). ^{31}P-NMR (162 MHz, $CDCl_3$): δ (ppm) = −60.6 (s). MS (ESI): m/z = 485.35 $[M + H]^+$, 407.34 $[M + Na]^+$.

Synthesis of Bis[2-(1,4-diisopropylimidazolyl)][4-(1,4-diisopropyl-imidazolyl)]phosphane (Iso-Pim^{iPr2}): This compound was synthesized in the same manner like Pim^{iPr2} with the exception of slightly higher temperatures in the deprotonation/lithiation of 1,4-diisopropylimidazole (inefficient cooling) and the crystallization directly out of a acetonitrile solution at room temperature. The product was obtained as a colorless solid with some crystals suitable for X-ray diffraction (1.05 g, 2.17 mmol, 9 % yield). ^{1}H-NMR (400 MHz, [D_6]acetone): δ (ppm) = 7.84 (s, 1H, 1 × Ar-CH), 7.09 (s, 2H, 2 × Ar-CH), 5.06 (quin, 1H, 1 × *i*Pr-CH), 4.50 (sext, 2H, 2 × *i*Pr-CH), 3.52–3.42 (m, 1H, 1 × *i*Pr-CH), 2.77 (quin, 2H, 2 × *i*Pr-CH), 1.42 (d, 6H, 1 × *i*Pr-CH_3), 1.22 (d, 6H, 1 × *i*Pr-CH_3), 1.19–1.13 (m, 18H, 3 × *i*Pr-CH_3), 1.08 (d, 6H, 1 × *i*Pr-CH_3). ^{13}C-NMR (100 MHz, $CDCl_3$): δ (ppm) = 159.3 (s, Ar-C_q), 151.7 (s, Ar-CH), 140.5 (d, Ar-C_q), 139.8 (d, Ar-C_q), 113.8 (s, Ar-CH),113.6 (d, Ar-C_q), 49.9 (d, *i*Pr-CH), 49.4 (s, *i*Pr-CH), 29.2 (s, *i*Pr-CH), 28.0 (d, *i*Pr-CH), 24.7 (s, *i*Pr-CH_3), 24.2 (s, *i*Pr-CH_3), 23.9 (s, *i*Pr-CH_3), 23.7 (s, *i*Pr-CH_3), 23.2 (s, *i*Pr-CH_3), 23.1 (s, *i*Pr-CH_3). ^{31}P-NMR (162 MHz, $CDCl_3$): δ (ppm) = −77.5 (s). MS (ESI): m/z = 485.35 $[M + H]^+$.

Synthesis of $[Cu(Pim^{iPr2})(CH_3CN)]CF_3SO_3$ ($1CF_3SO_3$): This Ligand was prepared according to the literature.[13] The product was obtained in form of colorless crystals suitable for X-ray diffraction (2.03 g, 2.75 mmol, 92 % yield). ^{1}H-NMR (400 MHz, $CDCl_3$): δ (ppm) = 6.78 (s, 3H, 3 × Ar-CH), 5.12–4.99 (m, 3H, 3 × *i*Pr-CH), 2.97 (quin, 3H, 3 × *i*Pr-CH), 2.38 (s, 3H, acetonitrile-CH_3), 1.48 (d, 18H, 6 × *i*Pr-CH_3), 1.28 (d, 18H, 6 × *i*Pr-CH_3). ^{13}C-NMR (100 MHz, $CDCl_3$): δ (ppm) = 151.6 (s, triflate-C_q), 137.8 (d, Ar-C_q), 138.4 (d, Ar-C_q), 114.4 (s, acetonitrile-C_q),113.3 (s, Ar-CH), 49.8 (d, *i*Pr-CH), 28.2 (s, *i*Pr-CH), 24.1 (s, *i*Pr-CH_3), 22.1 (s, *i*Pr-CH_3), 2.92 (s, acetonitrile-CH_3). ^{31}P-NMR (162 MHz, $CDCl_3$): δ (ppm) = −117.8 (s). MS (ESI): m/z = 547.27 $[M - CH_3CN - CF_3SO_3]^+$.

Synthesis of $[Cu_2(Pim^{iPr2})_2](CF_3SO_3)_2$: 242 mg of Pim^{iPr2} (0.50 mmol) were dissolved in 3 mL of methanol. A solution of 129 mg of copper(I) triflate toluene complex (0.25 mmol) in 3 mL of methanol was added dropwise to the ligand solution and the reaction mixture was stirred 30 min at room temperature. Diethyl ether was added to the green solution until the solution became cloudy. After few minutes at −30 °C colorless crystals suitable for X-ray diffraction were grown. The crystals were filtered off and washed with diethyl ether. The slightly green solid was dried in vacuo to obtain a colorless powder (245 mg, 0.18 mmol, 72 % yield). MS (ESI): m/z = 547.27 $[(0.5\ M) - CF_3SO_3]^+$.

Acknowledgments

Financial support is gratefully acknowledged by the Deutsche Forschungsgemeinschaft (DFG SPP1740, SCHI 377/13-1, HE5480/10-2). Furthermore, we would like to thank Prof. Thomas N. Sorrell (retired, previously at the Department of Chemistry, University of North Carolina Chapel Hill) for helpful discussions and for providing the first batch of complex **1**. The authors gratefully acknowledge the funding of this project by computing time provided by the Paderborn Center for Parallel

Computing (PC2). Especially, we would like to thank Prof. Rudi van Eldik (University of Erlangen-Nürnberg) for his help with the kinetic analysis. Open access funding enabled and organized by Projekt DEAL.

Keywords: Copper · Dioxygen · Peroxides · Kinetics · Superoxides

[1] a) K. D. Karlin, S. Itoh in *Copper Oxygen Chemistry, Vol. 4* (Ed.: S. E. Rokita), John Wiley & Sons, New York, **2011**; b) L. M. Mirica, X. Ottenwaelder, T. D. P. Stack, *Chem. Rev.* **2004**, *104*, 1013–1045; c) C. Würtele, O. Sander, V. Lutz, T. Waitz, F. Tuczek, S. Schindler, *J. Am. Chem. Soc.* **2009**, *131*, 7544–7545; d) A. L. Lewis, W. B. Tolman, *Chem. Rev.* **2004**, *104*, 1047–1076; e) L. Hatcher, K. D. Karlin, *J. Biol. Inorg. Chem.* **2004**, *9*, 669–683; f) S. Itoh, S. Fukuzumi, *Acc. Chem. Res.* **2007**, *40*, 592; g) M. Rolff, J. Schottenheim, H. Decker, F. Tuczek, *Chem. Soc. Rev.* **2011**, *40*, 4077–4098; h) C. Citek, S. Herres-Pawlis, T. D. Stack, *Acc. Chem. Res.* **2015**, *48*, 2424–2433; i) T. N. Sorrell, *Tetrahedron* **1989**, *45*, 3–68.

[2] a) K. V. N. Esguerra, Y. Fall, J.-P. Lumb, *Angew. Chem. Int. Ed.* **2014**, *53*, 5877–5881; *Angew. Chem.* **2014**, *126*, 5987; b) K. V. N. Esguerra, Y. Fall, L. Petitjean, J.-P. Lumb, *J. Am. Chem. Soc.* **2014**, *136*, 7662–7668; c) K. V. N. Esguerra, J. P. Lumb, *Angew. Chem. Int. Ed.* **2018**, *57*, 1514–1518; *Angew. Chem.* **2018**, *130*, 1530; d) M. Paul, M. Teubner, B. Grimm-Lebsanft, C. Golchert, Y. Meiners, L. Senft, K. Keisers, P. Liebhäuser, T. Rösener, F. Biebl, S. Buchenau, M. Naumova, V. Murzin, R. Krug, A. Hoffmann, J. Pietruszka, I. Ivanovic-Burmazovic, M. Rübhausen, S. Herres-Pawlis, *Chem. Eur. J.* **2020**, *26*, 7556–7562.

[3] a) S. M. Smith, S. Rawat, J. Telser, B. M. Hoffman, T. L. Stemmler, A. C. Rosenzweig, *Biochemistry* **2011**, *50*, 10231–10240; b) M. A. Culpepper, G. E. Cutsail 3rd, B. M. Hoffman, A. C. Rosenzweig, *J. Am. Chem. Soc.* **2012**, *134*, 7640–7643.

[4] a) R. R. Jacobsen, Z. Tyeklár, A. Farooq, K. D. Karlin, S. Liu, J. Zubieta, *J. Am. Chem. Soc.* **1988**, *110*, 3690; b) C. Würtele, E. Gaoutchenova, K. Harms, M. C. Holthausen, J. Sundermeyer, S. Schindler, *Angew. Chem. Int. Ed.* **2006**, *45*, 3867–3869; *Angew. Chem.* **2006**, *118*, 3951; c) S. Schindler, *Eur. J. Inorg. Chem.* **2000**, 2311–2326; d) T. Hoppe, S. Schaub, J. Becker, C. Würtele, S. Schindler, *Angew. Chem. Int. Ed.* **2013**, *52*, 870–873; *Angew. Chem.* **2013**, *125*, 904; e) K. Komiyama, H. Furutachi, S. Nagatomo, A. Hashimoto, H. Hayashi, S. Fujinami, M. Suzuki, T. Kitagawa, *Bull. Chem. Soc. Jpn.* **2004**, *77*, 59–72; f) M. J. Baldwin, D. E. Root, J. E. Pate, K. Fujisawa, N. Kitajima, E. I. Solomon, *J. Am. Chem. Soc.* **1992**, *114*, 10421–10431; g) S. Mahapatra, V. G. Young Jr., *Angew. Chem. Int. Ed. Engl.* **1997**, *36*, 130–133; *Angew. Chem.* **1997**, *109*, 125; h) J. A. Halfen, S. Mahapatra, *Science* **1996**, *271*, 1397–1400; i) C. J. Cramer, W. B. Tolman, *Acc. Chem. Res.* **2007**, *40*, 601–608; j) N. Kindermann, E. Bill, S. Dechert, S. Demeshko, E. J. Reijerse, F. Meyer, *Angew. Chem. Int. Ed.* **2015**, *54*, 1738–1743; *Angew. Chem.* **2015**, *127*, 1758; k) S. Mahapatra, S. Kaderli, A. Llobet, Y.-M. Neuhold, T. Palanché, J. A. Halfen, V. G. Young Jr., T. A. Kaden, L. Que Jr., A. D. Zuberbühler, W. B. Tolman, *Inorg. Chem.* **1997**, *36*, 6343–6356.

[5] a) L. M. Mirica, M. A. Vance, D. Jackson-Rudd, B. Hedman, K. O. Hodgson, E. I. Solomon, T. D. P. Stack, *Science* **2005**, *308*, 1890–1892; b) K. D. Karlin, N. Wei, B. Jung, S. Kaderli, P. Niklaus, J. Zuberbühler, *J. Am. Chem. Soc.* **1993**, *115*, 9506–9514; c) M. Weitzer, S. Schindler, *Inorg. Chem.* **2003**, *42*, 1800–1806; d) N. W. Aboelella, S. V. Kryatov, B. F. Gherman, W. W. Brennessel, V. G. Young Jr., R. Sarangi, E. V. Rybak-Akimova, K. O. Hodgson, B. Hedman, E. I. Solomon, C. J. Cramer, W. B. Tolman, *J. Am. Chem. Soc.* **2004**, *126*, 16896–16911; e) S. Mahapatra, J. A. Halfen, W. B. Tolman, *J. Am. Chem. Soc.* **1996**, *118*, 11575–11586; f) S. Itoh, H. Nakao, L. M. Berreau, T. Kondo, M. Komatsu, S. Fukuzumi, *J. Am. Chem. Soc.* **1998**, *120*, 2890–2899.

[6] M. Becker, F. W. Heinemann, F. Knoch, W. Donaubauer, G. Liehr, S. Schindler, G. Golub, H. Cohen, D. Meyerstein, *Eur. J. Inorg. Chem.* **2000**, 719–726.

[7] J. E. Bol, W. L. Driessen, R. Y. N. Ho, B. Maase, L. Que Jr., J. Reedijk, *Angew. Chem. Int. Ed. Engl.* **1997**, *36*, 998–1000; *Angew. Chem.* **1997**, *109*, 1022.

[8] W. E. Lynch, D. M. Kurtz Jr., S. Wang, R. A. Scott, *J. Am. Chem. Soc.* **1994**, *116*, 11030–11038.

[9] T. N. Sorrell, W. E. Allen, P. S. White, *Inorg. Chem.* **1995**, *34*, 952–960.

[10] a) H. Börzel, P. Comba, K. S. Hagen, M. Kerscher, H. Pritzkow, M. Schatz, S. Schindler, O. Walter, *Inorg. Chem.* **2002**, *41*, 5440–5452; b) M. Kodera, K. Katayama, Y. Tachi, K. Kano, S. Hirota, S. Fujinami, M. Suzuki, *J. Am. Chem. Soc.* **1999**, *121*, 11006–11007.

[11] G. J. Karahalis, A. Thangavel, B. Chica, J. Bacsa, R. B. Dyer, C. C. Scarborough, *Inorg. Chem.* **2016**, *55*, 1102–1107.

[12] a) F. Felis, F. Strassl, L. Laurini, N. Dietrich, A.-M. Billet, V. Roig, S. Herres-Pawlis, K. Loubière, *Chem. Eng. Sci.* **2019**, *207*, 1256–1269; b) M. Paul, F. Strassl, A. Hoffmann, M. Hoffmann, M. Schlüter, S. Herres-Pawlis, *Eur. J. Inorg. Chem.* **2018**, *2018*, 2101–2124; c) A. Miska, D. Schurr, G. Rinke, R. Dittmeyer, S. Schindler, *Chem. Eng. Sci.* **2018**, *190*, 459–465; d) Y. Nagami, T. Saito, *Particuology* **2013**, *11*, 158–169; e) Y. Bao, Z. Jiang, S. Tong, X. Huang, Z. Cai, Z. Gao, *Chem. Eng. Sci.* **2019**, *207*, 829–843; f) U. D. Kück, M. Schlüter, N. Räbiger, *J. Chem. Eng. Jpn.* **2012**, *45*, 708–712.

[13] W. E. Allen, T. N. Sorrell, *Inorg. Chem.* **1997**, *36*, 1732–1734.

[14] W. G. Dougherty, W. S. Kassel, *Inorg. Chim. Acta* **2010**, *364*, 120–124.

[15] a) J. Becker, P. Gupta, F. Angersbach, F. Tuczek, C. Nather, M. C. Holthausen, S. Schindler, *Chem. Eur. J.* **2015**, *21*, 11735–11744; b) A. Hoffmann, M. Wern, T. Hoppe, M. Witte, R. Haase, P. Liebhäuser, J. Glatthaar, S. Herres-Pawlis, S. Schindler, *Eur. J. Inorg. Chem.* **2016**, *2016*, 4744–4751; c) M. P. Jensen, E. L. Que, X. Shan, E. Rybak-Akimova, L. Que Jr., *Dalton Trans.* **2006**, 3523–3527.

[16] C. X. Zhang, S. Kaderli, M. Costas, E. K. Kim, Y.-M. Neuhold, K. D. Karlin, A. D. Zuberbühler, *Inorg. Chem.* **2003**, *42*, 1807–1824.

[17] a) H. V. Obias, Y. Lin, N. Murthy, E. Pidcock, E. I. Solomon, M. Ralle, N. J. Blackburn, Y.-M. Neuhold, A. D. Zuberbühler, K. D. Karlin, *J. Am. Chem. Soc.* **1998**, *120*, 12960–12961; b) S. Mahapatra, J. A. Halfen, E. C. Wilkinson, L. Que Jr., W. B. Tolman, *J. Am. Chem. Soc.* **1994**, *116*, 9785–9786; c) J. Astner, M. Weitzer, S. P. Foxon, S. Schindler, F. W. Heinemann, J. Mukherjee, R. Gupta, V. Mahadevan, R. Mukherjee, *Inorg. Chim. Acta* **2008**, *361*, 279–292.

[18] D. Projahn, S. Schindler, R. van Eldik, D. G. Fortier, C. R. Andrew, A. G. Sykes, *Inorg. Chem.* **1995**, *34*, 5935–5941.

[19] a) M. Becker, S. Schindler, R. van Eldik, *Inorg. Chem.* **1994**, *33*, 5370–5371; b) M. Becker, S. Schindler, K. D. Karlin, T. A. Kaden, S. Kaderli, T. Palanché, A. D. Zuberbühler, *Inorg. Chem.* **1999**, *38*, 1989–1995.

[20] K. D. Karlin, S. Kaderli, A. D. Zuberbühler, *Acc. Chem. Res.* **1997**, *30*, 139–147.

[21] S. Fukuzumi, K. D. Karlin, *Coord. Chem. Rev.* **2013**, *257*, 187–195.

[22] H.-C. Liang, K. D. Karlin, R. Dyson, S. Kaderli, B. Jung, A. D. Zuberbühler, *Inorg. Chem.* **2000**, *39*, 5884–5894.

[23] D. Schurr, F. Strassl, P. Liebhäuser, G. Rinke, R. Dittmeyer, S. Herres-Pawlis, *React. Chem. Eng.* **2016**, *1*, 485–493.

[24] A. Miska, J. Norbury, M. Lerch, S. Schindler, *Chem. Eng. Technol.* **2017**, *40*, 1522–1526.

[25] *Solubility Data Series*, Pergamon Press, Oxford, **1981**, p.

[26] M. Weitzer, M. Schatz, F. Hampel, F. W. Heinemann, S. Schindler, *J. Chem. Soc., Dalton Trans.* **2002**, 686–694.

[27] M. J. Frisch, G. W. Trucks, H. B. Schlegel, G. E. Scuseria, M. A. Robb, J. R. Cheeseman, G. Scalmani, V. Barone, B. Mennucci, G. A. Petersson, H. Nakatsuji, M. Caricato, X. Li, H. P. Hratchian, A. F. Izmaylov, J. Bloino, G. Zheng, J. L. Sonnenberg, M. Hada, M. Ehara, K. Toyota, R. Fukuda, J. Hasegawa, M. Ishida, T. Nakajima, Y. Honda, O. Kitao, H. Nakai, T. Vreven, J. A. Montgomery Jr., J. E. Peralta, F. Ogliaro, M. Bearpark, J. J. Heyd, E. Brothers, K. N. Kudin, V. N. Staroverov, R. Kobayashi, J. Normand, K. Raghavachari, A. Rendell, J. C. Burant, S. S. Iyengar, J. Tomasi, M. Cossi, N. Rega, J. M. Millam, M. Klene, J. E. Knox, J. B. Cross, V. Bakken, C. Adamo, J. Jaramillo, R. Gomperts, R. E. Stratmann, O. Yazyev, A. J. Austin, R. Cammi, C. Pomelli, J. W. Ochterski, R. L. Martin, K. Morokuma, V. G. Zakrzewski, G. A. Voth, P. Salvador, J. J. Dannenberg, S. Dapprich, A. D. Daniels, Ö. Farkas, J. B. Foresman, J. V. Ortiz, J. Cioslowski, D. J. Fox, *Gaussian 09, Revision B.01*, Gaussian, Inc., Wallingford CT, **2016**.

[28] a) M. Tao, J. P. Perdew, V. N. Staroverov, G. E. Scuseria, *Phys. Rev. Lett.* **2003**, *91*, 146401; b) V. N. Staroverov, G. E. Scuseria, J. Tao, J. P. Perdew, *J. Chem. Phys.* **2003**, *119*, 12129 and Erratum **2004**, *121*, 11507(E).

[29] a) F. Weigend, R. Ahlrichs, *Phys. Chem. Chem. Phys.* **2005**, *7*, 3297–305; b) A. Schäfer, C. Huber, R. Ahlrichs, *J. Chem. Phys.* **1994**, *100*, 5829; c) K. Eichkorn, F. Weigend, O. Treutler, R. Ahlrichs, *Theor. Chem. Acc.* **1997**, *97*, 119.

EurJIC
European Journal of Inorganic Chemistry

Full Paper
doi.org/10.1002/ejic.202000462

Chemistry Europe
European Chemical Societies Publishing

[30] a) S. Grimme, S. Ehrlich, L. Goerigk, *J. Comput. Chem.* **2011**, *32*, 1456; b) L. Goerigk, S. Grimme, *Phys. Chem. Chem. Phys.* **2011**, *13*, 6670; c) For TPSSh, the values of the original paper have been substituted by the corrected values kindly provided by S. Grimme as private communication and published in; d) A. Hoffmann, R. Grunzke, S. Herres-Pawlis, *J. Comput. Chem.* **2014**, *35*, 1943.

[31] A. A. Tolmachev, A. A. Yurchenko, A. S. Merculov, M. G. Semenova, E. V. Zarudnitskii, V. V. Ivanov, A. M. Pinchuk, *Heteroat. Chem.* **1999**, *10*, 585–597.

[32] Hätzelt in Vol. DE102007017657 A1 **2008**.

Received: May 10, 2020

Supporting Information

Kinetic Investigation of the Reaction of Dioxygen with the Copper(I) Complex [Cu(Pim^{iPr2})(CH$_3$CN)]CF$_3$SO$_3$ K1;Pim^{iPr2} = Tris[2-(1,4-diisopropylimidazolyl)]phosphineK2;

Markus Lerch, Markus Weitzer, Tim-Daniel J. Stumpf, Larissa Laurini, Alexander Hoffmann, Jonathan Becker, Andreas Miska, Richard Göttlich, Sonja Herres-Pawlis, Siegfried Schindler*

1 | Formation and decay of complex 2 (benchtop experiment)

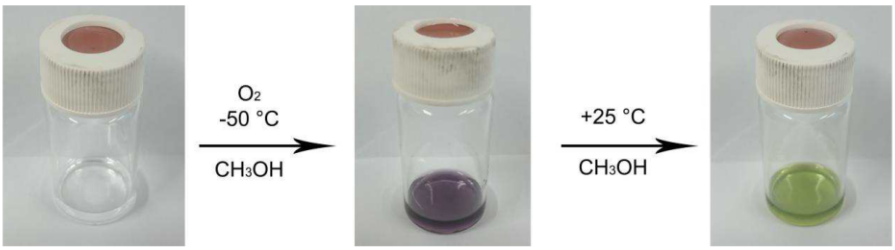

Figure S1. Benchtop experiment of the reaction of **1**CF_3SO_3 with O_2 in CH_3OH at -50 °C leading to the purple dinuclear peroxide complex. Warming the solution leads irreversibly to a green colored copper(II) complex solution.

2 | Tris[2-(1,4-diisopropylimidazolyl)]phosphine (Pim^{iPr2})

2.1 | ^{1}H-NMR, ^{13}C-NMR and ^{31}P-NMR spectra of Pim^{iPr2} ($CDCl_3$)

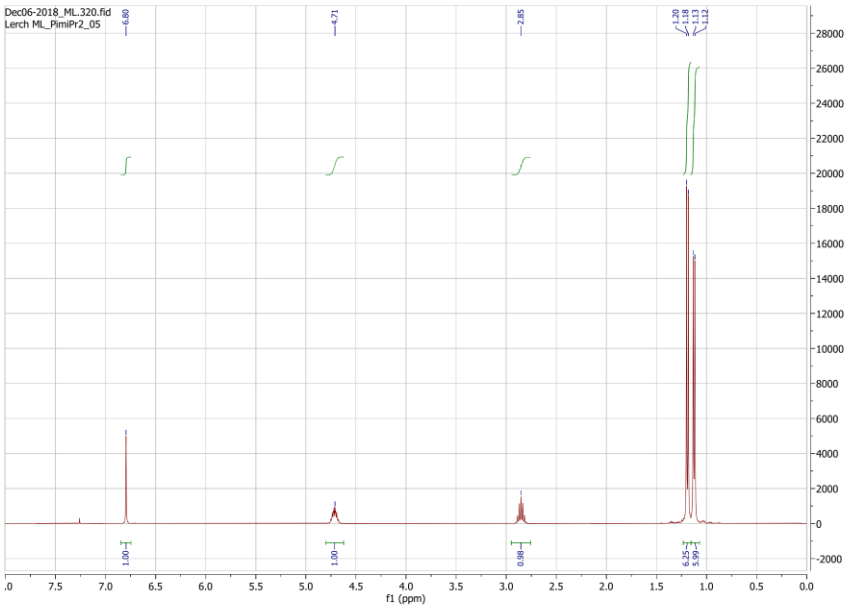

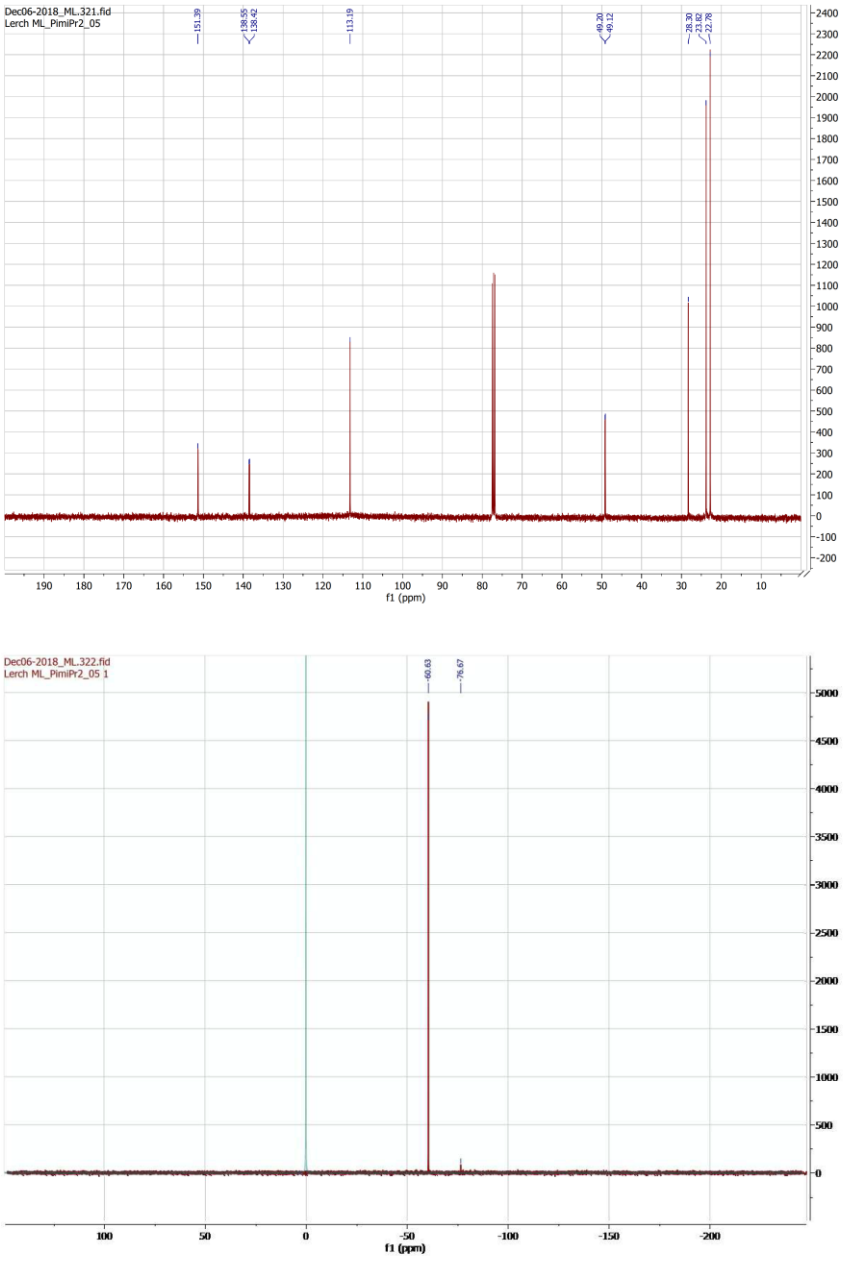

Figures S2.1 a, b, c

2.2 | ESI-MS spectrum of Pim^{iPr2} (positive mode, CH_3OH)

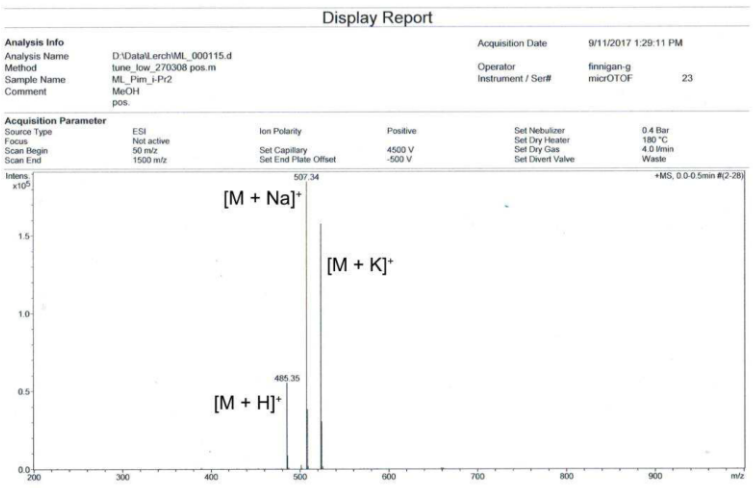

Figure S2.2

Crystallography

Diffraction data for all samples were collected at low temperatures (100K) using φ- and ω-scans on a BRUKER D8 Venture System equipped with dual IμS microfocus sources, a PHOTON100 detector and an OXFORD CRYOSYSTEMS 700 low temperature system. Mo-K_α radiation with a wavelength of 0.71073 Å and a collimating Quazar multilayer mirror were used.

Semi-empirical absorption corrections from equivalents were applied using SADABS[1]. The structures were solved by direct methods using SHELXT[2] and refined against F^2 on all data by full-matrix least squares using SHELXL[3]. All non-hydrogen atoms were refined anisotropically, O-H hydrogen atoms were located in the Fourier difference map and were set to ideal distances and C-H hydrogen atoms were positioned at geometrically calculated positions and refined using a riding model. The isotropic displacement parameters of all hydrogen atoms were fixed to 1.2x or 1.5x (OH and CH_3 hydrogens) the U_{eq} value of the atoms they are linked to. All crystallographic data were deposited with the Cambridge Crystallographic Database as 1998658, 1998659, 2001562 - 2001564 and can be obtained free of charge[4].

2.3 | Crystallographic data of Pim^{iPr2}

The crystal structure of Pim^{iPr2} was solved in the monoclinic space group $P2_1/n$. The asymmetric unit contains one ligand molecule.

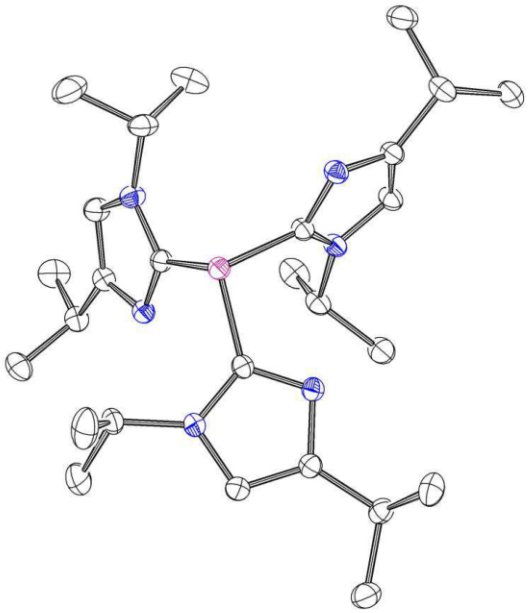

Figure S2.3. ORTEP plot of Pim^{iPr2}. Hydrogen atoms are omitted for clarity, thermal ellipsoids were set to 50%

Table S1. Crystal data and structure refinement for Pim^{iPr2}.

CCDC No	2001562	
Empirical formula	C_{27} H_{45} N_6 P	
Formula weight	484.66	
Temperature	100(2) K	
Wavelength	0.71073 Å	
Crystal system	Monoclinic	
Space group	$P2_1/n$	
Unit cell dimensions	a = 13.5018(8) Å	α= 90°.
	b = 14.3027(8) Å	β= 110.807(2)°.
	c = 15.7982(9) Å	γ = 90°.
Volume	2851.9(3) Å^3	
Z	4	
Density (calculated)	1.129 Mg/m^3	

Absorption coefficient	0.121 mm^{-1}
F(000)	1056
Crystal size	0.355 x 0.198 x 0.133 mm^3
Theta range for data collection	1.982 to 34.337°.
Index ranges	$-21 \le h \le 21$, $-22 \le k \le 22$, $-25 \le l \le 25$
Reflections collected	76864
Independent reflections	11944 [R(int) = 0.0639]
Completeness to theta = 25.242°	100.0 %
Absorption correction	Semi-empirical from equivalents
Refinement method	Full-matrix least-squares on F^2
Data / restraints / parameters	11944 / 0 / 319
Goodness-of-fit on F^2	1.026
Final R indices [I>2σ(I)]	R_1 = 0.0578, wR_2 = 0.1569
R indices (all data)	R_1 = 0.0742, wR_2 = 0.1691
Largest diff. peak and hole	2.448 and -0.550 $e.Å^{-3}$

3 | Isomer Iso-Pim^{iPr2}

3.1 | ^{1}H-NMR, ^{13}C-NMR and ^{31}P-NMR spectra of Iso-Pim^{iPr2} (acetone-d_6)

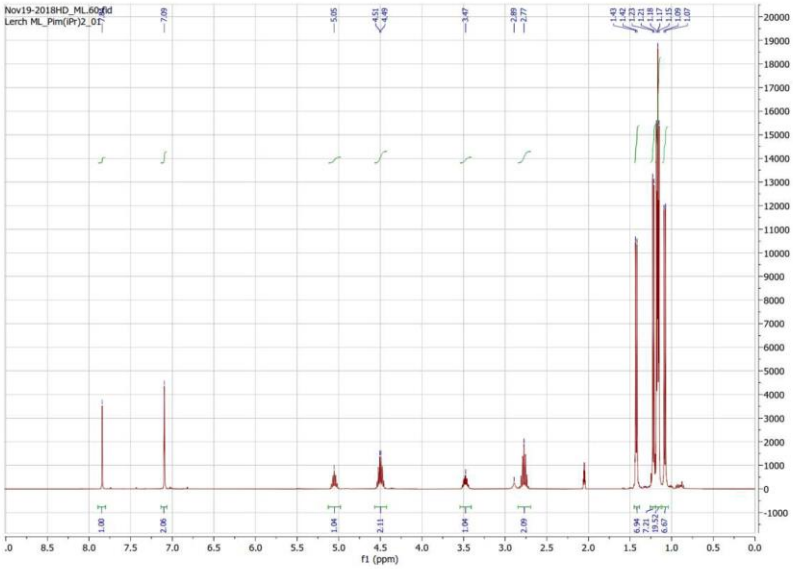

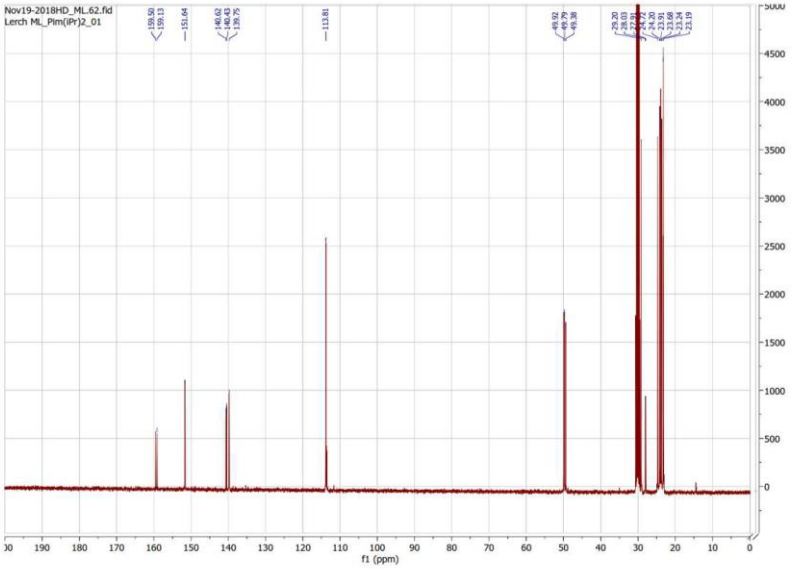

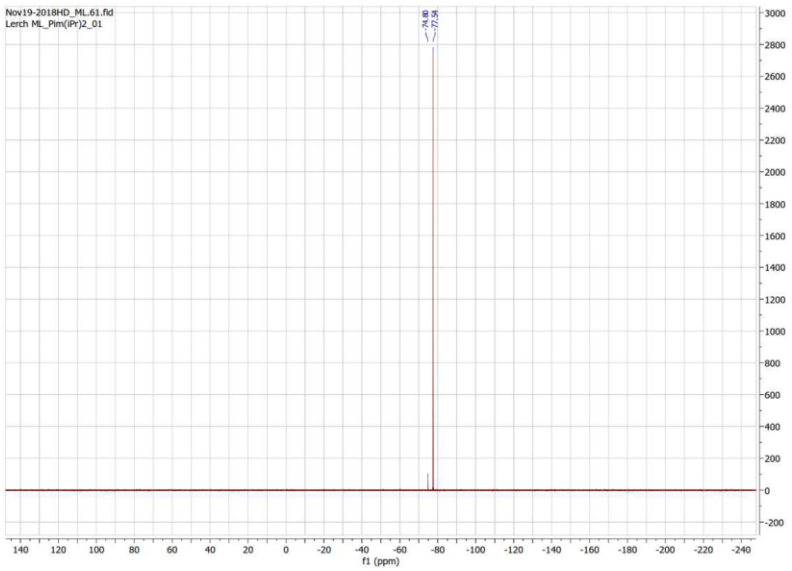

Figures S3.1 a, b, c

3.2 | Crystallographic data of Iso-Pim^{iPr2}

The crystal structure of the ligand isomer Iso-Pim^{iPr2} was solved in the monoclinic space group $P2_1$. The asymmetric unit contains one molecule which was found to be partially disordered in two positions. The disorder was refined with the help of similarity restraints on the anisotropic displacement parameters, advanced rigid bond restraints[5], same distance restraints and restraints to a common plane. Some atoms with positions close to each other were set to the same anisotropic displacement parameters[6]. The disorder ratios were allowed to refine freely and converged to 0.516(5) and 0.52(3). The absolute structure was successfully determined with a Parsons parameter of 0.032(36).[7]

Chemical formula of Iso-Pim^{iPr2}

iso-Pim$^{(iPr2)}$

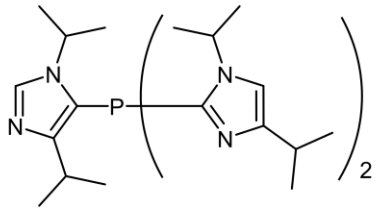

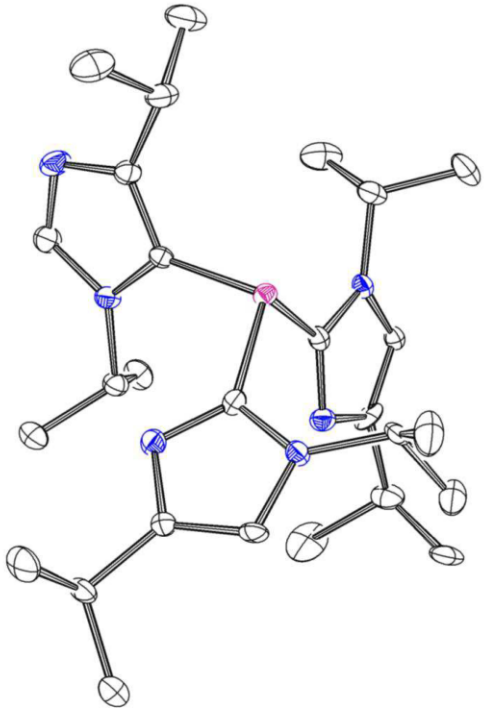

Figure S3.2. ORTEP plot of Iso-Pim^{iPr2}. Hydrogen atoms omitted for clarity and thermal ellipsoids set to 50%

Table S6. Crystal data and structure refinement for Iso-Pim^{iPr2}.

CCDC No	1998658	
Empirical formula	C_{27} H_{45} N_6 P	
Formula weight	484.66	
Temperature	100(2) K	
Wavelength	0.71073 Å	
Crystal system	Monoclinic	
Space group	$P2_1$	
Unit cell dimensions	a = 8.2805(3) Å	α= 90°.
	b = 15.3203(5) Å	β= 99.8398(17)°.
	c = 11.4740(4) Å	γ = 90°.
Volume	1434.18(9) Å^3	
Z	2	
Density (calculated)	1.122 Mg/m^3	
Absorption coefficient	0.121 mm^{-1}	
F(000)	528	
Crystal size	0.085 x 0.084 x 0.055 mm^3	
Theta range for data collection	2.239 to 27.484°.	
Index ranges	-10 ≤ h ≤ 10, -19 ≤ k ≤ 19, -14 ≤ l ≤ 14	
Reflections collected	50899	
Independent reflections	6561 [R(int) = 0.0840]	
Completeness to theta = 25.242°	100.0 %	
Absorption correction	Semi-empirical from equivalents	
Refinement method	Full-matrix least-squares on F^2	
Data / restraints / parameters	6561 / 1410 / 449	
Goodness-of-fit on F^2	1.032	
Final R indices [I>2σ(I)]	R_1 = 0.0380, wR_2 = 0.0765	
R indices (all data)	R_1 = 0.0530, wR_2 = 0.0816	
Absolute structure parameter	0.03(4)	
Largest diff. peak and hole	0.193 and -0.248 e.Å^{-3}	

4 | $[Cu(Pim^{Me})_2](CF_3SO_3)_2$

4.1 | Crystallographic data of $[Cu(Pim^{Me})_2](CF_3SO_3)_2$

The structure of $[Cu(Pim^{Me})_2](CF_3SO_3)_2$ was solved in the monoclinic space group $P2_1/n$. The asymmetric unit contains two half molecules of $[Cu(Pim^{Me})_2]$, two triflate anions, a methanol and two water molecules. The anions and the methanol molecule were found to be disordered over two or three positions. The disorder was refined with the help of advanced rigid bond restraints, similarity restraints on anisotropic displacement parameters and same distance restraints. The disorder ratios were refined freely and converged to 0.538(8), 0.860(3) and 0.799(3):0.116(2):0.085(2).

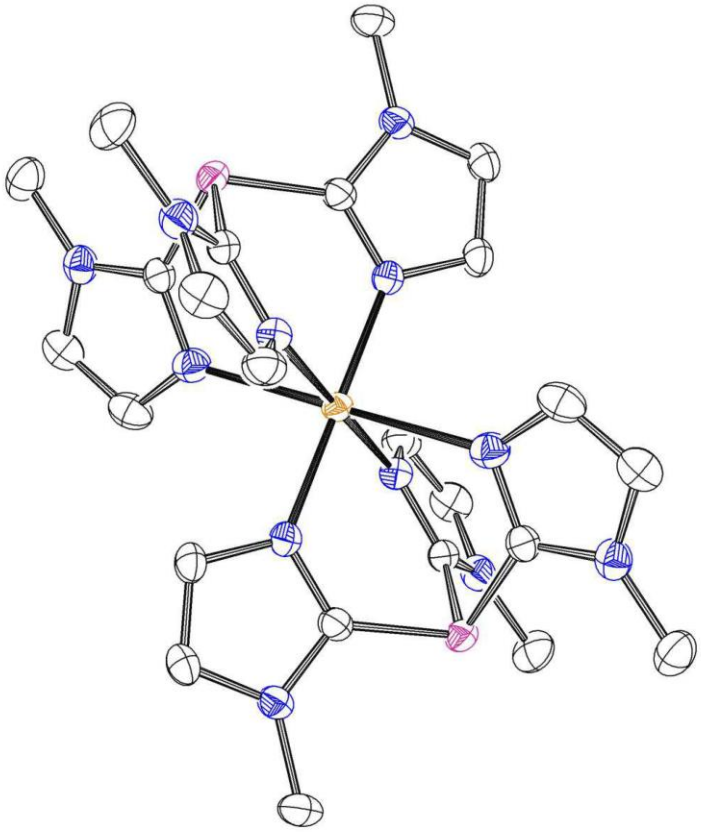

Figure S4.ORTEP plot of $[Cu(Pim^{Me})_2]$. Anions, solvent molecules and hydrogen atoms are omitted for clarity. One full molecule shown. Thermal ellipsoid propability set to 50%.

Table S 11. Crystal data and structure refinement for $[Cu(Pim^{Me})_2](CF_3SO_3)_2$.

CCDC No	2001563	
Empirical formula	$C_{27}\ H_{38}\ Cu\ F_6\ N_{12}\ O_9\ P_2\ S_2$	
Formula weight	978.29	
Temperature	100(2) K	
Wavelength	0.71073 Å	
Crystal system	Monoclinic	
Space group	$P2_1/n$	
Unit cell dimensions	a = 15.4791(6) Å	α= 90°.
	b = 12.0637(5) Å	β= 90.606(2)°.
	c = 21.1457(8) Å	γ = 90°.
Volume	3948.4(3) $Å^3$	
Z	4	
Density (calculated)	1.646 Mg/m^3	
Absorption coefficient	0.834 mm^{-1}	
F(000)	2004	
Crystal size	0.744 x 0.589 x 0.466 mm^3	
Theta range for data collection	2.341 to 28.282°.	
Index ranges	-20 ≤ h ≤ 20, -16 ≤ k ≤ 16, -28 ≤ l ≤ 28	
Reflections collected	65005	
Independent reflections	9807 [R(int) = 0.0599]	
Completeness to theta = 25.242°	99.9 %	
Absorption correction	Semi-empirical from equivalents	
Refinement method	Full-matrix least-squares on F^2	
Data / restraints / parameters	9807 / 2005 / 799	
Goodness-of-fit on F^2	1.028	
Final R indices [I>2σ(I)]	R_1 = 0.0482, wR_2 = 0.1254	
R indices (all data)	R_1 = 0.0682, wR_2 = 0.1391	
Largest diff. peak and hole	0.763 and -0.629 $e.Å^{-3}$	

5 | [Cu(Pim^{iPr2})CH$_3$CN]CF$_3$SO$_3$ (1 CF$_3$SO$_3$)

5.1 | ^{1}H-NMR, ^{13}C-NMR and ^{31}P-NMR spectra of [Cu(Pim^{iPr2})CH$_3$CN]CF$_3$SO$_3$ (CDCl$_3$)

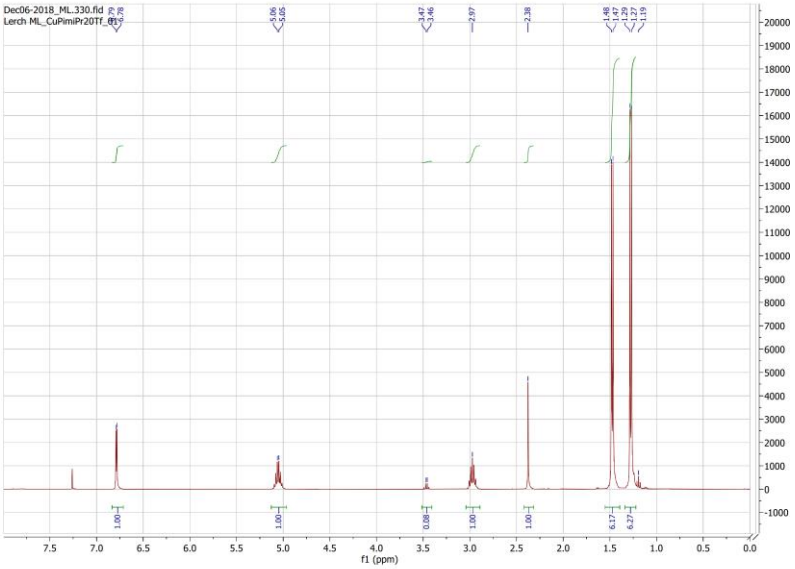

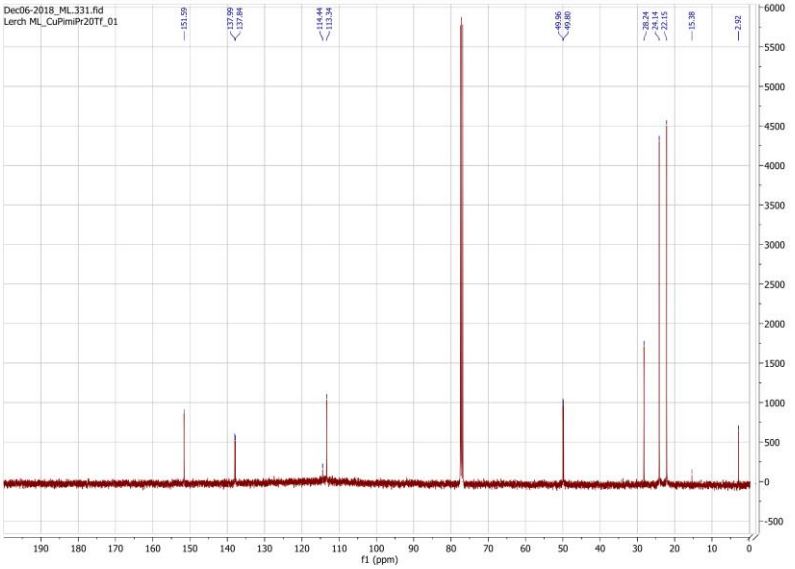

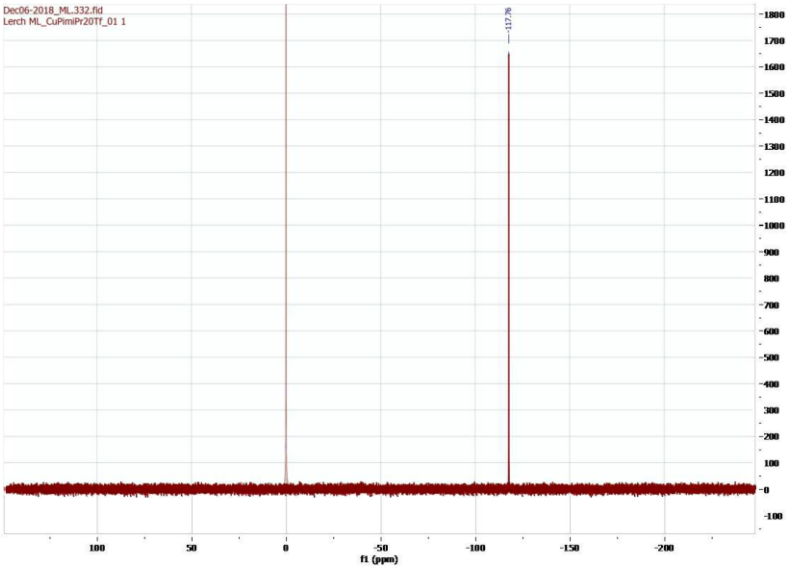

Figure S5.1 a,b,c

5.2 | ESI-MS spectrum of [Cu(Pim^{iPr2})CH$_3$CN]CF$_3$SO$_3$ (positive mode, in methanol)

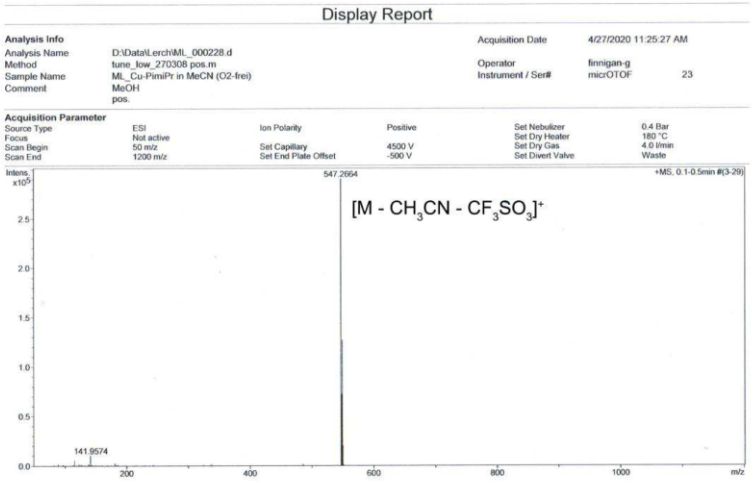

Figure S5.2

5.3 | Crystallographic data of [Cu(Pim^{iPr2})CH_3CN]CF_3SO_3

The structure of [Cu(Pim^{iPr2})CH_3CN]CF_3SO_3 was solved in the monoclinic space group *C*2. The asymmetric unit contains one full molecule and anion. The complex molecule was found to be nearly completely disordered over two positions, also the triflate anion was found to be disordered over two positions. The disorder was refined with the help of similarity restraints on anisotropic displacement parameters, advanced rigid bond restraints, same distance restraints and restraints to a common plane. Some disordered atoms close to each other were set to the same anisotropic displacement parameters. The disorder ratios were refined freely and converged to 0.596(5) and 0.456(5). Additional disordered solvent was found in the unit cell, but because no sufficient model could be found, SQUEEZE[8] as implemented in PLATON[9] was used to include a bulk solvent model into the refinement. SQUEEZE identified two voids in the crystal lattice located at 0.5 -0.1 0.0 and 0.0 0.4 0.0, each with a volume of 511 Å^3 and containing the equivalent of 221 electrons. The structure was refined as an inversion twin. The twin ratio was refined and converged to 0.504(3).

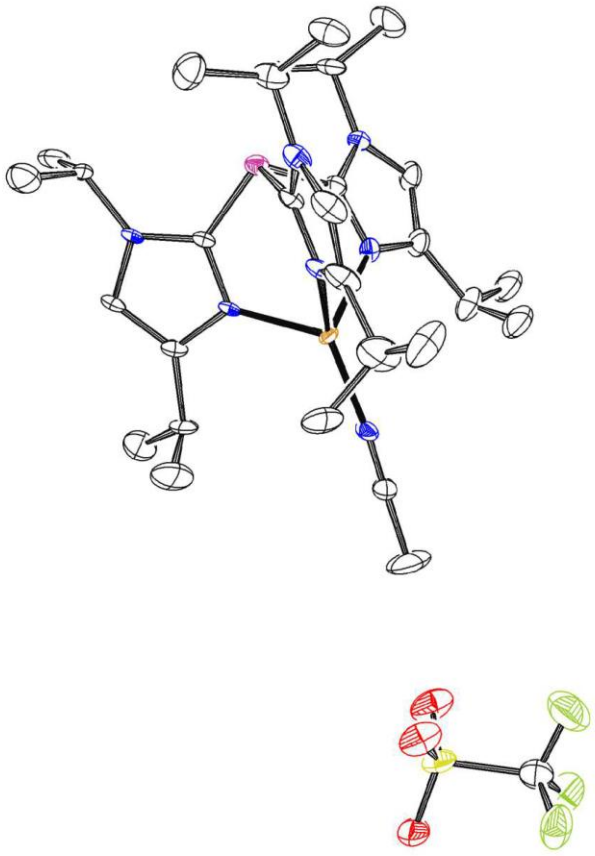

Figure S5.3. ORTEP plot of [Cu(Pim^{iPr2})CH_3CN]CF_3SO_3. Main disorder part shown, hydrogen atoms are omitted for clarity. Propability of thermal ellipsoids set to 50%.

Table S17. Crystal data and structure refinement for $[Cu(Pim^{iPr2})CH_3CN]CF_3SO_3$.

CCDC No	1998659	
Empirical formula	C_{30} H_{48} Cu F_3 N_7 O_3 P S	
Formula weight	738.32	
Temperature	100(2) K	
Wavelength	0.71073 Å	
Crystal system	Monoclinic	
Space group	*C*2	
Unit cell dimensions	a = 18.195(4) Å	α= 90°.
	b = 15.090(3) Å	β= 92.575(6)°.
	c = 17.200(3) Å	γ = 90°.
Volume	4717.7(17) Å^3	
Z	4	
Density (calculated)	1.040 Mg/m^3	
Absorption coefficient	0.584 mm^{-1}	
F(000)	1552	
Crystal size	0.328 x 0.160 x 0.120 mm^3	
Theta range for data collection	2.145 to 27.484°.	
Index ranges	-23 ≤ h ≤ 23, -19 ≤ k ≤ 19, -22 ≤ l ≤ 22	
Reflections collected	214798	
Independent reflections	10832 [R(int) = 0.0533]	
Completeness to theta = 25.242°	99.9 %	
Absorption correction	Semi-empirical from equivalents	
Refinement method	Full-matrix least-squares on F^2	
Data / restraints / parameters	10832 / 3065 / 761	
Goodness-of-fit on F^2	1.048	
Final R indices [I>2σ(I)]	R_1 = 0.0550, wR_2 = 0.1326	
R indices (all data)	R_1 = 0.0708, wR_2 = 0.1442	
Absolute structure parameter	0.50(3)	
Largest diff. peak and hole	1.094 and -0.458 e.Å^{-3}	

6 | DFT Calculations

Table S22. Geometric Key Parameters with TPSSh/def2-TZVP, MeOH and GD3BJ

	Cu…Cu [Å]	Cu-N(eq) [Å]	Cu-N(ax) [Å]	Cu-O [Å]	O-O [Å]	S2	E [H]	relative E [kcal/mol]
Oxo	2.825	1.944/1.947 1.960/1.996	2.722 2.518	1.793/1.811 1.802/1.817	2.231		- 6884,69228820	0,00
Peroxo	3.556	1.961/1.986 1.970/2.018	2.326 2.249	1.919/1.932 1.929/1.954	1.435		- 6884,70390730	-7,29
Peroxo BS	3.394	1.986/2.074 1.987/1.992	2.172 2.300	1.951/1.999 1.953/1.988	1.440	0.83	- 6884,71112610	-11,82

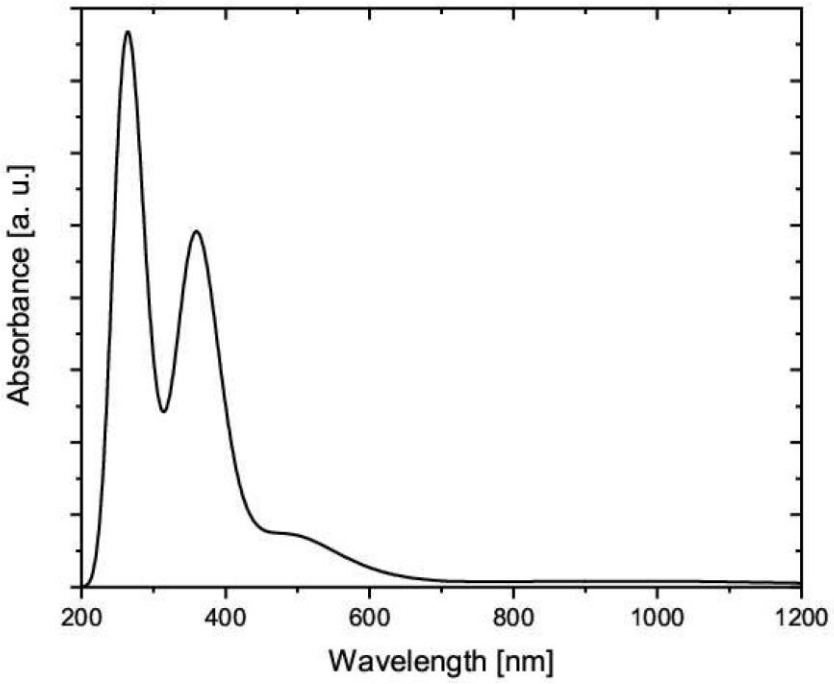

Figure S6. Calculated TD-DFT UV/vis spectrum of **2** (TPSSh/def2-TZVP, MeOH, GD3BJ, broken-symmetry)

7 | Time-resolved UV-Vis spectra of the reaction of 1CF_3SO_3 with dioxygen in methanol

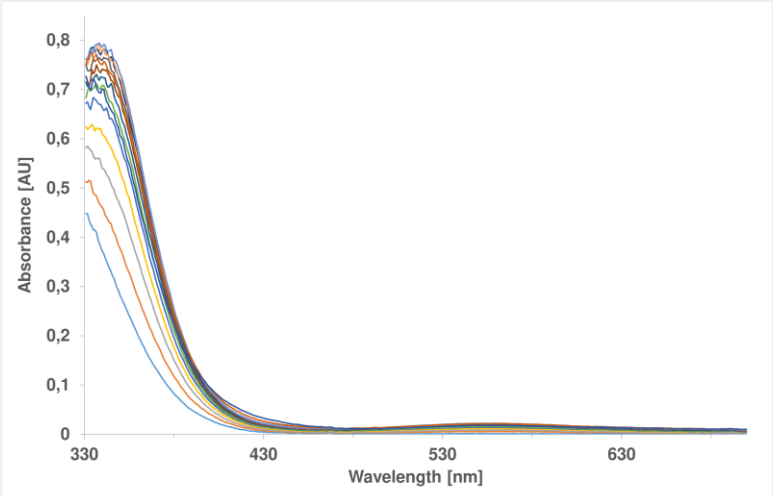

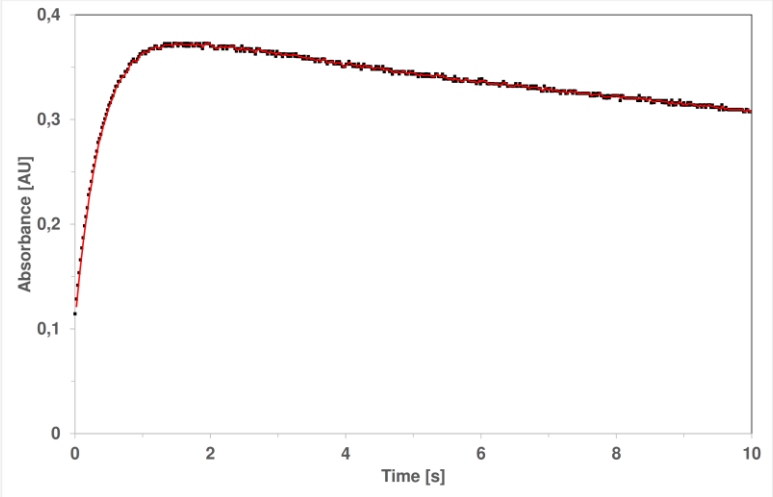

Bei 370 nm

Figure S7. (a)Time-resolved UV-Vis spectra of the reaction of **1**CF_3SO_3 with dioxygen in methanol (T = 25.0 °C, [complex] = 0.4 mmol/L, [O_2] = 5.2 mmol/L). (b): absorbance *vs.* time trace at 370 nm.

8 | Variation of complex (1) concentration

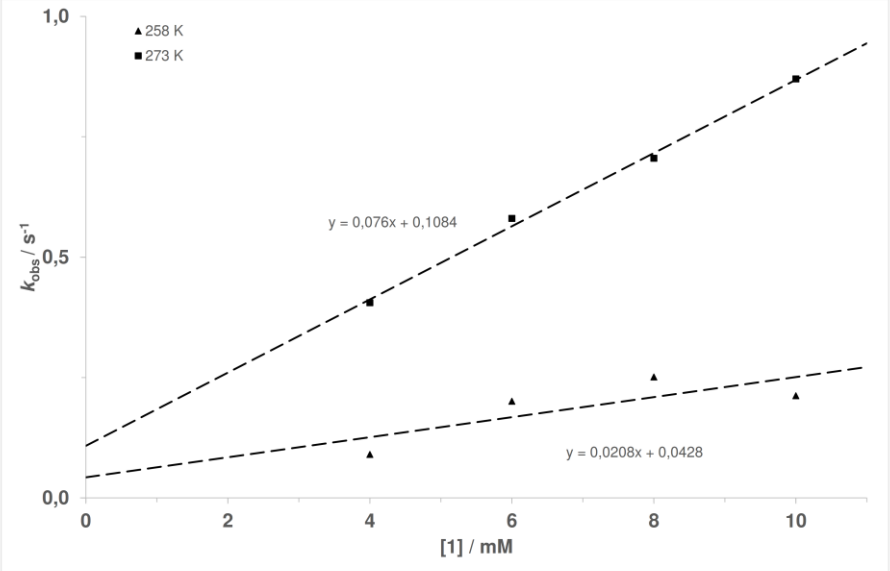

Figure S8. Variation of [**1**CF_3SO_3] from 4 to 10 mmol/L (after mixing) at different temperatures (-15.0 and 0.0 °C), [O_2] = 0.1 mmol/L)

9 | Derivation of steady state kinetics for the formation of a copper superoxido complex as an intermediate

Reactions: $Cu(I) + O_2 \rightleftharpoons Cu(II)O_2$

$$Cu(I) + Cu(II)O_2 \rightleftharpoons Cu_2(II)O_2$$

Simplified to: $A + B \rightleftharpoons C$ (with k_1 and k_{-1})

$$A + C \rightleftharpoons D \text{ (with } k_2 \text{ and } k_{-2})$$

Rate for formation of D: $d[D]/dt = k_2[A][C] - k_{-2}[D]$ **(eq 1)**

C as a reactive intermediate was not observed and can be treated applying the steady state approach $d[C]/dt = 0$ leading to:

$k_1[A][B] + k_{-2}[D] = k_2[A][C] + k_{-1}[C]$

Thus: $[C] = \frac{k_1[A][B]+k_{-2}[D]}{k_2[A]+k_{-1}}$ **(eq 2)**

Insertion of [C] from eq 2 into eq 1:

$$\frac{d[D]}{dt} = \frac{k_2k_1[A]^2[B] + k_2k_{-2}[A][D]}{k_2[A] + k_{-1}} - k_{-2}[D]$$

$$\frac{d[D]}{dt} = \frac{k_2k_1[A]^2[B] + k_2k_{-2}[A][D] - k_2k_{-2}[A][D] - k_{-2}k_{-1}[D]}{k_2[A] + k_{-1}}$$

$$\frac{d[D]}{dt} = \frac{k_2 k_1 [A]^2 [B] - k_{-2} k_{-1} [D]}{k_2 [A] + k_{-1}} \qquad (\boldsymbol{eq\ 3})$$

With: $[A]_0 = [A] + 2[D] = [A]_{eq} + 2[D]_{eq}$

And the equilibrium: A + C ⇌ D

$K = \frac{k_2}{k_{-2}} = \frac{[D]_{eq}}{[A]_{eq}[C]}$ and $\frac{k_1}{k_{-1}} = \frac{[C]}{[A]_{eq}[B]}$ With $\frac{k_1 [A]_{eq} [B]}{k_{-1}} = [C]$

$\frac{k_2}{k_{-2}} = \frac{[D]_{eq}}{[A]_{eq} \frac{k_1 [A]_{eq} [B]}{k_{-1}}}$ leading to $\frac{[D]_{eq}}{[A]_{eq}} =$ $\frac{k_2 k_1 [B]}{k_{-2} k_{-1}} = \frac{[D]_{eq}}{[A]_{eq}^2}$

or $k_2 k_1 [B] [A]_{eq}^2 = k_{-2} k_{-1} [D]_{eq}$

Expanding eq 3

$$\frac{d[D]}{dt} = \frac{k_2 k_1 [A]^2 [B] - k_{-2} k_{-1} [D]}{k_2 [A] + k_{-1}} \qquad (\boldsymbol{eq\ 3})$$

with $k_2 k_1 [B] [A]_{eq}^2$ (adding and subtracting this term and furthermore with

$$k_2 k_1 [B] [A]_{eq}^2 = k_{-2} k_{-1} [D]_{eq}$$

Leads to

$$\frac{d[D]}{dt} = \frac{k_2 k_1 [A]^2 [B] - k_2 k_1 [B] [A]_{eq}^2 + k_{-2} k_{-1} ([D]_{eq} - [D])}{k_2 [A] + k_{-1}}$$

$$\frac{d[D]}{dt} = \frac{k_2 k_1 [B]([A]^2 - [A]_{eq}^2) + k_{-2} k_{-1}([D]_{eq} - [D])}{k_2[A] + k_{-1}}$$

$$\frac{d[D]}{dt} = \frac{k_2 k_1 [B]([A] - [A]_{eq})([A] + [A]_{eq}) + k_{-2} k_{-1}([D]_{eq} - [D])}{k_2[A] + k_{-1}}$$

With $[A] = [A]_0 - 2[D]$

$$\frac{d[D]}{dt} = \frac{k_2 k_1 [B]([A]_0 - 2[D] - [A]_{eq})([A] + [A]_{eq}) + k_{-2} k_{-1}([D]_{eq} - [D])}{k_2[A] + k_{-1}}$$

And $[A]_0 - [A]_{eq} = 2[D]_{eq}$

$$\frac{d[D]}{dt} = \frac{k_2 k_1 [B] 2([D]_{eq} - [D])([A] + [A]_{eq}) + k_{-2} k_{-1}([D]_{eq} - [D])}{k_2[A] + k_{-1}}$$

And $[A]_{eq} = 2[D]_{eq} - [A]_0$

$$\frac{d[D]}{dt} = \frac{k_2 k_1 [B] 2([D]_{eq} - [D])([A]_0 - 2[D] + 2[D]_{eq} - [A]_0) + k_{-2} k_{-1}([D]_{eq} - [D])}{k_2[A] + k_{-1}}$$

$$\frac{d[D]}{dt} = \frac{k_2 k_1 [B] 2([D]_{eq} - [D])^2 + k_{-2} k_{-1}([D]_{eq} - [D])}{k_2[A] + k_{-1}}$$

$$\frac{d[D]}{dt[D]_{eq} - [D]} = \frac{k_2 k_1 2[B]([D]_{eq} - [D]) + k_{-2}k_{-1}}{k_2[A] + k_{-1}}$$

Substituting

$$[D]_{eq} - [D] = \frac{[A] - [A]_{eq}}{2}$$

Leads to

$$\frac{d[D]}{dt[D]_{eq} - [D]} = \frac{k_2 k_1 [B]([A] - [A]_{eq}) + k_{-2}k_{-1}}{k_2[A] + k_{-1}}$$

With $k_2[A] >> k_{-1}$ and

$[A] - [A]_{eq} \approx [A]$

This simplification can be used because $[A]_{eq}$ is coming from the equilibrium A + C ⇌ D (see above, here $[A]_{eq}$ as well as [C] are very small) and not from the overall equilibrium 2A + B ⇌ D.

$$k_{obs} = k_1[B] + \frac{k_{-2}k_{-1}}{k_2[A]}$$

10 | Eyring plot of k_1

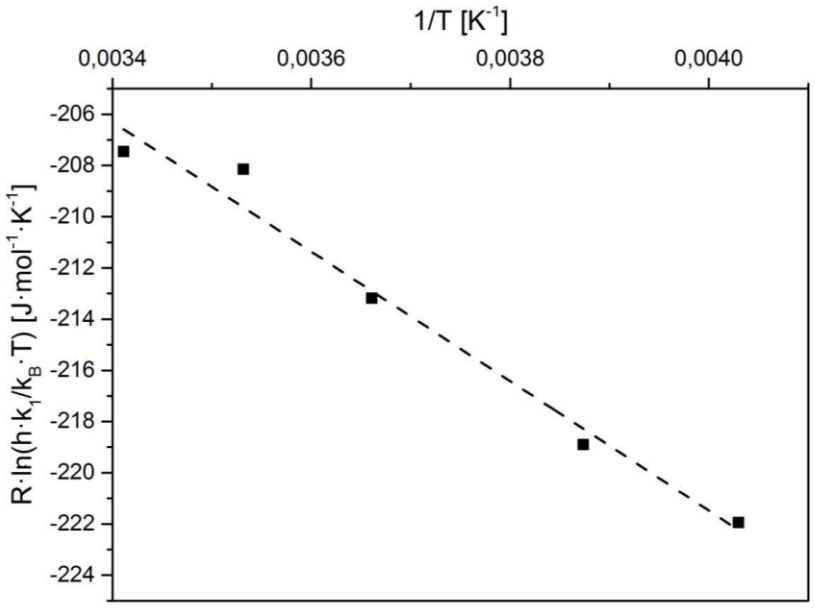

Figure S9. Eyring plot of k_1.

11 | Crystallographic data of $[Cu_2(Pim^{iPr2})_2](CF_3SO_3)_2$

The structure of $[Cu_2(Pim^{iPr2})_2](CF_3SO_3)_2$ was solved in the orthorhombic space group *Pnnm*. The asymmetric unit contains half of a dimer and one triflate anion summed up over several positions. The dimer and the anions are all located on the mirror planes, causing disorder of one iPr-group of the ligand and two of the triflate positions, which were also found to be disordered in itself. The structure was refined using similarity restraints on anisotropic displacement parameters and advanced rigid bond restraints and the disorder with the help of additional same distance restraints and restraints to U_{ij} components to approximate isotropic behavior. Some disordered atoms were set to the same anisotropic displacement parameters. The unit cell also contains heavily disordered solvent molecules, for which SQUEEZE was used to include a bulk solvent model into the refinement. SQUEEZE identified four independent voids located at 0.3 0.6 0.0, 0.7 0.4 0.0, 0.2 0.1 0.5 and 0.8 0.9 0.5, each containing the equivalent of 20 electrons in 92 Å^3.

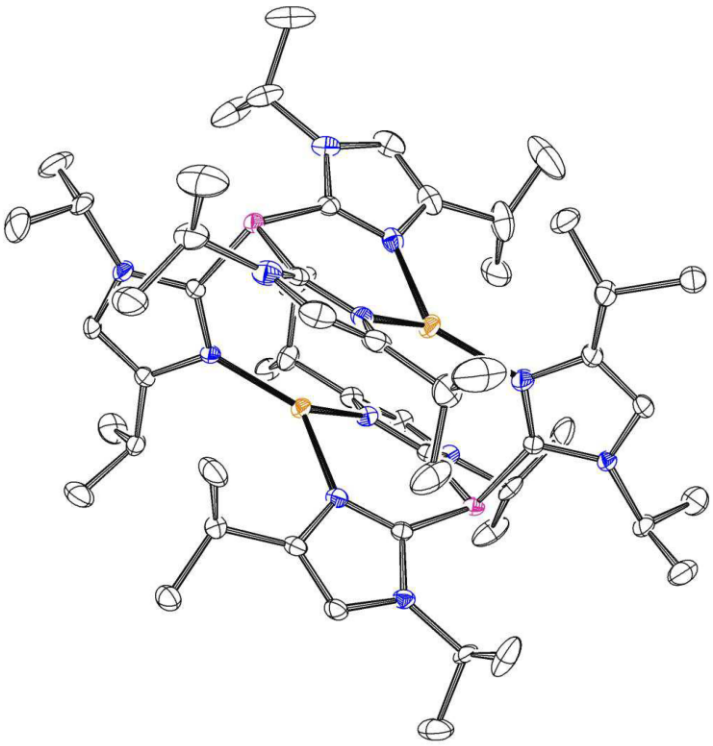

Figure S10. ORTEP plot of $[Cu_2(Pim^{iPr2})_2](CF_3SO_3)_2$. Anions, disorder and hydrogen atoms omitted for clarity. Thermal ellipsoid propability set to 50%.

Table 23. Crystal data and structure refinement for $[Cu_2(Pim^{iPr2})_2](CF_3SO_3)_2$.

CCDC No	2001564	
Empirical formula	$C_{56}\ H_{90}\ Cu_2\ F_6\ N_{12}\ O_6\ P_2\ S_2$	
Formula weight	1394.53	
Temperature	100(2) K	
Wavelength	0.71073 Å	
Crystal system	Orthorhombic	
Space group	*Pnnm*	
Unit cell dimensions	a = 19.7092(8) Å	α= 90°.
	b = 23.2380(9) Å	β= 90°.
	c = 15.2637(6) Å	γ = 90°.
Volume	6990.8(5) $Å^3$	
Z	4	
Density (calculated)	1.325 Mg/m^3	
Absorption coefficient	0.783 mm^{-1}	
F(000)	2928	
Crystal size	0.796 x 0.279 x 0.210 mm^3	
Theta range for data collection	1.596 to 25.027°.	
Index ranges	$-23 \le h \le 23, -27 \le k \le 27, -18 \le l \le 18$	
Reflections collected	106440	
Independent reflections	6438 [R(int) = 0.1332]	
Completeness to theta = 25.027°	100.0 %	
Absorption correction	Semi-empirical from equivalents	
Refinement method	Full-matrix least-squares on F^2	
Data / restraints / parameters	6438 / 1491 / 533	
Goodness-of-fit on F^2	1.060	
Final R indices [I>2σ(I)]	R_1 = 0.0511, wR_2 = 0.1147	
R indices (all data)	R_1 = 0.0887, wR_2 = 0.1317	
Largest diff. peak and hole	0.776 and -0.444 $e.Å^{-3}$	

12 | Superfocus mixer

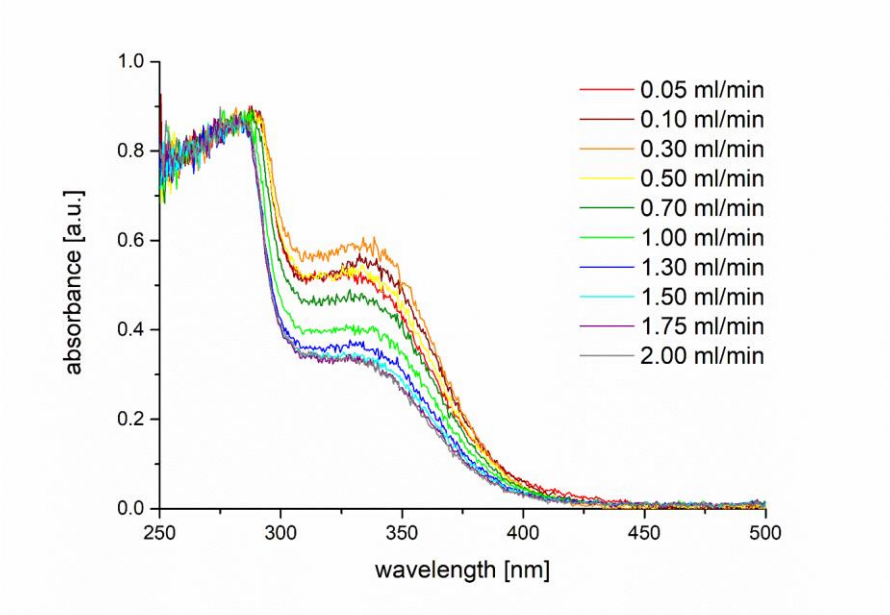

Figure S10.2. Measurements in a SuperFocus mixer at 25°C in methanol

13 | Decay of 2

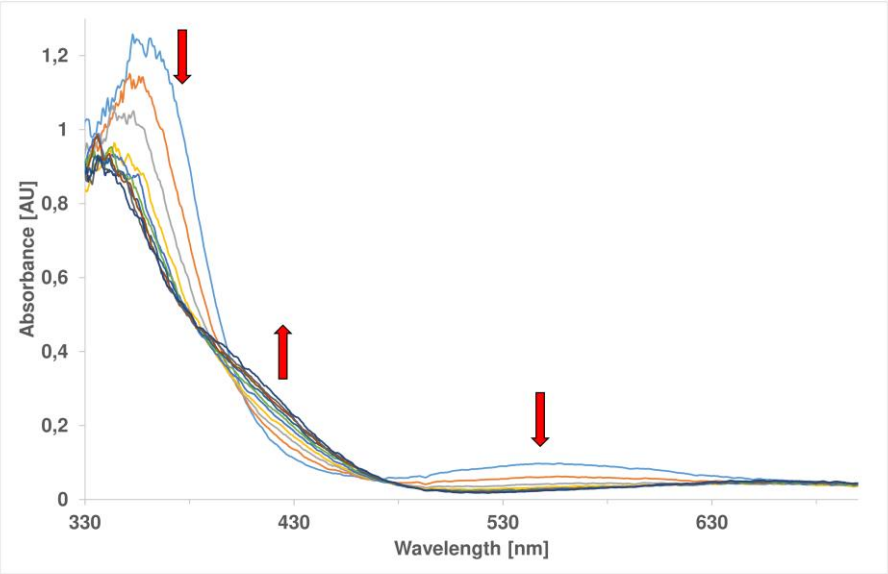

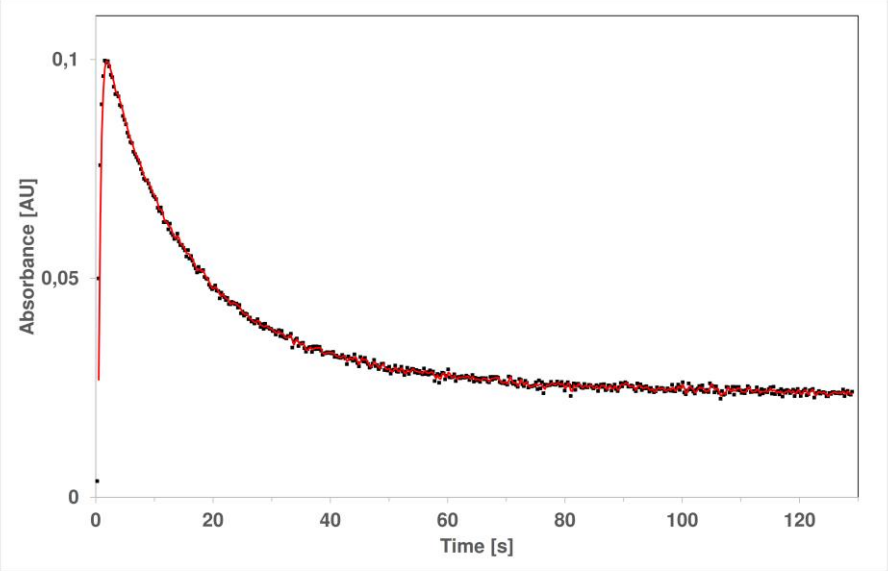

Figure S11. (a) Time resolved UV-Vis spectra for the decay of 2 in methanol ([1] = 0.4 mmol/L, $[O_2]$ = 5.2 mmol/L, T = 25 °C). (b) Absorbance vs. time trace and fit at 540 nm)

14 | Eyring plot for the decay of 2

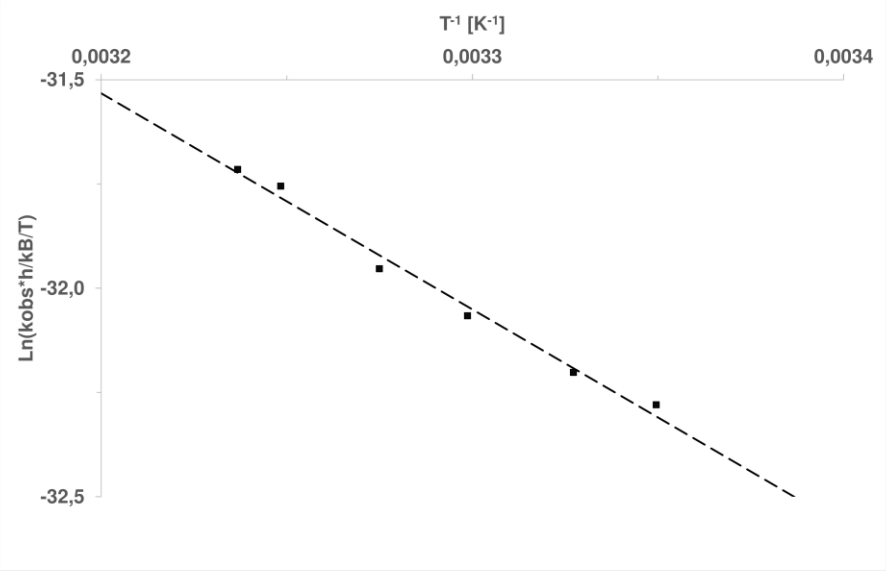

Figure S12. Eyring plot for the decay of 2 in methanol ([1] = 0.4 mmol/L, [O_2] = 5.2 mmol/L, temperature was varied between + 25 - 36 °C).

15 | References

[1] L. Krause, R. Herbst-Irmer, G. M. Sheldrick, D. J. Stalke *Appl. Cryst.* **2015**, 48, 3–10

[2] G. M. Sheldrick *Acta Cryst. A* **2015**, 71, 3–8

[3] G. M. Sheldrick *Acta Cryst. C* **2015**, 71, 3–8

[4] https://www.ccdc.cam.ac.uk/structures/

[5] P. Müller *Cryst. Rev.* **2009**, 15(1), 57

[6] A. Thorn, B. Dittrich, G. M. Sheldrick *Acta Cryst. A* **2012**, 68, 448

[7] H. Parsons, H. D. Flack, T. Wagner *Acta Cryst. A* **2013**, 69, 249-259

[8] A. L. Spek *Acta Cryst. C* **2015**, 71, 9

[9] A. L. Spek *Acta Cryst. D* **2009**, 65, 148

4.2 | Kinetische Studie zur Bildung von Eisen(III)-peroxido-Komplexen

Diese Arbeit wurde in der Fachzeitschrift *European Journal of Inorganic Chemistry* veröffentlicht.

A Mechanistic Study on the Reaction of Non-Heme Diiron(III)-Peroxido Complexes with Benzoyl Chloride

Markus Lerch, Andreas J. Achazi, Doreen Mollenhauer, Jonathan Becker, Siegfried Schindler, *Eur. J. Inorg. Chem.*, **2021**, 4122-4132.

doi.org/10.1002/ejic.202100711

EurJIC
European Journal of Inorganic Chemistry

Full Papers
doi.org/10.1002/ejic.202100711

Chemistry Europe
European Chemical Societies Publishing

VIP *Very Important Paper*

A Mechanistic Study on the Reaction of Non-Heme Diiron (III)-Peroxido Complexes with Benzoyl Chloride

Markus Lerch,[a] Andreas J. Achazi,[b] Doreen Mollenhauer,[b] Jonathan Becker,[a] and Siegfried Schindler*[a]

Dinuclear iron peroxido complexes are important intermediates for selective oxidation reactions. A detailed kinetic study of the reaction of benzoyl chloride (BzCl) with a dinuclear iron non-heme *cis end-on* peroxido complex with the ligand EtHPTB (*N,N,N′,N′*-tetrakis[(*N*-ethyl-2-benzimidazolyl)methyl]-2-hydroxy-1,3-diamino-propane) had been performed. The starting complex, the iron peroxido complex, can be obtained either by reaction of the iron(II) complex with O_2 or instead, applying the corresponding iron(III) complex together with hydrogen peroxide. Using low temperature stopped-flow measurements allowed to obtain activation parameters and in combination with a Hammet plot it was possible to postulate a mechanism for the formation of a perbenzoate complex prior to its decomposition. Furthermore, the direct reaction of the dinuclear iron(III) EtHPTB complex with peracetic acid was analyzed. Additionally, in comparison a mononuclear non-heme iron complex with the ligand bztpen (*N*-benzyl-*N,N′,N′*-tris(2-pyridylmethyl)ethane-1,2-diamine) was investigated as well.

Introduction

Selective oxidation/oxygenation reactions of organic substrates are important in the lab and in industry.[1] Efforts to substitute oxidants that are either expensive and/or quite toxic, e.g. chromium(VI) compounds, led to an intensive research on the development of functional model complexes for the active sites of metalloenzymes, especially oxygenases.[2] For example cyanobacterial aldehyde deformylating oxygenase (ADO) catalyzes the conversion of fatty aldehydes into alkanes and formate.[3] Recently Kaizer and co-workers reported the complex $[Fe^{III}_2(\mu\text{-}O_2)(MeBzim\text{-}Py)_4(MeCN)_2]^{4+}$ as a functional model for this enzyme by applying an iron complex with the ligand MeBzim-Py (2-(2′-pyridyl)-*N*-methylbenzimidazole; Scheme 1). In that context they furthermore pointed out the mechanistic versatility of peroxido-diiron(III) intermediates.[4]

We and others have been investigating in great detail the reactivity of iron complexes with the ligand RHPTB (Scheme 1) towards dioxygen and hydrogen peroxide.[5] The dinuclear iron (II) complex $[Fe_2(EtHPTB)(OBz)]^{2+}$ (**1a**, R=Et; EtHPTB = *N,N,N′,N′*-tetrakis[(*N*-ethyl-2-benzimidazolyl)methyl]-2-hydroxy-1,3-diamino-propane) reacts with O_2 to the *cis end-on* peroxido complex $[Fe_2(EtHPTB)(\mu\text{-}1,2\text{-}O_2)(OBz)(X)]^{n+}$ (**2a**, X = solvent or co-ligand).[5c] While under these conditions the formed peroxido complex is only persistent for a short time, it is possible to increase its stability by preparing it from the corresponding iron (III) complexes, $[Fe_2(RHPTB)(X)_m]^{n+}$ in combination with hydrogen peroxide.[5b] This reaction was investigated in acetonitrile as well as in methanol leading to the same results.[6] Furthermore, the reaction of the mononuclear iron(III) complex $[Fe(bztpen)(OMe)](ClO_4)_2$ (**3**$(ClO_4)_2$; bztpen = *N*-benzyl-*N,N′,N′*-tris(2-pyridylmethyl)ethane-1,2-diamine) with hydrogen peroxide had been analyzed.[7] An *end-on* hydroperoxido complex was formed that could be transformed into a *side-on* peroxido species after the addition of a base.[7b] Interestingly, the corresponding iron (II) complex did not react with dioxygen (neither with carbon monoxide), only with nitrogen oxide a reaction occurred.[7c]

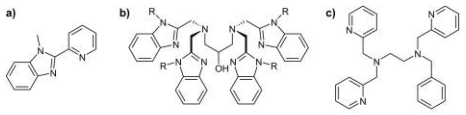

Scheme 1. a) MeBzim-Py, b) RHPTB (R = Et: EtHPTB), c) bztpen.

With regard to the formation of percarboxylate species as important intermediates in oxygenation reactions we report herein our results on the reaction of the iron(III) peroxido complex with EtHPTB as ligand and benzoyl chloride (BzCl) together with some related reactions.

Results and Discussion

The iron(III) complex $[Fe_2(EtHPTB)(OH)_2(MeOH)_2](ClO_4)_3$ (**1b**-$(ClO_4)_3$) was prepared in good yields by reacting the ligand

[a] *M. Lerch, Dr. J. Becker, Prof. Dr. S. Schindler*
Institute of Inorganic and Analytical Chemistry,
Justus-Liebig-Universität Gießen
Heinrich-Buff-Ring 17, 35392 Gießen, Germany
E-mail: siegfried.schindler@anorg.chemie.uni-giessen.de
https://www.uni-giessen.de/fbz/fb08/Inst/iaac/schindler
[b] *Dr. A. J. Achazi, Prof. Dr. D. Mollenhauer*
Institute of Physical Chemistry,
Justus-Liebig-Universität Gießen
Heinrich-Buff-Ring 17, 35392 Gießen, Germany

Supporting information for this article is available on the WWW under https://doi.org/10.1002/ejic.202100711

EurJIC
European Journal of Inorganic Chemistry

Full Papers
doi.org/10.1002/ejic.202100711

Chemistry Europe
European Chemical Societies Publishing

EtHPTB with iron(III) perchlorate and Et_3N in methanol. The molecular structure of **1 b** is shown in Figure 1 (crystallographic data of **1 b**$(ClO_4)_3$ are reported in the Supporting Information; Figure S2). The molecular structure of this complex is very similar to the complex $[Fe_2(EtHPTB)(H_2O)_2(OMe)(MeOH)](ClO_4)_4$ that had been reported previously by Avenier *et al.*[8] Here, water molecules are coordinated instead of hydroxide anions and one of the methanol ligands is deprotonated. A direct comparison of the two structures reveals that the angle spanned between the iron centers and the alcoholate oxygen is somewhat larger (angle Fe1-O1-Fe2: Avenier 131.1°; this work 128.5°) and this also results in a greater distance between the iron centers (distance Fe1–Fe2: Avenier 3.65 Å; this work 3.61 Å). In contrast to our synthetic protocol described herein, the authors did not apply triethylamine to prepare the iron(III) complex and did not recrystallize the product. Furthermore, **1 b** can be compared with $[Fe_2(HPTB)(\mu\text{-}OH)(NO_3)_2](NO_3)_2$ that had been investigated previously.[9]

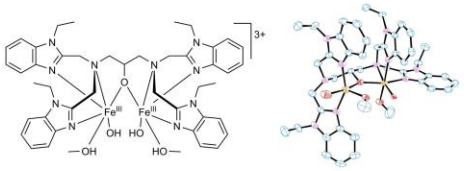

Figure 1. Complex **1 b** $[Fe_2(EtHPTB)(OH)_2(MeOH)_2]^{3+}$ (left). Molecular structure (ORTEP drawing; 50% probability) of the cation of **1 b**$(ClO_4)_3 \times 3$ MeOH. Uncoordinated 3 perchlorate anions and 3 methanol molecules are omitted for clarity (right).

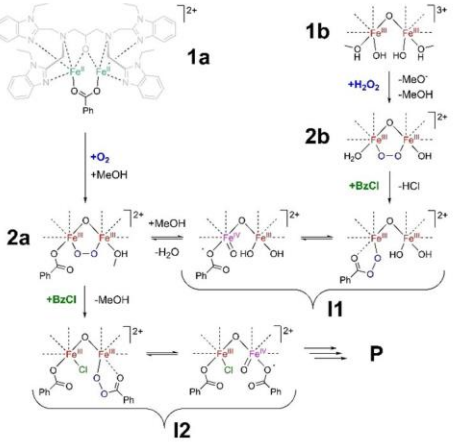

Scheme 2. Proposed reaction mechanism for the formation of **I2**.

Reaction of 1 b with H_2O_2

When a solution of **1 b**$(ClO_4)_3$ was reacted with hydrogen peroxide in methanol, a color change from a pale yellow color to a turquoise color was observed, which indicates the formation of an iron peroxido complex (**2 b**, Scheme 2) as described previously (Figure 2).[5b]

ESI-MS measurements support the assumption that the formation of the peroxido complex $\{[Fe_2(EtHPTB)(\mu\text{-}1,2\text{-}O_2)(OH)(H_2O)] + MeOH\}^{2+}$ is the main species under these conditions (compare Figure S5 and S6). One equivalent of H_2O_2 is enough for complete formation of **2 b** (Figure S9). The reaction in methanol is quite fast (completed within 1 s at RT) and the turquoise-colored solution is stable for a few minutes under these conditions. As previously described, this reaction can be followed by applying stopped-flow techniques.[5b] Time-resolved spectra are shown in Figure 3.

The peroxido complex is characterized by the main absorbance at 605 nm with a molar attenuation coefficient ε of 2200 $L\,mol^{-1}\,cm^{-1}$ under our conditions which compares well with data of the literature with other solvents.[5b,c]

Absorbance vs. time traces under pseudo-first-order conditions ($[H_2O_2] \gg [1\,b]$) could be fitted using single exponential functions. As observed previously a plot of the obtained rate constants k_{obs} vs. the hydrogen peroxide concentration at different temperatures exhibited a linear dependence without

Figure 2. Reaction of **1 b** with hydrogen peroxide, followed by the addition of benzoyl chloride.

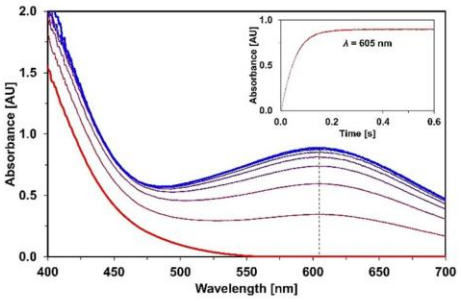

Figure 3. Time-resolved UV-vis spectra ($\Delta t = 0.03$ s) of the reaction between complex **1 b** ($c = 0.4$ mmol L^{-1}) and hydrogen peroxide ($c = 20.0$ mmol L^{-1}) at 25.0 °C in methanol (concentrations after mixing). The inset shows the time-trace of the reaction.

EurJIC
European Journal of Inorganic Chemistry

Full Papers
doi.org/10.1002/ejic.202100711

Chemistry Europe
European Chemical Societies Publishing

an intercept (Figure 4) and thus leading to an overall second-order rate law (Equation 1).

$$\frac{d[\mathbf{2b}]}{dt} = k_2\,[\mathbf{1b}]\,[H_2O_2] \quad (1)$$

An Eyring plot of the derived second-order rate constants over a much larger temperature range from −50.0 to +25.0 °C (Figure 5) allowed the calculation of the activation parameters to $\Delta H^{\ddagger} = 46 \pm 1$ kJ mol^{-1} and $\Delta S^{\ddagger} = -40 \pm 2$ J mol^{-1} K^{-1}. Data compare reasonable well with previous results of the $[Fe_2(HPTB)(\mu\text{-}OH)(NO_3)_2](NO_3)_2$ with $\triangle H^{\ddagger} = 53 \pm 3$ kJ mol^{-1} and $\triangle S^{\ddagger} = -17 \pm 1$ J mol^{-1} K^{-1} (see Table 1).[5b]

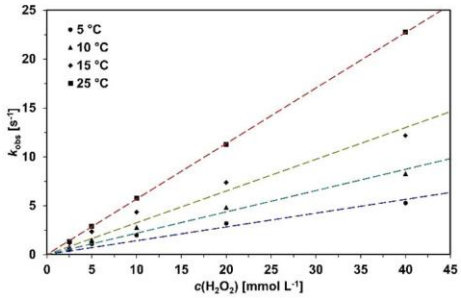

Figure 4. Plot of the rate constants k_{obs} versus H_2O_2 concentration at different temperatures. Complex concentration: $c = 0.2$ mmol L^{-1}. Second-order rate constant $k_{2(25°C)} = 568 \pm 2$ L mol^{-1} s^{-1}.

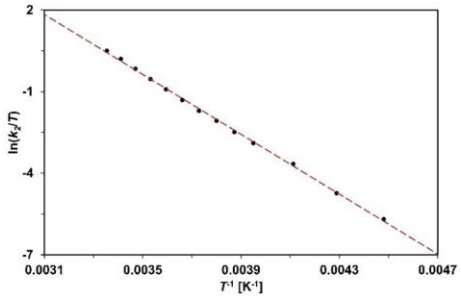

Figure 5. Eyring plot for the reaction of complex **1b** ($c = 0.4$ mmol L^{-1}) with H_2O_2 ($c = 20$ mmol L^{-1}) in the temperature range from −50.0 to 25.0 °C.

Table 1. Summary of molar attenuation coefficient, rate constants and activation parameters of the kinetically investigated reactions in this study.

Reaction in MeOH	BzCl derivative	λ_{max} [nm]	$k_{2\,(25\,°C)}$ [L mol^{-1} s^{-1}]	$\Delta H^{\ddagger}$ [kJ mol^{-1}]	$\Delta S^{\ddagger}$ [J K^{-1} mol^{-1}]
1b + H_2O_2 (→ **2b**)		600	568 ±2	46 ±1	-40 ±2
2b + BzCl (→ **I2**)	BzCl	445	ND	40 ±1	11 ±3
	BzCl	600	9.7 (±0.3) 10^5 [a]	40 ±1	10 ±3
	p NO_2-BzCl	445	ND	67 ±3	21 ±8
	p N(Me)$_2$-BzCl	445	ND	69 ±1	39 ±2
2a + BzCl (→ **I2**)	BzCl	450	243 ±10 [b]	36 ±1	-33 ±6
1b + PAA		440	455 ±25 [c]	32 ±1	-48 ±6

[a] k_3 third-order constant. ND = not determined. [b] At −60 °C. [c] At −65 °C.

Reaction of 2b with benzoyl chloride

The reaction of the peroxido complex **2b** with BzCl was investigated in methanol because no reaction was observed in acetonitrile (only decomposition of **2b** was detected). Furthermore, we did not assert an influence of different R-groups in RHPTB (Scheme 1) on the reactivity. Iron(III) complexes with the unsubstituted ligand HPTB (R=H) and BnHPTB (R=Bn) showed the same reactivity towards H_2O_2 and the subsequent reaction with benzoyl chloride. As shown in Figure 2 a rapid color change to a gold-brown-colored solution was observed when **2b** was reacted with benzoyl chloride in excess. Time-resolved UV-vis-spectra were recorded in stopped-flow measurements at low temperatures (Figure 6).

The decay of the absorbance maximum at 605 nm of **2b** (premixed immediately prior to the measurement applying an excess of H_2O_2) can be observed while at the same time a new compound is formed, characterized with an absorbance maximum at 445 nm. Two isosbestic points are observed at 415 and 515 nm. Absorbance vs. time traces again could be fitted perfectly well to a single exponential function, however a plot of k_{obs} vs. c(BzCl) turned out to be nonlinear. Instead, to obtain a linear correlation, it was necessary to plot k_{obs} vs. $c(\text{BzCl})^2$ (Figure 7) leading to a third-order rate law with $k_{obs} = k_3\,c(\text{BzCl})^2$ (Equation 2).

$$\frac{d[\mathbf{I2}]}{dt} = k_3\,[\mathbf{2b}]\,[\text{BzCl}]^2 \quad (2)$$

Third-order rate constants obtained here ($k_{3(25°C)} = 9.7 \pm 0.3 \times 10^5$ L^2 s^{-1} mol^{-2}) compare well with those measured for other

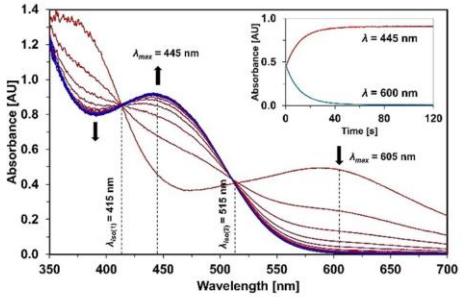

Figure 6. Time-resolved UV-vis spectra ($\Delta t = 7.4$ s) of the reaction between **2b** ($c = 0.2$ mmol L^{-1}, obtained by premixing **1b** with an excess of H_2O_2) and BzCl ($c = 20.0$ mmol L^{-1}) at −80.0 °C. Molar attenuation coefficient $\varepsilon_{445} = 4300$ L mol^{-1} cm^{-1}. The inset shows the time-traces of the reaction.

EurJIC
European Journal of Inorganic Chemistry

Full Papers
doi.org/10.1002/ejic.202100711

Chemistry Europe
European Chemical Societies Publishing

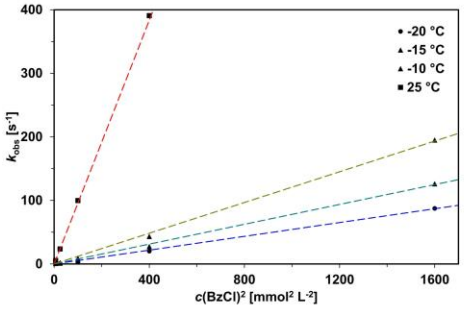

Figure 7. Plot of k_{obs} vs. $c(BzCl)^2$ at different temperatures. Concentration $c(\mathbf{2b}) = 0.2$ mmol L^{-1}.

reactions that showed a third-order rate law e.g. $NO + O_2$ with a rate constant of 2.1×10^6 $L^2 s^{-1} mol^{-2}$ at 25 °C[10] (depending on the conditions slightly different values)[11] in aqueous solutions and non-aqueous media were obtained.[12]

Since the sole kinetic interpretation does not yet provide any evidence that exactly two benzoyl chloride molecules react with the peroxido complex, a substoichiometric addition was also carried out here. A clear linearity can be seen up to the second equivalent benzoyl chloride added (Figure S10). This observation supports the assumption that exactly two molecules of benzoyl chloride react with **2b** during the reaction with benzoyl chloride. Furthermore, to exclude that benzoyl peroxide is an active reagent herein (it is synthesized in industry from benzoyl chloride with hydrogen peroxide in alkaline solutions), several test reactions with ABTS (2,2′-azino-bis(3-ethylbenzothiazoline-6-sulfonic acid) diammonium salt) were performed. ABTS is a reagent that is used to detect radicals and selectively peroxycarboxylic acids in the presence of H_2O_2.[13] Benzoyl peroxide reacts rapidly with ABTS, however, much slower in comparison with the reaction of complex **2b** with BzCl and hydrogen peroxide. BzCl together with hydrogen peroxide in methanol with a small amount of NaOH only reacts quite slowly with ABTS. Benzoyl peroxide itself does not react with complex **2b**. These experiments clearly indicate that the reaction occurs with BzCl.

From these results we propose that an intermediate, **I1**, is formed from **2b** and BzCl. The Intermediate **I1** stands in a rapid equilibrium with the peroxido complex **2a** which then reacts in a much slower reaction (rate-determining step, RDS) to the metastable product **I2** according to Scheme 2. Other third-order reactions in solution have been described previously (e.g.)[14] with a similar mechanistic scenario. After the very fast formation of **I2**, much slower decomposition reactions took place including the formation of products **P** such as benzoic acid, methyl benzoate, benzoic acid anhydride as well as iron(III) chloride (detected as $[FeCl_4]^-$). These products could be identified by ESI-MS measurements. An ESI-MS measurement of a dilute mixture of **2b** with BzCl in a ratio of 1:2 (measurement performed instantly after mixing) showed the possible formation of $[Fe_2(EtHPTB)(OOBz)(OH)_2]^{2+}$ with $m/z = 502.1$ as a direct derivative of **I1** (Figure S7). The formation of methyl benzoate and benzoic acid anhydride could be a hint of a free radical mechanism (iron(IV)oxido/benzoato radical-pathway), as these products are formed due to recombination reactions.

For a more detailed analysis we applied *para*-substituted BzCl derivatives with the electron-withdrawing groups –Cl, $-NO_2$ and electron-donating groups $-N(Me)_2$, –OMe, –Me for the reaction with **2b**. Besides BzCl (temperature range between −80.0 and 0.0 °C) we performed measurements with *p*$N(Me)_2$-BzCl and *p*NO_2-BzCl in a temperature range between 15.0 and 50.0 °C. From the temperature dependence the corresponding Eyring plots (Figure S11) allowed calculations of the activation parameters with BzCl: $\Delta H^{\neq} = 40 \pm 1$ kJ mol^{-1} and $\Delta S^{\neq} = 10 \pm 3$ J $mol^{-1} K^{-1}$; *p*$N(Me)_2$-BzCl: $\Delta H^{\neq} = 69 \pm 1$ kJ mol^{-1}, $\Delta S^{\neq} = 39 \pm 2$ J $mol^{-1} K^{-1}$; *p*NO_2-BzCl: $\Delta H^{\neq} = 67 \pm 3$ kJ mol^{-1}, $\Delta S^{\neq} = 21 \pm 8$ J $mol^{-1} K^{-1}$ (see Table 1). The slightly positive activation entropies indicate a dissociative interchange mechanism.

Hammett Plot

The Hammett correlation (a linear free energy relationship) is a widely used method to evaluate the impact of electrosterical effects on reactions. This correlation allows conclusions to be drawn about the transition state of the rate-determining step (RDS) of the observed reaction. Figure 8 shows the Hammett plot for the reaction of **2b** with *para*-substituted benzoyl chloride. In this study only *para*-substituted benzoyl chlorides were used, due to possible steric hindrance of *meta*-substituents. The Hammett plot leads to a V-shape from the two linearly fitted points that intersect near by a σ-value of 0 (unsubstituted BzCl).

Overall it is obvious, that electron-withdrawing (*p*Cl, *p*NO_2) and electron-donating (*p*$N(Me)_2$, *p*OMe, *p*Me) substituents slowed down the reaction. The V-shape indicates a change in the reaction mechanism, in which the electron-rich *p*$N(Me)_2$-BzCl is more nucleophilic ($\rho = -1.996$) and the electron-poor *p*NO_2-BzCl is more electrophilic ($\rho = 0.477$). This provides

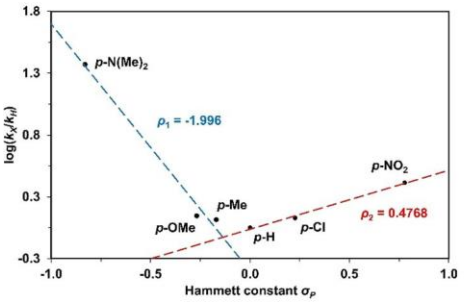

Figure 8. Hammett plot for the reactions of **2b** with *para*-substituted BzCl-derivatives (substituent = $-N(Me)_2$, –OMe, –Me, –Cl, $-NO_2$) at −60.0 °C in MeOH.

EurJIC
European Journal of Inorganic Chemistry

Full Papers
doi.org/10.1002/ejic.202100711

Chemistry Europe
European Chemical Societies Publishing

valuable information about the location of the RDS and transition state (TS). The strong negative ρ-value clearly indicates a build-up of a positive charge in the TS of the RDS, whereas the slightly positive ρ-value indicates a build-up of a positive charge in the TS of the RDS. In combination with the slightly positive activation entropies of the reaction between **2b** and pNO$_2$-BzCl resp. pN(Me)$_2$-BzCl (indicating a dissociative interchange mechanism) two different reaction pathways can be proposed. A possible mechanism for both reaction pathways is presented in Scheme 3.

In the reaction pathway with pN(Me)$_2$-BzCl, the C–Cl bond is severely weakened or even broken in the TS of the RDS, which is due to the high positive charge on the carbonyl carbon. On the other hand, the slightly positive ρ-value in the pNO$_2$–BzCl reaction pathway can be interpreted as a partially accomplished nucleophilic attack on the carbonyl carbon of the benzoyl chloride. In any case, it can be confirmed that benzoyl chloride is actively involved in the RDS of the whole reaction sequence.

In contrast to our system, no effect on para-substitution was observed with the system of Kripli and co-workers, where a ρ-value of zero was obtained.[4] Therefore, for their reaction mechanism a nucleophilic attack of the peroxido-diiron(III) complex as rate-determining step had been excluded.

Reaction of iron(II) complex 1a with O_2 and benzoyl chloride

As described in the introduction, the iron(II) complex $[Fe_2(EtHPTB)(OBz)]^{2+}$ (crystallographic data of **1a**$(BPh_4)_2$ are reported in the Supporting Information; see Figure S1) reacts with dioxygen to form the peroxido complex **2a** (Scheme 2). Therefore, to gain further support for the proposed mechanism of the reaction of **2b** with BzCl we also investigated the reaction of **2a** with BzCl (the benchtop experiment is reported in the Supporting Information, Figure S12 and S13). To accomplish this we used a double-mixing stopped-flow unit with four syringes (syringe 1: solution of **1a**; syringe 2: solvent saturated with dioxygen; syringe 3: solvent saturated with argon; syringe 4: solution of BzCl). Because of the poor solubility of **1a**$(BPh_4)_2$ in MeOH, the reaction was performed with 5% MeCN as co-solvent. Time-resolved UV-vis spectra of this reaction are presented in Figure 9.

A plot of the k_{obs}-values vs. BzCl-concentration allowed a linear fit with an intercept C (Figure S13) leading to an overall second-order rate law (Equation 3).

$$\frac{d[\mathbf{I2}]}{dt} = k_2\,[\mathbf{2a}]\,[\mathrm{BzCl}] + C \qquad (3)$$

The reaction is a bit faster than the reaction of **2b** with BzCl. However, this is easy to understand because here a benzoate is already coordinated to the complex and therefore only has to react further with BzCl. Overall, this supports our postulated mechanism (Scheme 2). The reaction was measured in a temperature range between −70.0 and −40.0 °C and from an Eyring plot (Figure S14) of the second-order rate constants the activation parameters could be calculated to $\Delta H^{\ddagger} = 36 \pm 1$ kJ mol^{-1} and $\Delta S^{\ddagger} = -33 \pm 6$ J mol^{-1} K^{-1} (see Table 1). The slightly negative activation entropy indicates an interchange associative mechanism, again in accordance with our postulated mechanism. The intercept we observed for the plot of the k_{obs}-values vs. c(BzCl) (Figure S14) is a bit more difficult to interpret. While we think we can exclude a reversible reaction at this point it could be possible that to some part acetonitrile is coordinated that needs to dissociate prior to the bonding of BzCl, leading to a reaction step independent of c(BzCl) and thus causing an intercept. However, it also could be caused by the equilibrium between **2a** and **I1**.

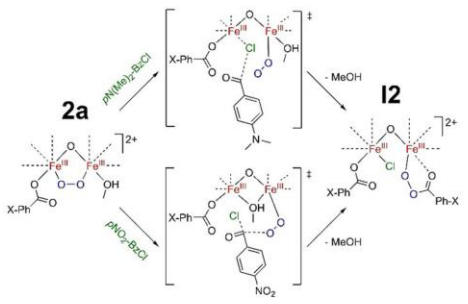

Scheme 3. Postulated mechanisms in dependence on different benzoyl chloride derivatives (electron-withdrawing or electron-donating groups in para position).

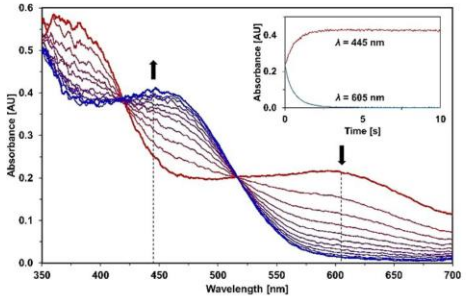

Figure 9. Time-resolved UV-vis spectra ($\Delta t = 0.14$ s) acquired from a double-mixing stopped-flow experiment in MeOH (5% MeCN) as cosolvent. The intermediate **2a** was generated by mixing 75 µL of solution **1a** ($c = 0.4$ mmol L^{-1}) with 75 µL oxygen-saturated methanol solution ($c = 10.4$ mmol L^{-1}). The first mixed solution was aged for 3 s. In the second mixing the generated peroxido complex **2a** reacted with 75 µL BzCl solution ($c = 40$ mmol L^{-1}) at −70 °C to trace the chromophore at $\lambda_{max} = 445$ nm (intermediate **I2**) and the decay of the peroxido complex **2a** at $\lambda_{max} = 605$ nm. The inset shows the time-traces over the course of 10 s.

EurJIC
European Journal of Inorganic Chemistry

Full Papers
doi.org/10.1002/ejic.202100711

Chemistry Europe
European Chemical Societies Publishing

DFT calculations

To gain further insights into the reaction from **2 b** with benzoyl chloride via the (assumed) **I1**, **2 a** and (assumed) **I2** to give a possible product **P**, a computational analysis was performed. The equilibrium structures and Gibbs energies of the involved complexes in solution were calculated with DFT for the concentrations used in the experiment (see Computational details). The results of the calculations are shown in Scheme 4.

The low-spin state with 0 unpaired electrons (singlet state with total spin quantum number $S=0$), the triplet state ($S=1$), quintet state ($S=2$), the septet state ($S=3$), nonet state ($S=4$) and the high-spin state with 12 unpaired electrons (tridecet state with total spin quantum number $S=6$) were energetically unfavorable for **2 b**, **I1-a**, **2 a** and **I2-a**. Instead, the undecet spin state ($S=5$) is most favorable for these iron complexes. The other iron complexes (Scheme 4) are very similar to **2 b**, **I1-a**, **2 a** and **I2-a**; therefore, we calculated them in an undecet spin state ($S=5$) as well. For the first step we assume that **2 b** reacts to **I1-a** (see Scheme 4). The reactions is exergonic and a Gibbs energy of $-48.1\ kJ\,mol^{-1}$ is gained. Three additional isomers (**I1-b** to **I1-d**) have been calculated for this step, but all are energetically less favorable. **I1-a** and **I1-c** are in agreement with the structures proposed in Scheme 2. The benzoate radical in complexes **I1-c** and **I1-d** is only loosely attached to the rest of the complex via π-π interaction and C–H···O hydrogen bonds. Thus, the iron atoms remain Fe^{III}. Furthermore, the spin state of the benzoate radical should have nearly no effect on the rest of the complex due to the large distance or loose attachment. Indeed, the nonet spin state ($S=4$) for **I1-c** and **I1-d** is energetically only $+0.1\ kJ\,mol^{-1}$ higher than the undecet spin state ($S=5$) for the same molecular structure.

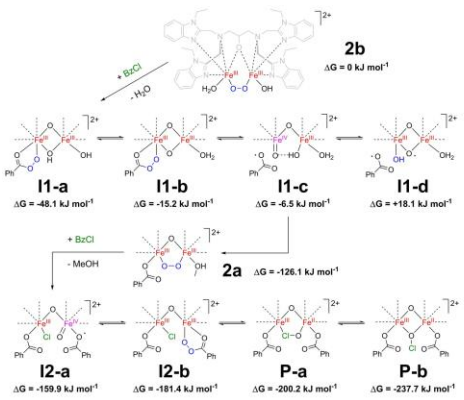

Scheme 4. Gibbs energies relative to **2 b** in conjugation with BzCl. $c(BzCl) = 0.04\ mol\,L^{-1}$. The electronic energies are calculated with B3LYP*-D3(BJ)/def2-TZVP COSMO(methanol). The ro-vibrational contributions are calculated with PBE0-D3(BJ)/def2-SVP, def2-TZVP. All iron complexes are in an undecet spin state ($S=5$).

Next an intramolecular formation takes place in **I1-a**, water is released, methanol binds to one iron atom resulting in **2 a**. The reaction is exergonic and a Gibbs energy of $-78.0\ kJ\,mol^{-1}$ is gained. From there, we assume that **2 a** reacts to **I2-a** and a Gibbs energy of $-33.8\ kJ\,mol^{-1}$ is gained. The shortest bond distance between an oxygen atom of the benzoate radical and the Fe^{IV}=O group of the undecet **I2-a** is 2.99 Å. This is a very long, and therefore, a weak bond. For comparison the bond distance between the benzoate anion and the Fe–Cl group of the undecet **I2-a** is only 1.96 Å. Like for **I1-c** and **I1-d**, the spin state of the loosely attached benzoate radical has nearly no effect on the rest of the **I2-a** complex. Hence, the nonet spin state is energetically very close to the undecet spin state (only $+0.5\ kJ\,mol^{-1}$ higher for the same molecular structure). As shown in Scheme 4, the benzoate radical in **I2-a** can react to a peroxybenzoate (**I2-b**). This intramolecular reaction is exergonic by $-21.5\ kJ\,mol^{-1}$ and both, the third oxygen of the peroxybenzoate and the chloride form weak bonds to the iron, which is connected to the peroxybenzoate. These results are in agreement with the proposed reaction in Scheme 2.

A possible next step is the intramolecular formation of a hypochlorite (**P-a**). The hypochlorite can reorient itself forming **P-b**, which is the most stable complex found in this study. The reaction from **2 a** over **I2-a**, **I2-b**, and **P-a** up to **P-b** is thermodynamically favorable. The formations of **I2-a**, **I2-b**, and **P-a** involve either the breaking or formation of an oxygen-oxygen bond as a key step. Thus, possible reaction barriers can be expected to be similar in all these cases.

Reactions of 1 b with peracids

To gain a better understanding of the overall mechanistic scenario **1 b** was furthermore reacted with percarboxylic acids. We excluded perbenzoic acid due to the danger involved with this compound and chose peracetic acid (PAA), *m*-chloroperbenzoic acid (mCPBA) and perdecanoic acid (PDA) instead. Perdecanoic acid was prepared according to the synthesis reported by Sitko *et al.*, however, so far no crystal structure of this compound had been reported.[15] We obtained crystals of perdecanic acid and the molecular structure together with crystallographic data are presented in the Supporting Information (Figure S4 and Table S4).

When **1 b** was reacted with an excess PAA in methanol, an orange-brown-colored solution formed (Figure S15) and peracetic acid adduct compounds could be detected in an ESI-MS spectrum (Figure S8). A *m/z* ratio at 1123.1 shows the presence of the peracetato complex $[Fe_2(EtHPTB)(OOAc)(OH)](+2ClO_4)^+$. In Figure 10 the characteristic UV-vis bands of the intermediates (**1 a** + O_2 + BzCl, **1 b** + H_2O_2 + BzCl and **1 b** + PAA) are compared.

Comparison with data from the literature for UV-vis data for iron(III) peroxyacetate complexes (in acetonitrile) are in accordance with our data and therefore also support our assignment of a peroxybenzoate complex discussed above.[16]

Efforts to crystallize and structurally characterize the intermediates **I1/I2** have been unsuccessful. So far (to the best of our knowledge) only one example of a structurally character-

EurJIC
European Journal of Inorganic Chemistry

Full Papers
doi.org/10.1002/ejic.202100711

Chemistry Europe
European Chemical Societies Publishing

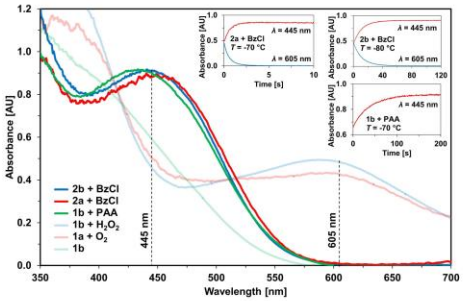

Figure 10. Comparison of the UV-vis spectra. The spectra of the monitored reactions were used, which showed the maximum absorption at 445 nm and 605 nm.

ized mononuclear non-heme iron(III) complex with a coordinating percarboxylic acid (PAA) had been reported.[17] However its UV-vis spectrum is completely different to the other known peroxyacetate iron complexes.

Time-resolved UV-vis spectra of the reaction of **1 b** with an excess of PAA (formation of **I2'**) at low temperatures are reported in the Supporting Information (Figure S15). A plot of k_{obs} values vs. c(PAA) could be fitted linear through the origin (Figure S16) leading to a second-order rate law (Equation 4).

$$\frac{d[\mathbf{I2'}]}{dt} = k_2\,[\mathbf{1b}]\,[PAA] \qquad (4)$$

An Eyring plot at temperatures between −70.0 and −40.0 °C (Figure S17) provides the activation parameters: $\Delta H^{\neq} = 32 \pm 1$ kJ mol^{-1} and $\Delta S^{\neq} = -48 \pm 3$ J mol^{-1} K^{-1} (see Table 1) indicating an interchange associative mechanism.

Reaction of **1 b** with mCPBA was sluggish and was not investigated further. A similar observation was described previously by Furutachi and co-workers.[17] PDA was applied in order to be able to react a highly pure peracid with complex **1 b** and thus to exclude other interfering components such as water. When analyzing time-resolved UV-vis spectra, only the formation of a peroxido adduct could be detected at low concentrations of percarboxylic acids. This is probably due to the direct oxidation of the coordinated hydroxides. However, applying high concentrations of the peracids PAA, mCPBA or PDA the formation of gold-brown-colored product solutions was observed. While the PAA adduct is stable for weeks at low temperatures the solutions of the mCPBA and PDA adducts turned to a blue-green-colored solution at −80 °C in less than an hour. Furthermore, PAA as well as mCPBA were tested for their reaction towards ABTS. The reaction turned out to be quite slow: about 3 min for peracetic acid and approximately 10 min for mCPBA.

Reactions with NEt_3

If the percarboxylate complex formed by the reaction of **2 b** + BzCl was reacted with NEt_3, a peroxido complex formed (the benchtop reaction is shown in Figure S18). Time-resolved spectra of the reaction of NEt_3 with premixed **2 b** + BzCl were obtained again with our double-mixing stopped-flow unit with four syringes and are presented in Figure 11. A plot of k_{obs} vs. [NEt_3] showed a linear dependence with intercepts (Figure S19).

This indicates a parallel or back reaction, most likely based on an acid/base equilibrium under the conditions applied.

An Eyring plot obtained from the k_2 values of the main reaction (Figure S20) did lead to the activation parameter $\Delta H^{\neq} = 49 \pm 1$ kJ mol^{-1}, $\Delta S^{\neq} = 9 \pm 4$ J mol^{-1} K^{-1}. With an activation entropy close to 0 this reaction follows an interchange pathway. The same reaction behavior was observed when premixed **1 a** + PAA (instead of **2 b** + BzCl) was reacted with NEt_3.

Reaction of $[Fe(bztpen)OOH]^{2+}$ with BzCl

To compare our results of a dinuclear iron complex system with a mononuclear iron complex we also investigated the reaction of the iron(III) complex with bztpen as ligand (Scheme 1). The complex [Fe(bztpen)(OMe)]$(ClO_4)_2$ (**3**$(ClO_4)_2$) has been prepared under aerobic conditions in methanol by combining bztpen, $Fe(ClO_4)_3$ and Et_3N in a ratio of 1:1:1. Crystals were obtained and the molecular structure together with crystallographic data are reported in the Supporting Information (Figure S3 and Table S3). The molecular structure compares well with [Fe^{III}-(bztpen)(OMe)]$(PF_6)_2$ reported previously.[18] It is well known from previous work that this complex reacts with hydrogen peroxide to a purple-colored *end-on* hydroperoxido complex, $[Fe(bztpen)(OOH)]^{2+}$.[7b] Time-resolved UV-vis spectra of this reaction are reported in the Supporting Information (Figure S21)

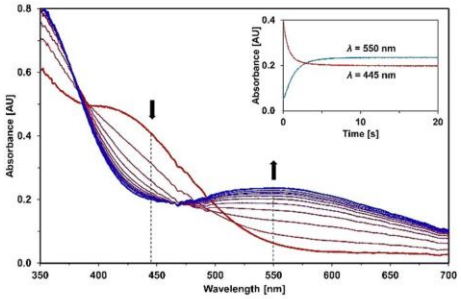

Figure 11. Time-resolved UV-vis spectra ($\Delta t = 0.42$ s) acquired from a double-mixing stopped-flow experiment in MeOH. The intermediate **I2** was generated by mixing 75 µL of a premixed solution of **2 b** ($c = 0.4$ mmol L^{-1}) with 75 µL H_2O_2 solution ($c = 20$ mmol L^{-1}). The first mixed solution was aged for 5 s. In the second mixing the generated intermediate **I2** reacted with 75 µL of an Et_3N solution ($c = 80$ mmol L^{-1}) at 0 °C to trace the decay at $\lambda = 445$ nm (**I2**) and the formation of a peroxido complex at $\lambda_{max} = 550$ nm. The diagram in the right corner shows the time-trace over the course of 20 s.

and kinetic data fit well with our previous results. However, in contrast to the reaction of **2b** with BzCl the reaction of $[Fe(bztpen)(OOH)]^{2+}$ with BzCl is complex (time resolved UV-vis spectra of this reaction are reported in the Supporting Information, Figure S22), indicating additional reactions take place that so far could not be analyzed.

In a subsequent reaction with a base such as Et_3N the hydroperoxido complex reacts to the corresponding *side-on* peroxido complex (turquoise). Interestingly, while the hydroperoxido complex reacts quite fast with benzoyl chloride the *side-on* peroxido complex did not react at all with BzCl.

Summary and Conclusion

In summary, we have studied the kinetics of the formation of peroxido complex **2b** (Fe^{III} complex **1b** + H_2O_2) and the subsequent reaction with benzoyl chloride in methanol in detail. We assume that the chromophore formed with λ_{max} = 445 nm is an iron(IV)oxido/carboxylato radical species **I1** that alternatively had been described as an iron(V)oxido-/carboxylato species (for PAA systems) according to the following equilibria presented in Scheme 5.[16a–c,e–i,19]

It turned out that the peroxido complex **2a**, formed in the reaction between Fe^{II} complex **1a** and O_2, was also able to react in the same way to form the chromophore at λ_{max} = 445 nm.

In contrast to previous publications that reported formation of iron(III)percarboxylates (mainly peracetate) in acetonitrile, our intermediates **I1/I2** herein were formed in the protic solvent methanol. Detailed kinetic studies were performed for the reaction of the peroxido complexes with benzoyl chloride and furthermore, the reaction of the iron(III) complex **1b** with peracetic acid.

From our kinetic investigations including a Hammet analysis we could propose a mechanism for the formation of the reactive intermediates, which is supported by a thermodynamic consideration of various intermediates using DFT calculations. They showed that the iron(III) species are more stable than the species with higher oxidized iron. The intermediates finally decompose to an almost colorless mixture of products that only in part could be identified.

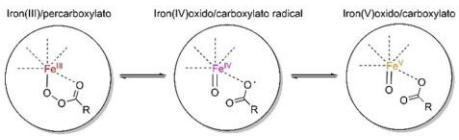

Scheme 5. Illustration of the possible equilibria between iron(III)/percarboxylato-, iron(IV)oxido/carboxylato radical- and iron(V)oxido/carboxylato-species.

Experimental Section

General: All solvents were distilled before use. Extra dry and oxygen-free solvents were distilled using desiccants under an argon atmosphere. Commercially available chemicals were used without further purification. Abbreviations of the supplier: Alfa Aesar (AA), CARL ROTH (CR), J&K Scientific (J&K), PanReac AppliChem ITW Reagents (PRAC), ACROS ORGANIC (AO), Sigma Aldrich (SA), FluoroChem (FC). Methanol extra dry (AO; 99.9%), acetonitrile extra dry (AO; 99.9%), 4-(dimethylamino)benzoyl chloride (J&K, 97%), 4-methoxybenzoyl chloride (J&K, 99%), 4-methylbenzoyl chloride (J&K, 98%), benzoyl chloride (SA; 99%), 4-chlorobenzoyl chloride (J&K, 99%), 4-nitrobenzoyl chloride (SA; 99%), 1,3-diamino-2-propanol-*N,N,N′,N′*-tetraacetic acid (TCI; 98%), 1,2-phenylenediamine (AA; 98%), 2-chloromethyl-pyridine hydrochloride (FC; 97%), *N*-benzylethylenediamine (AA; 98%), trifluoromethanesulphonic acid (abcr; 99%), iron powder (AA; 99%), iron(III) perchlorate nonahydrate (SA; 98%), iron(III)triflate (AA; 90%), benzoic acid (AA; 99%); decanoic acid (TCI; 98.0%), hydrogen peroxide (CR; 50% solution in H_2O), peracetic acid (PRAC; 15% solution in H_2O), urea hydrogen peroxide (SA; 97%), 2,2′-azino-bis(3-ethylbenzothiazoline-6-sulfonic acid) diammonium salt (AA; 98%). Pure iron(II) triflate•diacetonitrile salt was synthesized according to the literature.[20]

Physical Measurements: ^{1}H- and ^{13}C-NMR spectra were recorded on a Bruker Avance II 200 spectrometer (^{1}H at 200 MHz; ^{13}C at 50 MHz), Bruker Avance II 400 spectrometer (^{1}H at 400 MHz; ^{13}C at 100 MHz) and Bruker Avance III HD 400 spectrometer (^{1}H at 400 MHz; ^{13}C at 100 MHz) in deuterated solvents using TMS as internal standard. The ^{1}H- and ^{13}C-NMR spectra were calibrated against the proton and carbon signals of tetramethylsilane.

ESI-MS Measurements: Electrospray-ionization MS (ESI-MS) measurements in MeOH were performed on a Bruker micro-TOF mass spectrometer. When measuring any percarboxylato species, the corresponding solutions were pre-cooled to a temperature just above the melting point of methanol using liquid nitrogen. After mixing of the complex and the reagent, the cooled solution was measured immediately.

Stopped-Flow-Technique: Kinetic studies of the reactions of hydrogen peroxide with iron(III)complexes were recorded on a modified Hi Tech SF-3L low-temperature stopped-flow unit (modification for possible double-mixing measurements; Salisbury, U.K.) equipped with a J&M TIDAS 16-500 diode array spectrophotometer (J&M, Aalen, Germany). The kinetic data were treated by a global analysis fitting routine using the program Kinetic Studio (v.4.0.113798, T_gK Scientific) and/or by extracting single absorbance vs. time traces at different wavelengths. These traces were fitted to single-exponential functions using the integrated J&M software Kinspec. Hydrogen peroxide solutions were prepared by adding hydrogen peroxide (50%, cerimetric titration) with micropipets to the solution. In order to investigate the Intermediates **I1/I2** using the stopped-flow technique, complex **1b** was treated with an excess of H_2O_2. This premixed solution is taken up in the stopped-flow syringes and used as usually. For measurements where moisture and or air/oxygen should be avoided, the stopped-flow syringes were prepared in a glovebox by MBraun under an argon atmosphere. The reaction between **1a** and O_2 and the subsequent reaction with benzoyl chloride was performed with the double-mixing stopped-flow option. Dioxygen concentration in a saturated methanol solution has been reported to be 10.4 mmol L^{-1} at 25 °C.[21]

Computational Details: All structure optimizations were performed with B3LYP*-D3(BJ)/def2-TZVP,[24] the multipole accelerated resolution-of-identity (RI) approximation for *J* (MARI-*J*, with default parameters), Fermi-smearing, the "multiple grid" m4 for the

EurJIC
European Journal of Inorganic Chemistry

Full Papers
doi.org/10.1002/ejic.202100711

Chemistry Europe
European Chemical Societies Publishing

quadrature of exchange-correlation terms,[24f] and the dielectric continuum solvent model COSMO[25] (simulating methanol, relative permittivity $\varepsilon_r = 32.6$, refractive index $n_D = 1.3288$) using the Turbomole 7.5 software package.[26] Several studies have shown that for iron complexes, B3LYP with 15% HF exchange (called B3LYP*)[24c] is the density functional that comes closest to the experimental data.[24c,27] Furthermore, Kepp[27b] showed that the results for B3LYP* (with 15% HF exchange) can be improved by adding the D3(BJ) dispersion correction of the original B3LYP density functional. The ro-vibrational contributions are calculated for all molecules at the PBE0-D3(BJ)/def2-SVP, def2-TZVP[24,28] level seminumerical with the NumForce script including the fast contribution of the solvent in Turbomole 7.3 software package.[29] The def2-SVP[24f,28d] basis set was used for all atoms except iron. For iron the def2-TZVP[24e] was employed. For MARI-*J* the default parameter from older Turbomole versions were used to speed up calculations: precision: 10^{-6}, Imaxmom: 10, thrmom: 10^{-18}. The frequency calculations also verified the found molecular structures as minima (at the PBE0-D3(BJ)/def2-SVP, def2-TZVP level of theory). At the B3LYP*-D3(BJ)/def2-TZVP level of theory various spin states ($S = 0$, $S = 1$, $S = 2$, $S = 3$, $S = 4$, $S = 5$ and $S = 6$) were tested and the undecet spin state was found to be the most stable. The same concentration was used as in the experiment starting from the peroxide complex **2b**: Methanol 24.66 mol L^{-1}, benzoyl chloride 0.04 mol L^{-1}, and all the iron complexes 0.4 mmol L^{-1}. The experiments starting from **2a** were performed with a benzoyl chloride concentration of 20 mmol L^{-1}, the results are given in Scheme 4. The concentration is included via the translational entropy. This results in the following correction term G_{corr} for the Gibbs energy (Equation 5).

$$G_{corr} = -RT\ln\left(\frac{V_m^{new}}{V_m^{old}}\right) \quad (5)$$

with the molar gas constant R, the temperature T and the new (V_m^{new}) and old ($V_m^{old} = 0.024789598\ m^3$) volume of 1 mol of substance.

Synthesis of *N,N,N′,N′*-Tetrakis(2-benzimidazolylmethyl)-2-hydroxo-1,3-di-aminopropane (HPTB): The synthesis was performed according to the procedure by McKee *et al.*[22] 5.00 g diamino-2-propanol-*N,N,N′,N′*-tetraacetic acid (15.5 mmol) and 10.07 g *o*-phenylenediamine (93.09 mmol) were grounded together. The powder was taken up in a 250 mL Schlenk-flask and heated to 180 °C over 1.5 h. After cooling to RT the reddish glass was grounded and dissolved in 250 mL 4 mol L^{-1} HCl. After a few minutes a colorless solid precipitated. The solids were filtered and washed with ice-cold water. The filter residue was dissolved in 250 mL water. The solution was basified by adding 5 mol L^{-1} NaOH solution. After 10 min the colorless solid was filtered and washed a few times with water until the filtrate shows no alkaline reaction. The filter residue was air dried and then dissolved in 200 mL of hot acetone. At room temperature the mixture was mixed with 100 mL H_2O. The precipitation was completed at 4 °C overnight. The solids were filtered and washed with water. The filter residue was first air-dried and then dried in a desiccator over P_2O_5 under vacuum. The product was obtained as voluminous colorless powder (8.615 g, 14.10 mmol, yield 91%). ^{1}H-NMR (400 MHz, DMSO-d_6, TMS): $\delta =$ 7.60–7.53 (m, 8H, Ar-CH), 7.25–7.18 (m, 8H, Ar-CH), 6.37 (s[br], Ar-NH + H_2O), 4.19 (q, 8H, CH_2), 2.81 (q, 2H, CH_2), 2.57 (q, 2H, CH_2). ^{13}C-NMR (400 MHz, DMSO-d_6, TMS): $\delta =$ 152.5 (s, Ar-Cq), 136.5 (s, Ar-Cq), 122.5 (s, Ar-CH), 114.5 (s, Ar-CH), 66.6 (s, CH), 58.6 (s, CH_2), 51.9 (s, CH_2), MS (ESI; in MeOH): $m/z = [M + 2Na]^{2+} = 393.23$, $[M + H]^+ =$ 611.30, $[M + Na]^+ = 633.28$.

Synthesis of *N,N,N′,N′*-Tetrakis(2-(1-ethylbenzimidazolyl-methyl))-2-hydroxo-1,3-di-aminopropane (EtHPTB): In a 100 mL round-bottom flask 1.344 g fine-powdered NaOH (33.60 mmol) was suspended in 50 mL tetrahydrofuran. 4.885 g HPTB (8.000 mmol) was added and stirred for 30 h at room temperature to completely dissolve the ligand. Afterwards 10 mL bromoethane (14.6 g, 134 mmol) was added. The mixture was stirred for 48 h at room temperature. The milky suspension was evaporated to dryness and the faint yellow residue was extracted 3 times with 25 mL chloroform. The combined extracts were dried with sodium sulfate, filtrated and the filtrate was reduced to a minimal volume. The concentrated solution was added dropwise to 250 mL *n*-hexane under vigorous stirring to precipitate the product. The formed suspension was filtrated, the filter residue was under vacuum. The product was obtained as a colorless powder (5.343 g, 7.391 mmol, yield 92%). ^{1}H-NMR (400 MHz, $CDCl_3$, TMS): $\delta =$ 7.71–7.64 (m, 4H, 4× Ar–CH), 7.25–7.16 (m, 12H, 12× Ar–CH), 5.06 (s[br], 1H, OH), 4.20 (m, 16H, 4×CH_2 + 4×CH_2), 3.77 (p, 1H, CH), 2.73 (dd, 4H, 2×CH_2), 1.11 (t, 12H, 4×CH_3). ^{13}C-NMR (400 MHz, $CDCl_3$, TMS): $\delta =$ 151.4 (s, Ar–Cq), 142.3 (s, Ar–Cq), 134.7 (s, Ar–Cq), 122.6 (s, Ar–CH), 121.9 (s, Ar–CH), 119.5 (s, Ar–CH), 109.5 (s, Ar–CH), 68.9 (s, CH), 60.3 (s, CH_2), 52.0 (s, CH_2), 38.2 (s, CH_3). MS (ESI): $m/z = [M + 2H]^{2+} = 362.22$, $[M + 2Na]^{2+} = 393.17$; $[M + H]^+ = 723.43$; $[M + Na]^+ = 745.4060$.

Synthesis of $[Fe_2(EtHPTB)(OBz)](BPh_4)_2$ (1a): The synthesis was performed under inert conditions. 361 mg EtHPTB (0.50 mmol) and 50.5 mg Et_3N (0.50 mmol) were dissolved in 10 mL MeOH. A solution of 436 mg $Fe(OTf)_2 \times 2MeCN$ (1.00 mmol) in 3 mL MeOH was added to the ligand solution. After 5 min a solution of 61 mg and 50.5 mg Et_3N (0.50 mmol) was added dropwise to the complex solution. A precipitate was formed immediately. After 20 min the suspension was filtered and the filter residue was washed with MeOH and Et_2O. The crude product was dissolved in a minimal amount of acetone and stirred with 342 mg $NaBPh_4$ (1.00 mmol) overnight. After the solution was filtered, Et_2O was added until the solution became slightly cloudy. After two days at −30 °C light green crystals grew, which were suitable for single crystal X-ray diffraction analysis. The product was obtained as a slightly green powder (414 mg, 0.26 mmol, yield 51%). MS (ESI, 0.1% formic acid): $m/z = [Fe_2(EtHPTB)(OBz)(CHO_2H)]^+ = 1000.37$, $[Fe_2(EtHPTB)(CHO_2H)]^{2+} = 439.67$.

Synthesis of $[Fe_2(EtHPTB)(OH)_2(MeOH)_2](ClO_4)_3$ (1b): CAUTION! All perchlorate salts in this study should be handled with care because of their potential explosiveness. In a 250 mL round-bottom flask 2.184 g EtHPTB (3.000 mmol) were dissolved in 100 mL MeOH. A solution of 3.098 g $Fe(ClO_4)_3 \times 9\ H_2O$ (6.000 mmol) in 50 mL MeOH was added to this mixture. After 5 min 304 mg Et_3N (3.00 mmol) was added and stirred for 10 min. To the dark red solution another portion of 607 mg Et_3N (6.00 mmol) in 50 mL MeOH was added dropwise. The orange suspension was stirred for 30 min and then heated under reflux conditions for 30 min. After hot filtration of the solution the product was crystallized at room temperature. The crystals were filtered off and recrystallized twice in hot MeOH. The yellow crystals were filtered off and dried under vacuum. The obtained crystals were analyzed by single crystal X-ray diffraction. The product composition was determined by elemental analysis. The product was obtained as amber-colored powder (1.439 g, 1.170 mmol, yield 39%). MS (ESI; in MeOH): $m/z = [Fe_2(EtHPTB)(OMe)_3]^{2+} = 463.17$, $[Fe_2(EtHPTB)(OMe)_2(ClO_4)]^{2+} = 497.14$, $[Fe_2(EtHPTB)(OMe)_3(ClO_4)]^+ = 1025.29$. Elemental analysis calcd. (%) for $C_{45}H_{59}Cl_3Fe_2N_{10}O_{17}(+2H_2O)$: C(42.69), H(5.02), N(11.06). Found: C(42.50), H(4.85), N(11.19).

Synthesis of *N*-benzyl-*N,N′,N′*-tris(2-methylpyridyl)-ethylenediamine (bztpen): The synthesis was performed according to the procedure of Duelund *et al.*[23] In a 50 mL Schlenk-flask 751 mg *N*-benzylethylenediamine (5.00 mmol) and 2.63 g 2-Chloromethylpyridine hydrochloride (16.0 mmol) were dissolved in a mixture of 7.5 mL dichloromethane and 7.5 mL water. A solution of 1.28 g

EurJIC
European Journal of Inorganic Chemistry

Full Papers
doi.org/10.1002/ejic.202100711

Chemistry Europe
European Chemical Societies Publishing

NaOH (32 mmol) in 5 mL water was prepared. A third of this solution was added for the first 3 days. After the addition was complete, the solution was stirred for an additional 3 days at room temperature. The product was extracted 3 times with 10 mL dichloromethane. The combined organic phase was extracted with brine. The dichloromethane extract was dried over Na_2SO_4. The solvent was evaporated and the crude product was purified by column chromatography with silica as stationary phase (eluent: dichloromethane/MeOH). The product was obtained as a pale yellow solid (1.36 g, 3.21 mmol, yield 64%). ^{1}H-NMR (400 MHz, $CDCl_3$, TMS): δ = 8.52–8.44 (m, 3H, 3×Ar–CH), 7.60–7.53 (m, 3H, 3×Ar–CH), 7.49–7.39 (m, 3H, 3×Ar–CH), 7.32–7.17 (m, 5H, 5×Ar–CH), 7.14–7.07 (m, 3H, 3×Ar–CH), 3.78 (s, 4H, 2×CH_2), 3.72 (s, 2H, –CH_2), 3.59 (s, 2H, –CH_2), 2.82–2.62 (m, 4H, 2×CH_2). ^{13}C-NMR (400 MHz, $CDCl_3$, TMS): δ = 150.0 (s, Ar–CH), 148.9 (s, Ar–Cq), 136.3 (s, Ar–CH), 128.8 (s, Ar–Cq), 128.2 (s, Ar–CH), 126.9 (s, Ar–Cq), 122.8 (s, Ar–CH), 121.8 (s, Ar–CH), 121.6 (s, Ar–CH), 60.8 (s, 2×CH_2), 60.6 (s, –CH_2), 59.0 (s, –CH_2), 52.2 (s, –CH_2), 51.4 (s, –CH_2). MS (ESI): m/z = $[M+H]^+$ = 424.25.

Synthesis of [Fe(bztpen)(OMe)](ClO$_4$)$_2$ (3): CAUTION! All perchlorate salts in this study should be handled with care because of their potential explosiveness. In a 25 mL round-bottom flask 847 mg bztpen (2.00 mmol) were dissolved in 15 mL MeOH. A solution of 1.03 g $Fe(ClO_4)_3 \times 9H_2O$ (2.00 mmol) in 5 mL MeOH was added dropwise to this mixture. With vigorous stirring, the solution was triturated with 291 µL Et_3N (2.10 mmol). After 15 min the product was precipitated by adding Et_2O to the yellow solution. The crude product was recrystallized in hot MeOH. The yellow crystals were filtered off and dried under vacuum. The obtained crystals were suitable for single crystal X-ray diffraction. The product was obtained as yellow powder (1.10 g, 1.36 mmol, yield 68%). MS (ESI): m/z = $[M+MeO]^+$ = 541.22. Elemental analysis calcd. (%) for $C_{28}H_{32}Cl_2FeN_5O_9(+H_2O)$: C(46.24), H(4.71), N(9.63). Found: C(46.22), H(4.40), N(9.54).

Synthesis of perdecanoic acid (PDA): Synthesized according to literature.[15] In a 250 mL round-bottom flask 10.0 g decanoic acid (58.1 mmol) were dissolved in 20 mL conc. sulfuric acid (ω = 98%). The mixture was cooled in an ice bath to keep the temperature around 10 °C. Under stirring and proceeded cooling 5 mL of a H_2O_2 solution (ω = 50%) was added dropwise over the course of 20 min. The temperature should not rise above 20 °C during the addition. After the addition, the mixture was allowed to stir for another 50 min at 10 °C. The reaction mixture was then slowly diluted with 75 mL ice-cold water, in which the temperature should not rise above 30 °C. The product was extracted five times with 15 mL Et_2O using a separatory funnel. The combined organic phase was extracted twice with 15 mL water. The organic phase was dried over Na_2SO_4 and the filtrate was removed on a rotary evaporator at 25 °C (CAUTION!). The colorless residue was dissolved in 100 mL *n*-hexane and crystallized at −30 °C overnight. The crystals were filtered off and rinsed with cold *n*-hexane. The product was carefully dried under vacuum. The product was obtained as colorless crystals (6.77 g, 36.0 mmol, yield 62%). ^{1}H-NMR (400 MHz, $CDCl_3$, TMS): δ = 11.49 (s[br], 1H, –CO_3H), 2.42 (t, 2H, –CH_2), 1.70 (quint, 2H, –CH_2), 1.40–1.19 (m, 12H, 6×CH_2), 0.88 (t, 3H, –CH_3). ^{13}C-NMR (400 MHz, $CDCl_3$, TMS): δ = 174.7 (s, Cq), 31.8 (s, –CH_2), 30.4 (s, –CH_2), 29.3 (s, –CH_2), 29.2 (s, –CH_2), 29.1 (s, –CH_2), 28.9 (s, –CH_2), 24.6 (s, –CH_2), 22.7 (s, –CH_2), 14.1 (s, –CH_3). MS (ESI): m/z = $[M+H]^+$ = 189.15, $[M+Na]^+$ = 211.13.

Deposition Numbers 2088347 (for **3**), 2088348 (for **1b**(ClO_4)$_3$), 2088349 (for **1a**(BPh_4)$_2$), and 2101789 (for PDA) contain the supplementary crystallographic data for this paper. These data are provided free of charge by the joint Cambridge Crystallographic Data Centre and Fachinformationszentrum Karlsruhe Access Structures service www.ccdc.cam.ac.uk/structures.

Acknowledgements

We gratefully acknowledge support by the Justus-Liebig-Universität Gießen. A.J.A. and D.M. wish to express thanks for the support by the administrators of the JustHPC-cluster of the Justus-Liebig-Universität, Gießen. Open Access funding enabled and organized by Projekt DEAL.

Conflict of Interest

The authors declare no conflict of interest.

Keywords: Iron · Kinetics · Reaction mechanisms · Substituent effects · Time-resolved spectroscopy

[1] a) J. Piera, J.-E. Bäckvall, *Angew. Chem. Int. Ed.* **2008**, *47*, 3506–352; *Angew. Chem.* **2008**, *120*, 3558–35763; b) J. Dong, E. Fernández-Fueyo, F. Hollmann, C. E. Paul, M. Pesic, S. Schmidt, Y. Wang, S. Younes, W. Zhang, *Angew. Chem. Int. Ed.* **2018**, *57*, 9238–926; *Angew. Chem.* **2018**, *130*, 9380–94041.
[2] A. L. Feig, S. J. Lippard, *J. Am. Chem. Soc.* **1994**, *116*, 8410–8411.
[3] U. K. Bagha, J. K. Satpathy, G. Mukherjee, C. V. Sastri, S. P. de Visser, *Org. Biomol. Chem.* **2021**, *19*, 1879–1899.
[4] B. Kripli, F. V. Csendes, P. Török, G. Speier, J. Kaizer, *Chem. Eur. J.* **2019**, *25*, 14290–14294.
[5] a) Y. Dong, S. Yan, V. G. Young Jr., L. Que Jr., *Angew. Chem. Int. Ed.* **1996**, *35*, 618–620; *Angew. Chem.* **1996**, *108*, 673–676; b) L. Westerheide, F. K. Müller, R. Than, B. Krebs, J. Dietrich, S. Schindler, *Inorg. Chem.* **2001**, *40*, 1951–1961; c) A. L. Feig, M. Becker, S. Schindler, R. van Eldik, S. J. Lippard, *Inorg. Chem.* **1996**, *35*, 2590–2601; d) Y. Dong, S. Menage, B. A. Brennan, T. E. Elgren, H. G. Jang, L. L. Pearce, L. Que Jr., *J. Am. Chem. Soc.* **1993**, *115*, 1851–1859.
[6] A. Miska, D. Schurr, G. Rinke, R. Dittmeyer, S. Schindler, *Chem. Eng. Sci.* **2018**, *190*, 459–465.
[7] a) I. Bernal, I. M. Jensen, K. B. Jensen, C. J. McKenzie, H. Toftlund, J.-P. Tuchagues, *J. Chem. Soc. Dalton Trans.* **1995**, 3667–3675; b) A. Hazell, C. J. McKenzie, L. P. Nielsen, S. Schindler, M. Weitzer, *J. Chem. Soc. Dalton Trans.* **2002**, 310; c) T. Nebe, A. Beitat, C. Würtele, C. Dücker-Benfer, R. van Eldik, C. J. McKenzie, S. Schindler, *Dalton Trans.* **2010**, *39*, 7768–7773.
[8] F. Avenier, C. Herrero, W. Leibl, A. Desbois, R. Guillot, J.-P. Mahy, A. Aukauloo, *Angew. Chem. Int. Ed.* **2013**, *52*, 3634–3637; *Angew. Chem.* **2013**, *125*, 3722–3725.
[9] a) R. Than, A. Schrodt, L. Westerheide, R. van Eldik, B. Krebs, *Eur. J. Inorg. Chem.* **1999**, *1999*, 1537–1543; b) B. A. Brennan, Q. Chen, C. Juarez-Garcia, A. E. True, C. J. O'Connor, L. Que, *Inorg. Chem.* **1991**, *30*, 1937–1943;
[10] H. H. Awad, D. M. Stanbury, *Int. J. Chem. Kinet.* **1993**, *25*, 375–381.
[11] D. A. Wink, J. F. Darbyshire, R. W. Nims, J. E. Saavedra, P. C. Ford, *Chem. Res. Toxicol.* **1993**, *6*, 23–27.
[12] W. C. Nottingham, J. R. Sutter, *Int. J. Chem. Kinet.* **1986**, *18*, 1289–1302.
[13] U. Pinkernell, H.-J. Lüke, U. Karst, *Analyst* **1997**, *122*, 567–571.
[14] S. Hochreuther, S. T. Nandibewoor, R. Puchta, R. van Eldik, *Dalton Trans.* **2012**, *41*, 512–522.
[15] M. Sitko, A. Szelwicka, A. Wojewódka, A. Skwarek, D. Tadasiewicz, L. Schimmelpfennig, K. Dziuba, M. Morawiec-Witczak, A. Chrobok, *RSC Adv.* **2019**, *9*, 30012–30018.
[16] a) A. M. Zima, O. Y. Lyakin, R. V. Ottenbacher, K. P. Bryliakov, E. P. Talsi, *ACS Catal.* **2017**, *7*, 60–69; b) J. Serrano-Plana, W. N. Oloo, L. Acosta-Rueda, K. K. Meier, B. Verdejo, E. Garcia-Espana, M. G. Basallote, E. Münck, L. Que Jr., A. Company, M. Costas, *J. Am. Chem. Soc.* **2015**, *137*, 15833–15842; c) Y. Wang, D. Janardanan, D. Usharani, K. Han, L. Que Jr., S. Shaik, *ACS Catal.* **2013**, *3*, 1334–1341; d) C. Wegeberg, W. R. Browne, C. J. McKenzie, *ACS Catal.* **2018**, *8*, 9980–9991; e) J. Serrano-Plana, F. Acuña-Parés, V. Dantignana, W. N. Oloo, E. Castillo, A. Draksharapu, C. J. Whiteoak, V. Martin-Diaconescu, M. G. Basallote, J. M. Luis, L. Que, M. Costas, A. Company, *Chem. Eur. J.* **2018**, *24*, 5331–5340; f) S. Kal, S. Xu, L.

EurJIC
European Journal of Inorganic Chemistry

Full Papers
doi.org/10.1002/ejic.202100711

Chemistry Europe
European Chemical Societies Publishing

Que Jr., *Angew. Chem. Int. Ed.* **2020**, *59*, 7332–7349; *Angew. Chem.* **2020**, *132*, 7400–7419; g) R. Fan, J. Serrano-Plana, W. N. Oloo, A. Draksharapu, E. Delgado-Pinar, A. Company, V. Martin-Diaconescu, M. Borrell, J. Lloret-Fillol, E. Garcia-Espana, Y. Guo, E. L. Bominaar, L. Que Jr., M. Costas, E. Münck, *J. Am. Chem. Soc.* **2018**, *140*, 3916–3928; h) J. Serrano-Plana, A. Aguinaco, R. Belda, E. García-España, M. G. Basallote, A. Company, M. Costas, *Angew. Chem. Int. Ed.* **2016**, *55*, 6310–6314; *Angew. Chem.* **2016**, *128*, 6418–6422; i) W. N. Oloo, R. Banerjee, J. D. Lipscomb, L. Que Jr., *J. Am. Chem. Soc.* **2017**, *139*, 17313–17326.

[17] X. Zhang, H. Furutachi, T. Tojo, T. Tsugawa, S. Fujinami, T. Sakurai, M. Suzuki, *Chem. Lett.* **2011**, *40*, 515–517.

[18] N. A. Ortega-Villar, M. C. Munoz, J. A. Real, *Eur. J. Inorg. Chem.* **2010**, *2010*, 5563–5567.

[19] J. R. Khusnutdinova, J. Luo, N. P. Rath, L. M. Mirica, *Inorg. Chem.* **2013**, *52*, 3920–3932.

[20] A. Zhou, S. T. Kleespies, K. M. van Heuvelen, L. Que Jr., *Chem. Commun.* **2015**, *51*, 14326–14329.

[21] H. Miyamoto, Y. Yampolski, C. L. Young, *J. Phys. Chem. Ref. Data.* **2014**, *43*, 33102.

[22] V. McKee, M. Zvagulis, J. V. Dagdigian, M. G. Patch, C. A. Reed, *J. Am. Chem. Soc.* **1984**, *106*, 4765–4772.

[23] L. Duelund, R. Hazell, C. J. McKenzie, L. Preuss Nielsen, H. Toftlund, *J. Chem. Soc. Dalton Trans.* **2001**, 152–156.

[24] a) S. Grimme, S. Ehrlich, L. Goerigk, *J. Comput. Chem.* **2011**, *32*, 1456–1465; b) S. Grimme, J. Antony, S. Ehrlich, H. Krieg, *J. Chem. Phys.* **2010**, *132*, 154104; c) M. Reiher, O. Salomon, B. Artur Hess, *Theor. Chem. Acc.* **2001**, *107*, 48–55; d) F. Weigend, M. Häser, H. Patzelt, R. Ahlrichs, *Chem. Phys. Lett.* **1998**, *294*, 143–152; e) F. Weigend, R. Ahlrichs, *Phys. Chem. Chem. Phys.* **2005**, *7*, 3297–3305; f) K. Eichkorn, F. Weigend, O. Treutler, R. Ahlrichs, *Theor. Chem. Acc.* **1997**, *97*, 119–124; g) S. H. Vosko, L. Wilk, M. Nusair, *Can. J. Phys.* **1980**, *58*, 1200–1211; h) J. C. Slater, *Phys. Rev.* **1951**, *81*, 385–390; i) *Proc. R. Soc. Lond. A* **1929**, *123*, 714–733; j) A. D. Becke, *J. Chem. Phys.* **1993**, *98*, 5648–5652; k) Lee, Yang, Parr, *Phys. Rev. B Condens Matter* **1988**, *37*, 785–789; l) Becke, *Phys. Rev. A Gen. Phys.* **1988**, *38*, 3098–3100.

[25] a) A. Klamt, G. Schüürmann, *J. Chem. Soc. Perkin Trans. 2* **1993**, 799–805; b) A. Schäfer, A. Klamt, D. Sattel, J. C. W. Lohrenz, F. Eckert, *Phys. Chem. Chem. Phys.* **2000**, *2*, 2187–2193;

[26] a) S. G. Balasubramani, G. P. Chen, S. Coriani, M. Diedenhofen, M. S. Frank, Y. J. Franzke, F. Furche, R. Grotjahn, M. E. Harding, C. Hättig, A. Hellweg, B. Helmich-Paris, C. Holzer, U. Huniar, M. Kaupp, A. Marefat Khah, S. Karbalaei Khani, T. Müller, F. Mack, B. D. Nguyen, S. M. Parker, E. Perlt, D. Rappoport, K. Reiter, S. Roy, M. Rückert, G. Schmitz, M. Sierka, E. Tapavicza, D. P. Tew, C. van Wüllen, V. K. Voora, F. Weigend, A. Wodyński, J. M. Yu, *J. Chem. Phys.* **2020**, *152*, 184107; b) TURBOMOLE V7.5 2020, a development of University of Karlsruhe and Forschungszentrum Karlsruhe GmbH, 1989–2007, *TURBOMOLE GmbH*, since **2007**; available from *https://www.turbomole.org*.

[27] a) M. Reiher, *Inorg. Chem.* **2002**, *41*, 6928–6935; b) K. P. Kepp, *Inorg. Chem.* **2016**, *55*, 2717–2727; c) O. Salomon, M. Reiher, B. A. Hess, *J. Chem. Phys.* **2002**, *117*, 4729–4737.

[28] a) Perdew, Burke, Ernzerhof, *Phys. Rev. Lett.* **1996**, *77*, 3865–3868; b) Perdew, Wang, *Phys. Rev. B Condens.Matter* .**1992**, *45*, 13244–13249; c) J. P. Perdew, M. Ernzerhof, K. Burke, *J. Chem. Phys.* **1996**, *105*, 9982–9985; d) A. Schäfer, H. Horn, R. Ahlrichs, *J. Chem. Phys.* **1992**, *97*, 2571–2577.

[29] a) R. Ahlrichs, M. Bär, M. Häser, H. Horn, C. Kölmel, *Chem. Phys. Lett.* **1989**, *162*, 165–169; b) P. Deglmann, F. Furche, *J. Chem. Phys.* **2002**, *117*, 9535–9538; c) P. Deglmann, F. Furche, R. Ahlrichs, *Chem. Phys. Lett.* **2002**, *362*, 511–518; d) TURBOMOLE V7.3 2018, a development of University of Karlsruhe and Forschungszentrum Karlsruhe GmbH, 1989–2007, *TURBOMOLE GmbH*, since **2007**; available from *http://www.turbomole.com*.

Manuscript received: August 16, 2021
Revised manuscript received: September 10, 2021
Accepted manuscript online: September 14, 2021

European Journal of Inorganic Chemistry

Supporting Information

A Mechanistic Study on the Reaction of Non-Heme Diiron (III)-Peroxido Complexes with Benzoyl Chloride

Markus Lerch, Andreas J. Achazi, Doreen Mollenhauer, Jonathan Becker, and Siegfried Schindler*

Content

1 | Crystal Structures

Single crystal diffraction data for **1a**, **1b** and **3** were collected at low temperatures (100 K) using φ- and ω-scans on a BRUKER D8 Venture system equipped with dual IμS microfocus sources, a PHOTON100 detector and an OXFORD CRYOSYSTEMS 700 low temperature system. Mo-K_α radiation with wavelength 0.71073 Å and a collimating Quazar multilayer mirror were used. Semi-empirical absorption correction from equivalents was applied using SADABS-2016/2[1] and the structures were solved by direct methods using SHELXT2014/5.[2] Refinement was performed against F^2 on all data by full-matrix least squares using SHELXL2018/3.[3] All non-hydrogen atoms were refined anisotropically and C-H hydrogen atoms were positioned at geometrically calculated positions and refined using a riding model. OH hydrogen atoms were, where possible, located in the Fourier difference map and set to ideal distances. All other OH hydrogen atoms were positioned at geometrically calculated positions considering hydrogen bond acceptors. The isotropic displacement parameters of all hydrogen atoms were fixed to 1.2x or 1.5x (OH and CH_3 hydrogen atoms) the U_{eq} value of the atoms they are linked to. The crystallographic data have been deposited with the Cambridge Crystallographic Data Centre as CCDC No. 2088347-2088349 and 2101789 and can be obtained free of charge.[4]

1.1 | $[Fe_2(EtHPTB)(OBz)](BPh_4)_2$ (+ 2 Acetone) (Compound 1a + 2 Acetone)

The structure was solved in the monoclinic space group $P2_1$ and refined as racemic twin. The asymmetric unit contains two complex cations, four anions and four acetone molecules. Both EtHPTB ligands were found to be fully disordered. The disorder was refined with the help of same distance restraints, similarity restraints on anisotropic displacement parameters, restraints to a common plane[5] and advanced rigid bond restraints.[6] Additionally, atoms with very similar positions were set to the same anisotropic displacement parameters. The disorder rations were allowed to refine freely and converged to 0.518(4) and 0.777(7).

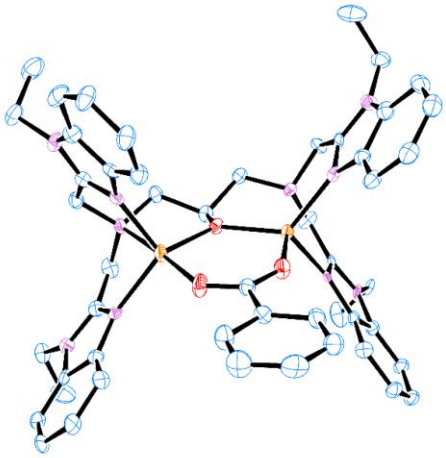

Figure S1. ORTEP[7] drawing of $[Fe_2(EtHPTB)(OBz)](BPh_4)_2$ × 2 acetone. The thermal ellipsoids are set at a 50 % probability level. Hydrogen atoms, solvent molecules and tetraphenylborate anions are omitted for clarity.

Table S1. Crystal data and structure refinement for **1a**.

CCDC No	2088349	
Empirical formula	C_{104} H_{106} B_2 Fe_2 N_{10} O_5	
Formula weight	1709.30	
Temperature	100(2) K	
Wavelength	0.71073 Å	
Crystal system	Monoclinic	
Space group	$P2_1$	
Unit cell dimensions	a = 17.605(2) Å	α = 90°.
	b = 26.247(3) Å	β = 101.709(4)°.
	c = 19.622(2) Å	γ = 90°.
Volume	8878.6(18) $Å^3$	
Z	4	
Density (calculated)	1.279 Mg/m^3	
Absorption coefficient	0.388 mm^{-1}	
F(000)	3608	
Crystal size	0.510 x 0.419 x 0.411 mm^3	
Theta range for data collection	1.313 to 26.021°.	
Index ranges	-21 ≤ h ≤ 21, -32 ≤ k ≤ 32, -24 ≤ l ≤ 24	
Reflections collected	301545	
Independent reflections	35014 [R(int) = 0.0827]	
Completeness to theta = 25.242°	100.0 %	
Absorption correction	Semi-empirical from equivalents	
Refinement method	Full-matrix least-squares on F^2	
Data / restraints / parameters	35014 / 7443 / 2772	
Goodness-of-fit on F^2	1.038	
Final R indices [I>2σ(I)]	R1 = 0.0419, wR2 = 0.0974	
R indices (all data)	R1 = 0.0538, wR2 = 0.1037	
Absolute structure parameter	0.496(10)	
Largest diff. peak and hole	0.445 and -0.467 $e.Å^{-3}$	

1.2 | $[Fe_2(EtHPTB)(OH)_2(MeOH)_2](ClO_4)_3$ (+ 3MeOH) (Compound 1b + 3 MeOH)

The crystal structure was solved in the triclinic space group $P\bar{1}$. The asymmetric unit contains the complex, perchlorate anions, hydroxide anions and methanol molecules. Both iron atoms at their "open" coordination site are coordinated by either hydroxide or methanol. This was found to be disordered so that the position of hydroxide and methanol are switched. The disorder ratio refined to 0.54(1). Additionally, all perchlorate anions were found to be disordered over two positions each. The disorders were refined and converged to 0.78(1), 0.84(2) and 0.828(6). All disorders were refined using same distance restraints, similarity restraints on anisotropic displacement parameters and advanced rigid bond restraints. Some atoms with very similar positions were set to the same anisotropic displacement parameters.

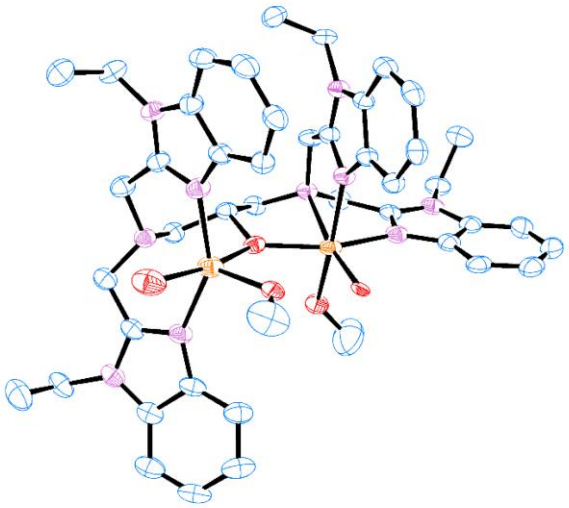

Figure S2. ORTEP[7] drawing of $[Fe_2(EtHPTB)(OH)_2(MeOH)_2](ClO_4)_3$ × 3MeOH. The thermal ellipsoids are set at a 50 % probability level. Hydrogen atoms, solvent molecules and perchlorate anions are omitted for clarity.

Table S2. Crystal data and structure refinement for **1b**.

CCDC No	2088348	
Empirical formula	$C_{47.5}\ H_{69}\ Cl_3\ Fe_2\ N_{10}\ O_{19.5}$	
Formula weight	1310.17	
Temperature	100(2) K	
Wavelength	0.71073 Å	
Crystal system	Triclinic	
Space group	$P\bar{1}$	
Unit cell dimensions	a = 14.0065(11) Å	α = 98.102(2)°.
	b = 15.5793(12) Å	β = 104.766(2)°.
	c = 16.1202(12) Å	γ = 112.138(2)°.
Volume	3038.4(4) $Å^3$	
Z	2	
Density (calculated)	1.432 Mg/m^3	
Absorption coefficient	0.687 mm^{-1}	
F(000)	1366	
Crystal size	0.256 x 0.075 x 0.015 mm^3	
Theta range for data collection	2.045 to 25.026°.	
Index ranges	-16 ≤ h ≤ 16, -18 ≤ k ≤ 18, -19 ≤ l ≤ 19	
Reflections collected	48325	
Independent reflections	10523 [R(int) = 0.0848]	
Completeness to theta = 25.026°	98.0 %	
Absorption correction	Semi-empirical from equivalents	
Refinement method	Full-matrix least-squares on F^2	
Data / restraints / parameters	10523 / 2479 / 922	
Goodness-of-fit on F^2	1.020	
Final R indices [I>2σ(I)]	R1 = 0.0741, wR2 = 0.2015	
R indices (all data)	R1 = 0.1128, wR2 = 0.2315	
Extinction coefficient	0.0031(8)	
Largest diff. peak and hole	2.342 and -1.609 $e{\cdot}Å^{-3}$	

1.3 | [Fe(bztpen)(OMe)](ClO$_4$)$_2$ (Compound 3)

The structure of **3** was solved in the orthorhombic space group *Pbca*. The asymmetric unit contains the full cation and two anions. One of the perchlorate anions was found to be disordered over two positions. The disorder was refined using same distance restraints, similarity restraints on anisotropic displacement parameters and by setting all atoms of the very low occupied second disorder position to the same anisotropic displacement parameters. The disorder ratio was allowed to refine freely and converged to 0.938(3).

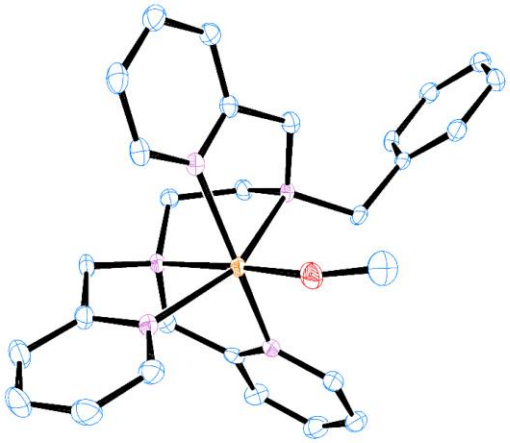

Figure S3. ORTEP[7] drawing of [Fe(bztpen)(OMe)](ClO$_4$)$_2$. The thermal ellipsoids are set at a 50 % probability level. Hydrogen atoms and perchlorate anions are omitted for clarity.

Table S3. Crystal data and structure refinement for **3**.

CCDC No	2088347	
Empirical formula	C_{28} H_{32} Cl_2 Fe N_5 O_9	
Formula weight	709.33	
Temperature	100(2) K	
Wavelength	0.71073 Å	
Crystal system	Orthorhombic	
Space group	*Pbca*	
Unit cell dimensions	a = 17.106(3) Å	α = 90°.
	b = 17.882(3) Å	β = 90°.
	c = 19.412(3) Å	γ = 90°.
Volume	5937.9(15) $Å^3$	
Z	8	
Density (calculated)	1.587 Mg/m^3	
Absorption coefficient	0.752 mm^{-1}	
F(000)	2936	
Crystal size	0.164 x 0.055 x 0.021 mm^3	
Theta range for data collection	1.953 to 25.681°.	
Index ranges	-20 ≤ h ≤ 20, -21 ≤ k ≤ 21, -23 ≤ l ≤ 23	
Reflections collected	111041	
Independent reflections	5639 [R(int) = 0.1117]	
Completeness to theta = 25.242°	100.0 %	
Absorption correction	Semi-empirical from equivalents	
Refinement method	Full-matrix least-squares on F^2	
Data / restraints / parameters	5639 / 164 / 429	
Goodness-of-fit on F^2	1.035	
Final R indices [I>2σ(I)]	R1 = 0.0393, wR2 = 0.0874	
R indices (all data)	R1 = 0.0589, wR2 = 0.0974	
Largest diff. peak and hole	0.490 and -0.411 $e·Å^{-3}$	

1.4 | Perdecanoic acid

The structure of **perdecanoic acid** was solved in the monoclinic space group $P2_1/c$. The asymmetric unit contains one full molecule. The molecules of **perdecanoic acid** in the structure are connected via hydrogen bonds and form an infinite chain.

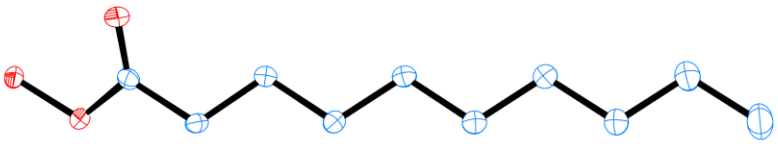

Figure S4. ORTEP[7] drawing of perdecanoic acid. The thermal ellipsoids are set at a 50 % probability level, hydrogen atoms are omitted for clarity.

Table S4. Crystal data and structure refinement for perdecanoic acid.

CCDC No	2101789	
Empirical formula	C_{10} H_{20} O_3	
Formula weight	188.26	
Temperature	100(2) K	
Wavelength	0.71073 Å	
Crystal system	Monoclinic	
Space group	$P2_1/c$	
Unit cell dimensions	a = 24.397(5) Å	α= 90°.
	b = 4.6770(9) Å	β= 90.211(7)°.
	c = 9.5082(18) Å	γ = 90°.
Volume	1084.9(4) $Å^3$	
Z	4	
Density (calculated)	1.153 Mg/m^3	
Absorption coefficient	0.083 mm^{-1}	
F(000)	416	
Crystal size	0.304 x 0.064 x 0.020 mm^3	
Theta range for data collection	1.669 to 25.027°.	
Index ranges	-29 ≤ h ≤ 29, -4 ≤ k ≤ 5, -11 ≤ l ≤ 11	
Reflections collected	12710	
Independent reflections	1922 [R(int) = 0.0967]	
Completeness to theta = 25.027°	99.9 %	
Absorption correction	Semi-empirical from equivalents	
Refinement method	Full-matrix least-squares on F^2	
Data / restraints / parameters	1922 / 1 / 122	
Goodness-of-fit on F^2	1.046	
Final R indices [I>2σ(I)]	R1 = 0.0554, wR2 = 0.1261	
R indices (all data)	R1 = 0.0990, wR2 = 0.1504	
Largest diff. peak and hole	0.229 and -0.263 $e \cdot Å^{-3}$	

2 | ESI-MS Spectra

2.1 | ESI-MS Spectrum of Complex 1b in MeOH

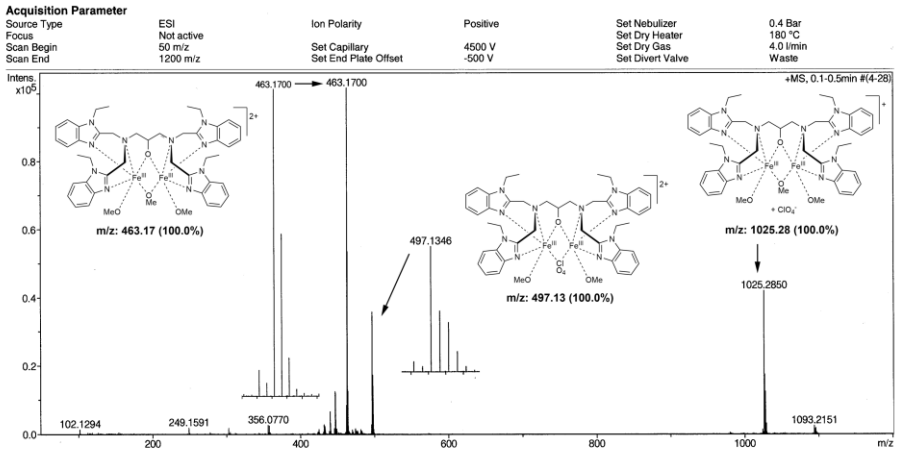

Figure S5. ESI-MS spectrum measured in the positive-ion mode for compound **1b** dissolved in methanol. The signal at 463.2 shows the *m/z* ratio of the complex $[Fe_2(EtHPTB)(OMe)_3]^{2+}$.

2.2 | ESI-MS Spectrum of Peroxido Complex 2b in MeOH

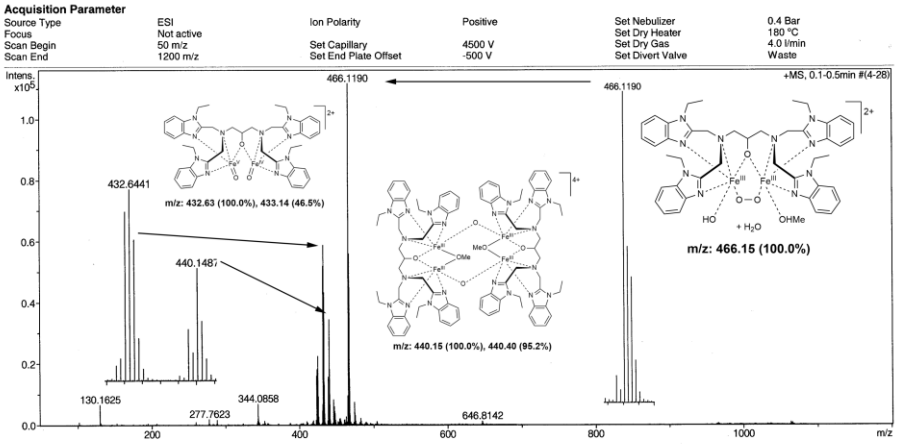

Figure S6. ESI-MS spectrum measured in the positive-ion mode for compound **1b** dissolved in methanol and additional addition of an excess of hydrogen peroxide. The signal at 466.1 shows the *m/z* ratio of the peroxido complex $[Fe_2(EtHPTB)(\mu\text{-}1,2\text{-}O_2)(H_2O)_2(OMe)]^{2+}$.

2.3 | ESI-MS Spectrum of a Mixture of Complex 2b and BzCl in MeOH

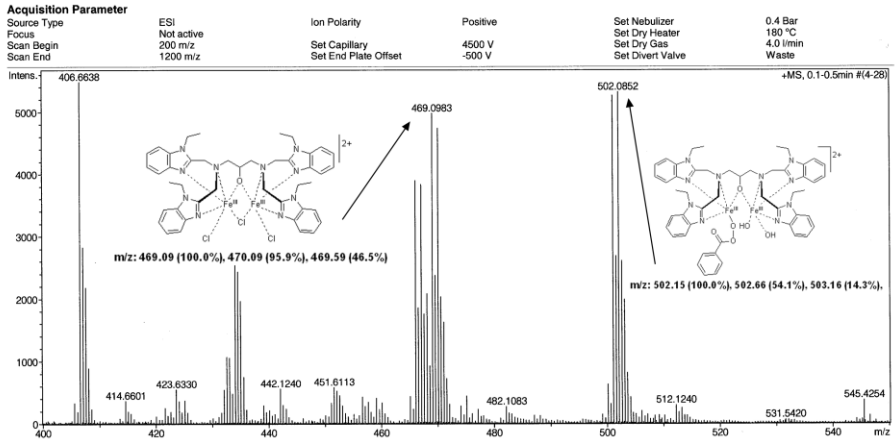

Figure S7. ESI-MS spectrum measured in the positive-ion mode for compound **2b** and the addition of about 2 eq. of benzoyl chloride. It is assumed that the signal at a *m/z* ratio of 502.1 can be ascribed to be the intermediate **I1** with the formula $[Fe_2(EtHPTB)(OOBz)(OH)_2]^{2+}$.

2.4 | ESI-MS Spectrum of a Mixture of Complex 1b and PAA in MeOH

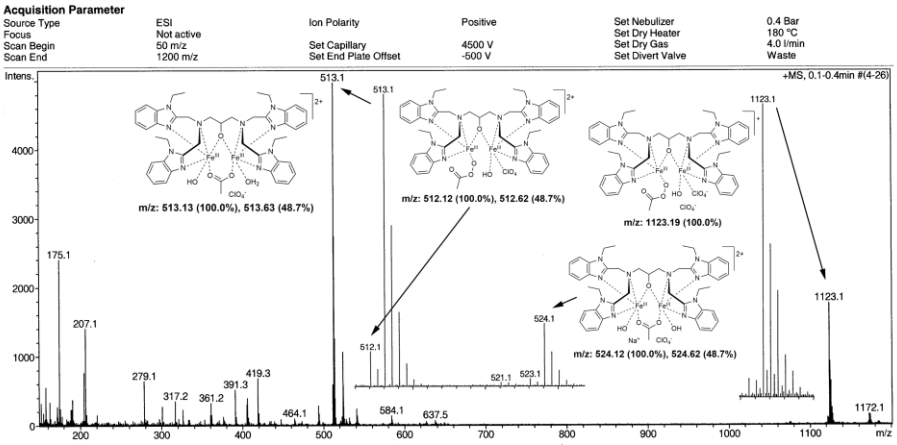

Figure S8. ESI-MS spectrum measured in the positive-ion mode for compound **1b** dissolved in methanol and the addition of an excess peracetic acid. The signal at 1123.1 shows the *m/z* ratio of the peracetato complex $[Fe_2(EtHPTB)(OOAc)(OH)(ClO_4)_2]^+$.

3 | Kinetic Data and Related Information

3.1 | Reaction of Complex 1b with Hydrogen Peroxide

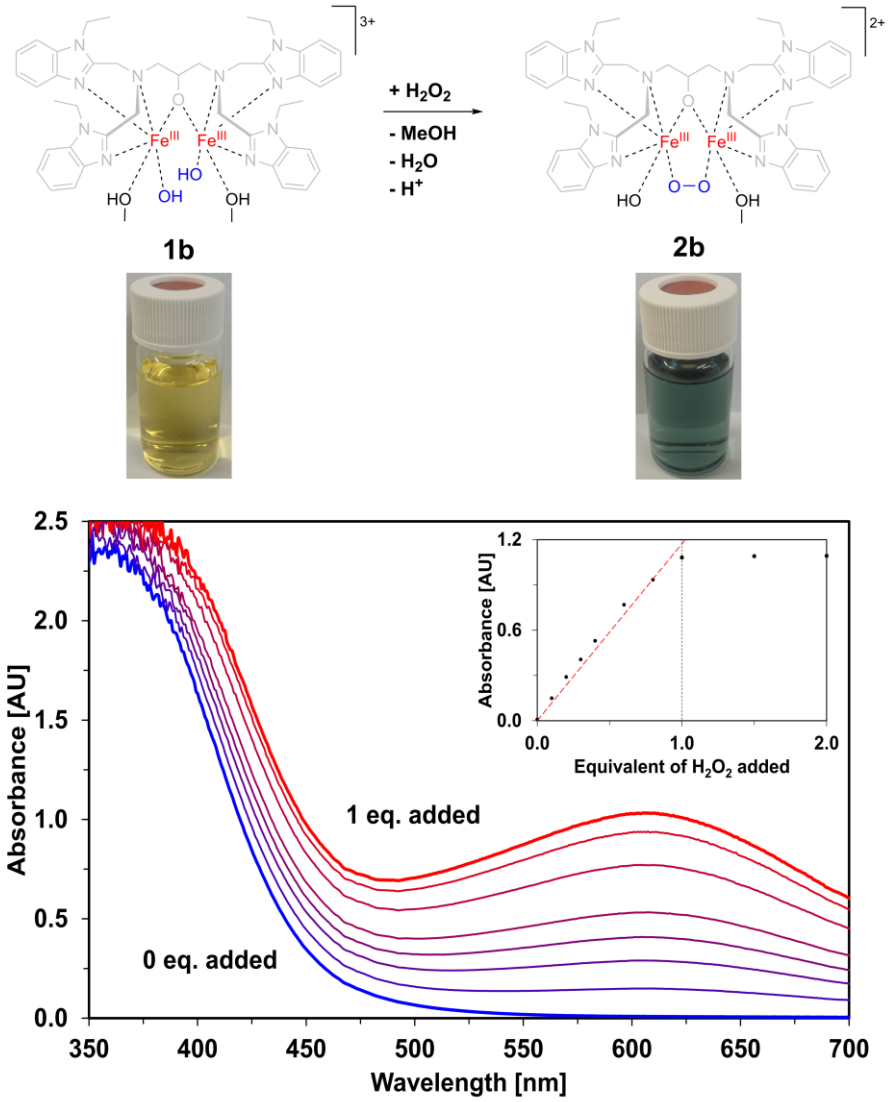

Figure S9. UV-vis spectral changes of a 0.4 mmol L^{-1} solution of complex **1b** in methanol upon the gradual addition of H_2O_2 (up to 1.0 eq.) at 25.0 °C. The diagram in the right corner shows the saturation point at the addition of 1.0 eq. H_2O_2 over the course of the addition of 2.0 eq. of H_2O_2.

3.2 | Reaction of Peroxide Complex 2b with Benzoyl Chloride

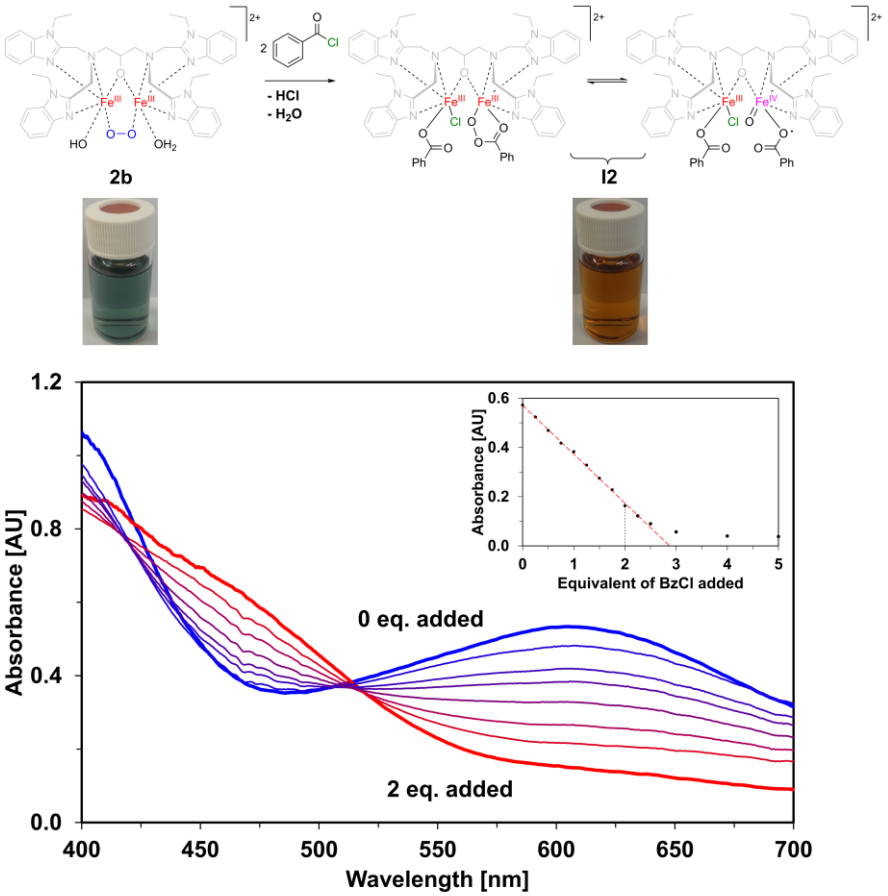

Figure S10. UV-vis spectral changes of a 0.2 mmol L^{-1} solution of the peroxido-complex **2b** in methanol upon the gradual addition of BzCl (up to 2.0 eq.) at 25.0 °C. The diagram in the right corner shows the saturation point at the addition of 2.0 eq. BzCl over the course of the addition of 5.0 eq. of BzCl.

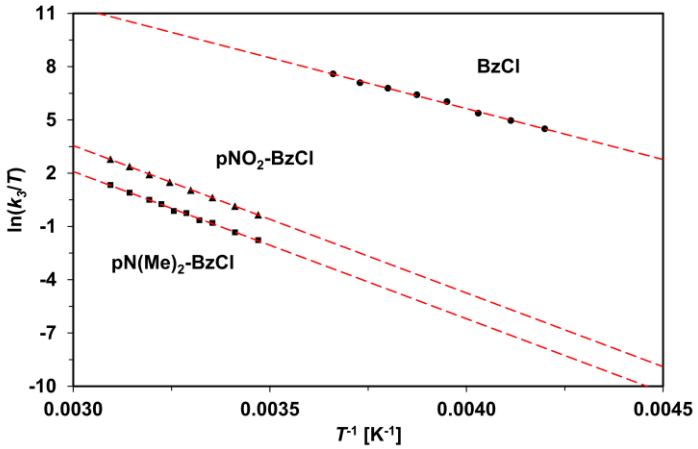

Figure S11. Eyring plot for the reaction of the peroxido-complex **2b** (c = 0.2 mmol L^{-1}) with BzCl (c = 20.0 mmol L^{-1}) based on the observed rate constants (fitted for first order reaction) determined from the kinetic measurements in the temperature range -80.0 to 0.0 °C. Determinated activation parameters: $\Delta H^{\neq}$ (BzCl, 445 nm) = 40 ± 1 kJ mol^{-1} and $\Delta H^{\neq}$ (BzCl, 600 nm) = 40 ± 1 kJ mol^{-1}. $\Delta S^{\neq}$ (BzCl, 445 nm) = 10 ± 3 J mol^{-1} K^{-1} and $\Delta S^{\neq}$ (BzCl, 600 nm) = 11 ± 3 J mol^{-1} K^{-1}. $\Delta H^{\neq}$ ($p$$NO_2$-BzCl, 600 nm) = 67 ± 3 kJ mol^{-1} and $\Delta H^{\neq}$ ($p$$N(Me)_2$-BzCl, 600 nm) = 69 ± 1 kJ mol^{-1}. $\Delta S^{\neq}$ ($p$$NO_2$-BzCl, 600 nm) = 21 ± 8 kJ mol^{-1} and $\Delta S^{\neq}$ ($p$$N(Me)_2$-BzCl, 600 nm) = 39 ± 2 kJ mol^{-1}. $\Delta G^{\neq}$ (BzCl, 600 nm) = 37 ± 8 kJ mol^{-1}, $\Delta G^{\neq}$ ($p$$NO_2$-BzCl, 600 nm) = 61 ± 2 kJ mol^{-1} and $\Delta G^{\neq}$ ($p$$N(Me)_2$-BzCl, 600 nm) = 57 ± 1 kJ mol^{-1}.

3.3 | Reaction of Complex 1a with O_2 and BzCl

Figure S12. Scheme of the reaction of compound 1a with O_2 (formation of **2a**) and the subsequent reaction with an excess of benzoyl chloride (formation of **I2**).

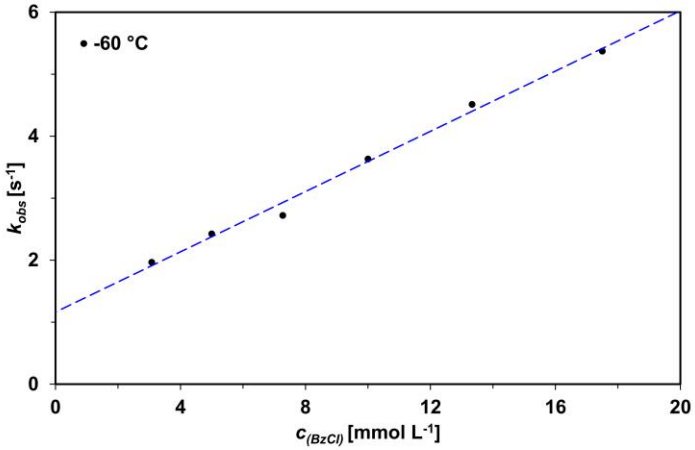

Figure S13. Plot of the rate constants k_{obs} versus the BzCl-concentration at -60 °C. Kinetic data were acquired by double-mixing Stopped-Flow experiments. The intermediate **2a** was generated by mixing a solution of **1a** (c = 0.4 mmol L^{-1}) with 75 µL oxygen saturated methanol solution (c = 10.4 mmol L^{-1}). The first mixed solution was aged for 3 s. In the second mixing the generated peroxido complex **2a** reacted with different volumes of a BzCl solution (c = 40 mmol L^{-1}) to trace the decay of the peroxido complex **2a** at λ_{max} = 600 nm. Second-order rate constant at -60 °C: $k_{2(-60°C)}$ = 243 ± 11 L s^{-1} mol^{-1}.

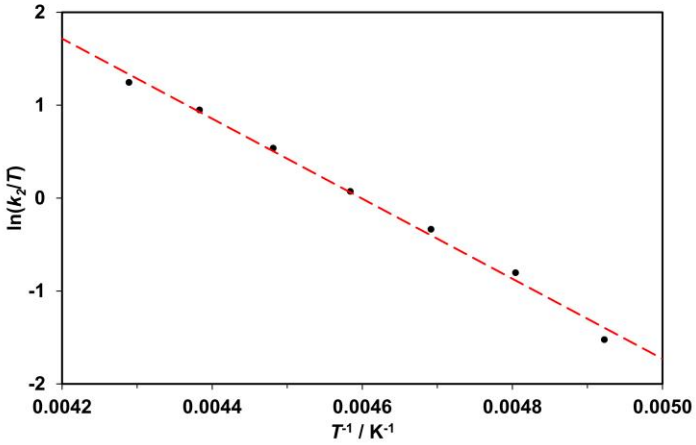

Figure S14. Eyring plot acquired from double-mixing Stopped-Flow experiments in a temperature range -70.0 to -40.0 °C. The intermediate **2a** was generated by mixing 75 µL of solution **1a** (c = 0.4 mmol L^{-1}) with 75 µL oxygen saturated methanol solution (c = 10.4 mmol L^{-1}). The first mixed solution was aged for 3 s. In the second mixing the generated peroxido complex **2a** reacted with 75 µL BzCl solution (c = 40 mmol L^{-1}) to trace the decay of the peroxido complex **2a** at λ_{max} = 605 nm. Determinated activation parameters: $\Delta H^{\neq}$ = 36 ± 1 kJ mol^{-1}, $\Delta S^{\neq}$ = -33 ± 6 J mol^{-1} K^{-1} and $\Delta G^{\neq}$ = 46 ± 1 kJ mol^{-1}.

3.4 | Reaction of 1b with Peracetic Acid

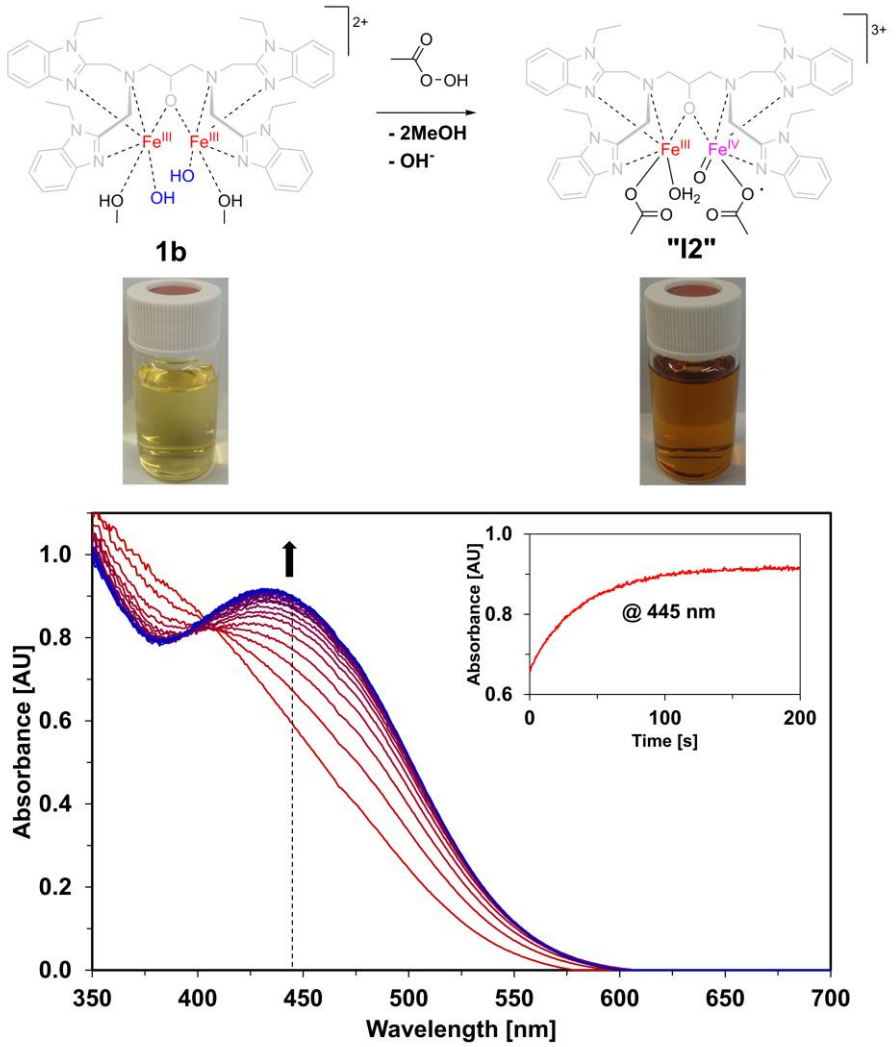

Figure S15. Time-resolved UV-vis spectra (Δt = 9.9 s) of the reaction of **1b** (c = 0.2 mmol L^{-1}) with an excess PAA (c = 50.0 mmol L^{-1}) at -70.0 °C to trace the formation at λ = 445 nm (intermediate **I2**). The diagram in the right corner shows the time-trace over the course of 200 s.

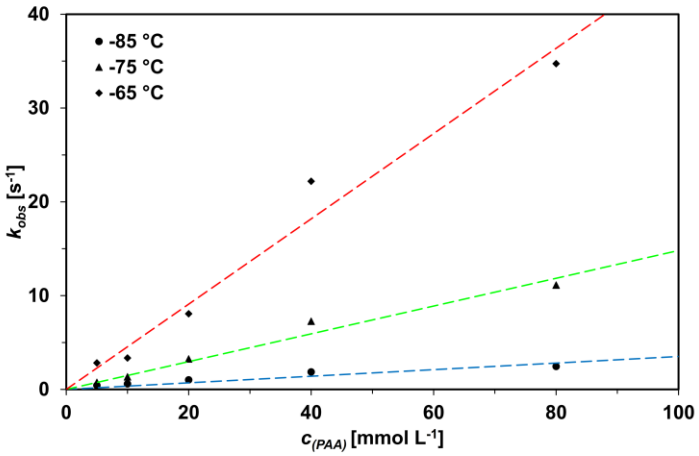

Figure S16. Plot of the rate constants k_{obs} versus the PAA-concentration at different temperatures. Concentration of **1b**: c = 0.2 mmol L^{-1}. Measurement at 445 nm. Second-order rate constant at -65 °C: $k_{2(-65°C)}$ = 455 ± 25 L s^{-1} mol^{-1}.

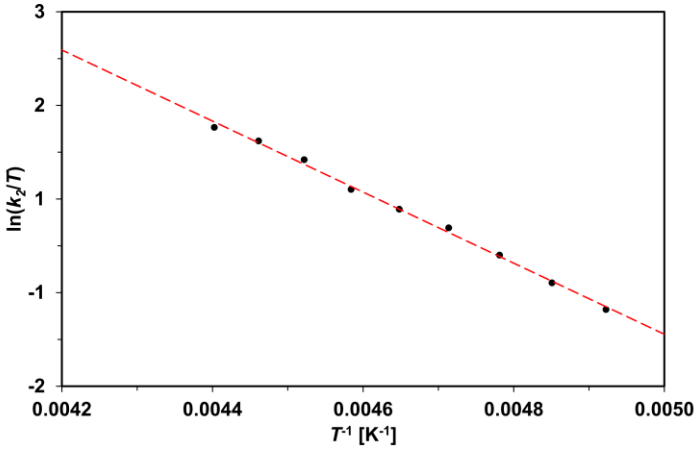

Figure S17. Eyring plot for the reaction of the reaction of **1b** (c = 0.2 mmol L^{-1}) with an excess PAA (c = 50.0 mmol L^{-1}) based on the observed rate constants (fitted for first order reaction) determined from the kinetic measurements in the temperature range -70.0 to -40.0 °C. Determinated activation parameters: $\Delta H^{\neq}$ = 32 ± 1 kJ mol^{-1}, $\Delta S^{\neq}$ = -48 ± 3 J mol^{-1} K^{-1} and $\Delta H^{\neq}$ = 46 ± 2 kJ mol^{-1}.

3.5 | Reaction of I2 with Et_3N

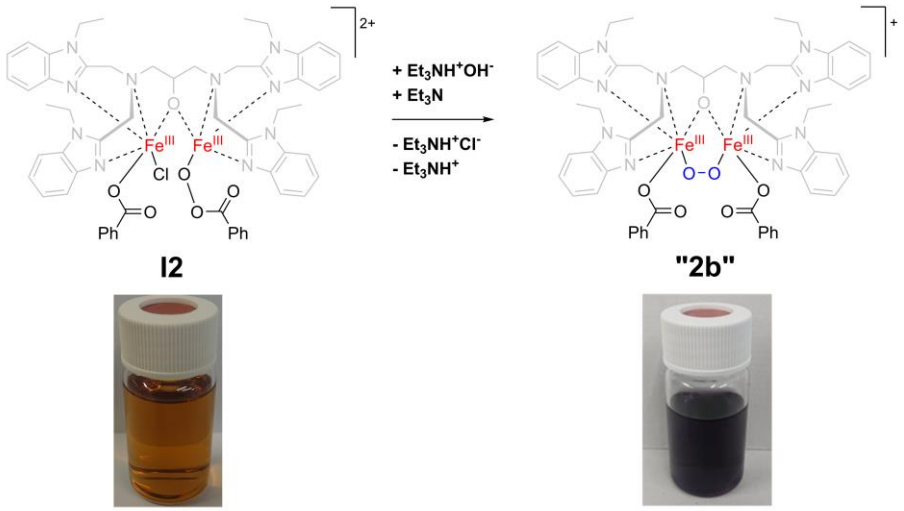

Figure S18. Scheme of the reaction of product **I2** with hydroxide ions (generated by Et_3N in methanol with water residues).

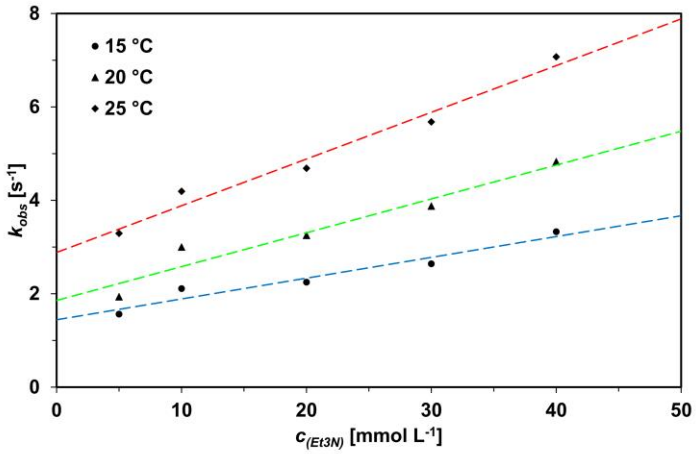

Figure S19. Plot of the rate constants k_{obs} versus the BzCl-concentration at different temperatures. Kinetic data were acquired by double-mixing Stopped-Flow experiments. The intermediate **I2** was generated by mixing a premixed solution of **2b** (c = 0.8 mmol L^{-1}) with 75 µL of a BzCl solution (c = 10 mmol L^{-1}). The first mixed solution was aged for 5 s. In the second mixing the generated intermediate **I2** reacted with 75 µL of a Et_3N solution (c = 5 - 40 mmol L^{-1}) to trace the formation of the peroxido species at λ_{max} = 550 nm. Second-order rate constant at 25 °C: $k_{2(25°C)}$ = 100 ± 9 L s^{-1} mol^{-1}.

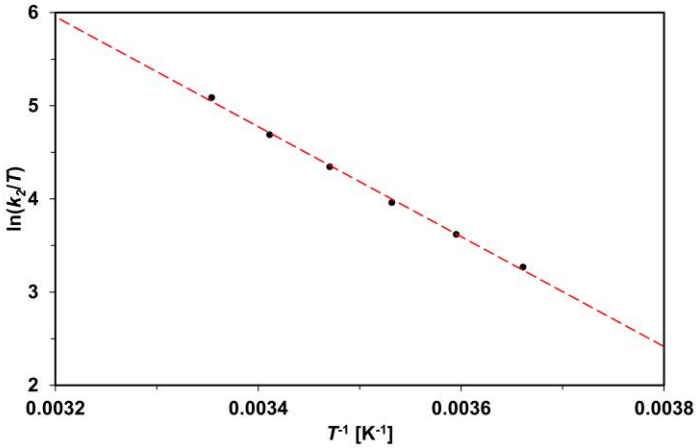

Figure S20. Eyring plot acquired from double-mixing Stopped-Flow experiments in a temperature range 0 °C to 25 °C. The intermediate **I2** was generated by mixing 75 µL of a premixed solution of **2b** (c = 0.4 mmol L^{-1}) with 75 µL H_2O_2 solution (c = 20 mmol L^{-1}). The first mixed solution was aged for 5 s. In the second mixing the generated intermediate **I2** reacted with 75 µL of an Et_3N solution (c = 80 mmol L^{-1}) to trace the formation of the peroxido species at λ_{max} = 550 nm. Determinated activation parameters: $\Delta H^{\neq}$ = 49 ± 1 kJ mol^{-1}, $\Delta S^{\neq}$ = 9 ± 4 J mol^{-1} K^{-1} and $\Delta G^{\neq}$ = 46 ± 1 kJ mol^{-1}.

3.6 | Reaction of $[Fe(bztpen)(OOH)]^{2+}$ with BzCl

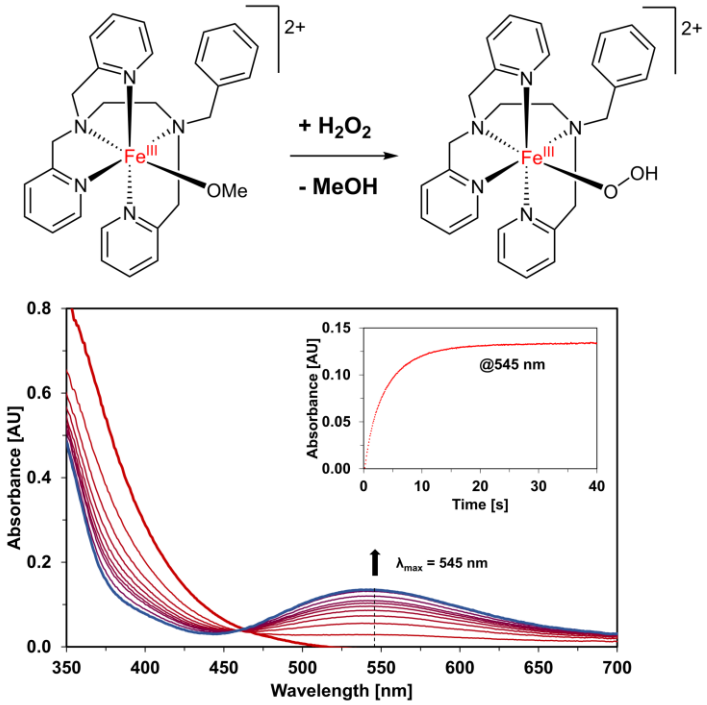

Figure S21. Time-resolved UV-vis spectra of the reaction of complex **[Fe(bztpen)(OMe)]$^{2+}$** (c = 0.1 mmol L^{-1}) with an excess H_2O_2 (c = 10.0 mmol L^{-1}) at -50.0 °C to trace the formation at λ_{max} = 545 nm (intermediate **[Fe(bztpen)(OOH)]$^{2+}$**). The diagram in the right corner shows the time-trace over the course of 40 s.

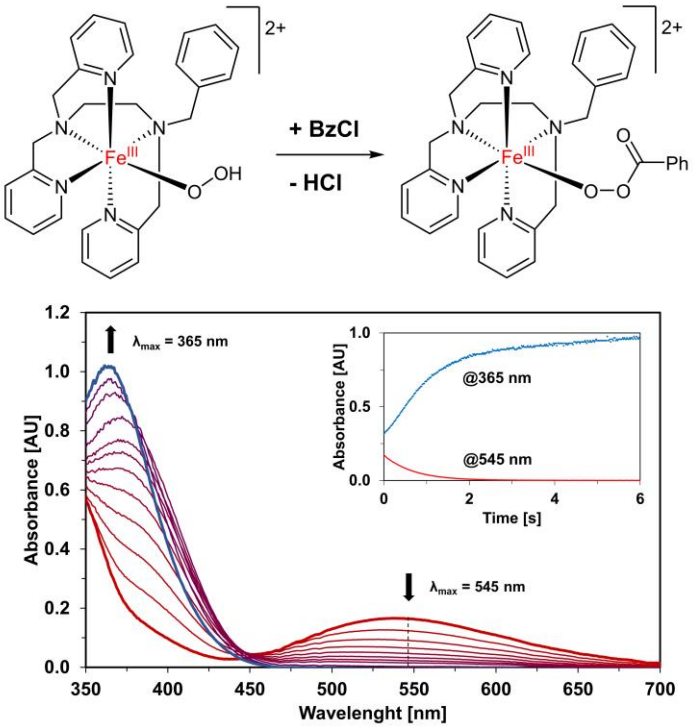

Figure S22. Time-resolved UV-vis spectra acquired from a double-mixing Stopped-Flow experiment in MeOH as solvent. The hydroperoxido complex was generated by mixing 75 µL of a solution of **[Fe(bztpen)(OMe)]$^{2+}$** (c = 0.4 mmol L^{-1}) with 75 µL H_2O_2 solution (c = 40 mmol L^{-1}) in the first mixing-step. The mixed solution was aged for 20 s (at -50 °C). In the second mixing-step the generated intermediate **[Fe(bztpen)(OOH)]$^{2+}$** reacted with 75 µL of a BzCl solution (c = 80 mmol L^{-1}) at -50 °C to trace the decay at λ_{max} = 545 nm and the formation of the unknown chromophore at λ_{max} = 365 nm. The diagram in the right corner shows the time-trace over the course of 6 s.

4 | Computational Details

The results for the Gibbs-Energies where the electronic energies are calculated using B3LYP*-D3(BJ)/def2-TZVP COSMO(methanol),[8-10] a benzoyl chloride concentration of 0.04 mol L^{-1} was used, and ro-vibrational contributions were calculated with PBE0-D3(BJ)/def2-SVP, def2-TZVP [8a,8b,8h,8i,8j,8k,11,12] are shown in Scheme 4. Figure S23 shows the results for benzoyl chloride concentration of 0.02 mol L^{-1}. The results where the electronic energies are calculated using PBE0-D3(BJ)/def2-SVP, def2-TZVP are shown in Figure S24 and Figure S25. The trends of the Gibbs-Energies from **2b** over **I1-a**, **2a**, **I2-a** to **P-b** calculated with PBE0-D3(BJ)/def2-SVP, def2-TZVP electronic energies are overall similar to the Gibbs-Energies where the electronic energy is calculated with B3LYP*-D3(BJ)/def2-TZVP.

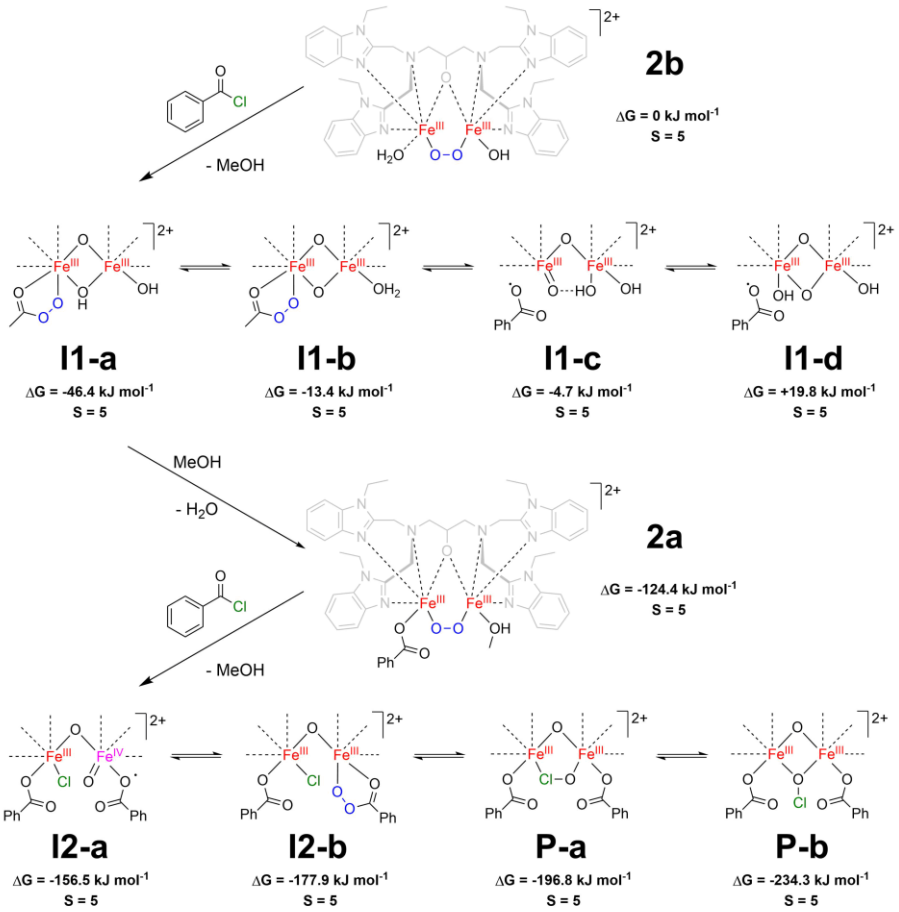

Figure S23: Gibbs energies relative to **2b** in conjugation with a benzyl chloride in kJ mol^{-1}. The electronic energies are calculated with B3LYP*-D3(BJ)/def2-TZVP COSMO(methanol), a benzoyl chloride concentration of 0.02 mol L^{-1} is used, and the ro-vibrational contributions are calculated with PBE0-D3(BJ)/def2-SVP, def2-TZVP. All iron complexes are in an undecet spin state (S = 5).

5 | NMR Spectra

5.1 | NMR Spectra of HPTB

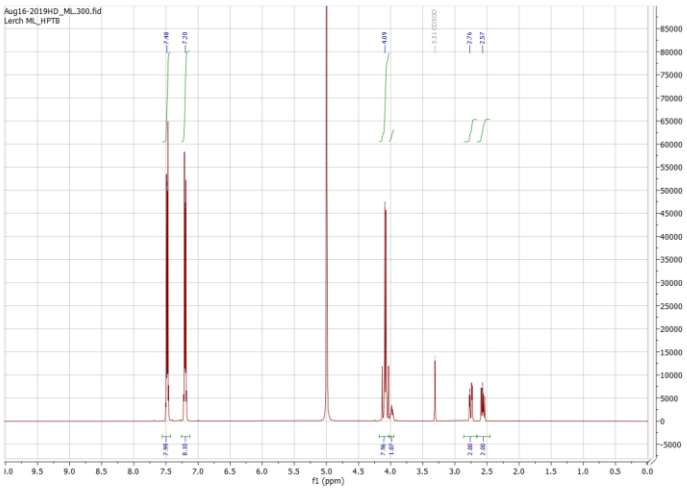

Figure S26. ^{1}H-NMR of HPTB. The sample was dissolved in methanol-d_4. The residual solvent signal of methanol-d_4 was used as reference for the ^{1}H-NMR spectrum.

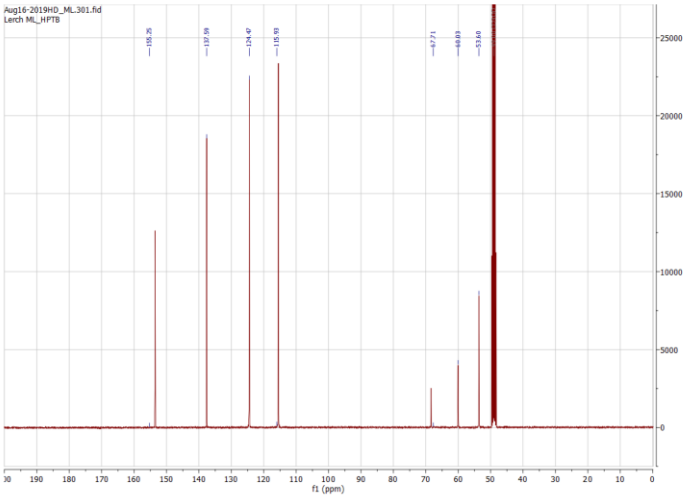

Figure S27. ^{13}C-NMR of HPTB. The sample was dissolved in methanol-d_4. The residual solvent signal of methanol-d was used as reference for the ^{13}C-NMR spectrum.

5.2 | NMR Spectra of EtHPTB

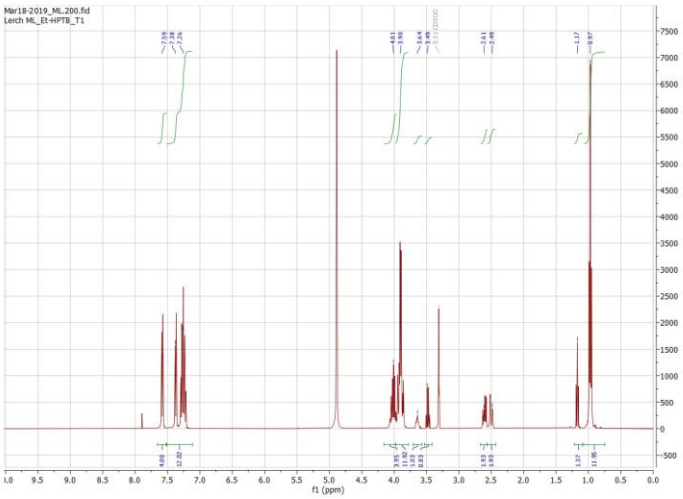

Figure S28. ^{1}H-NMR of EtHPTB. The sample was dissolved in chloroform-*d*. TCM was used as reference for the ^{1}H-NMR spectrum.

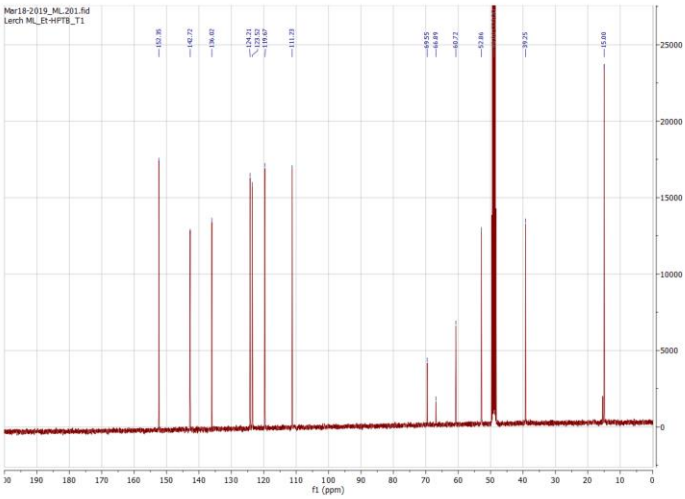

Figure S29. ^{13}C-NMR of EtHPTB. The sample was dissolved in chloroform-*d*. TCM was used as reference for the ^{13}C-NMR spectrum.

5.3 | NMR Spectra of bztpen

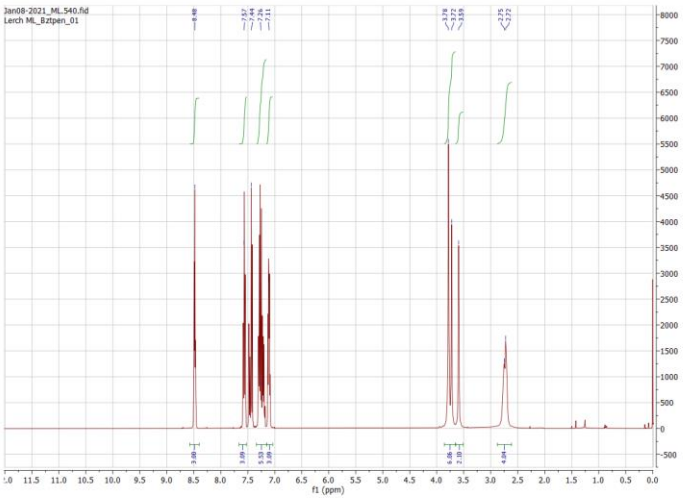

Figure S30. ^{1}H-NMR of bztpen. The sample was dissolved in chloroform-*d*. TCM was used as reference for the ^{1}H-NMR spectrum.

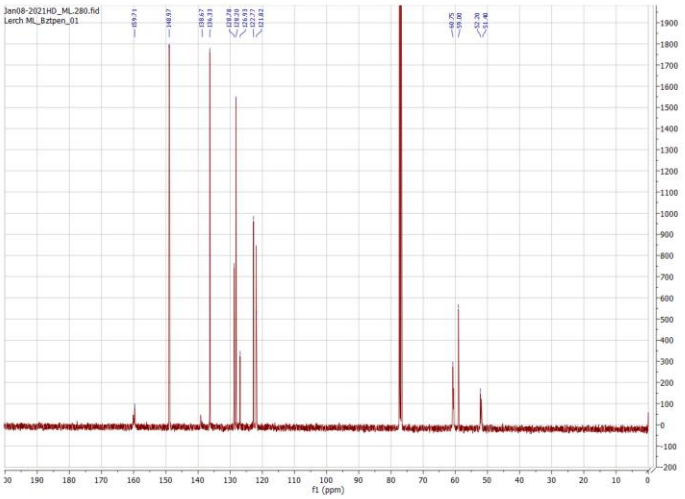

Figure S31. ^{13}C-NMR of bztpen. The sample was dissolved in chloroform-*d*. TCM was used as reference for the ^{13}C-NMR spectrum.

5.4 | NMR Spectra of Perdecanoic Acid

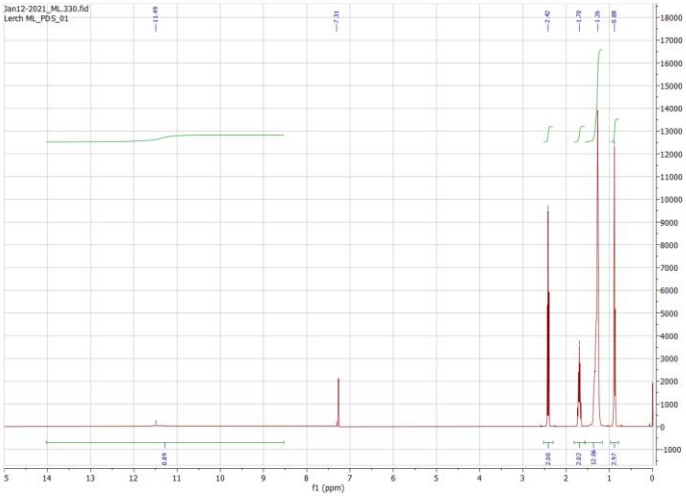

Figure S32. ^{1}H-NMR of perdecanoic acid. The sample was dissolved in chloroform-*d*. TCM was used as reference for the ^{1}H-NMR spectrum.

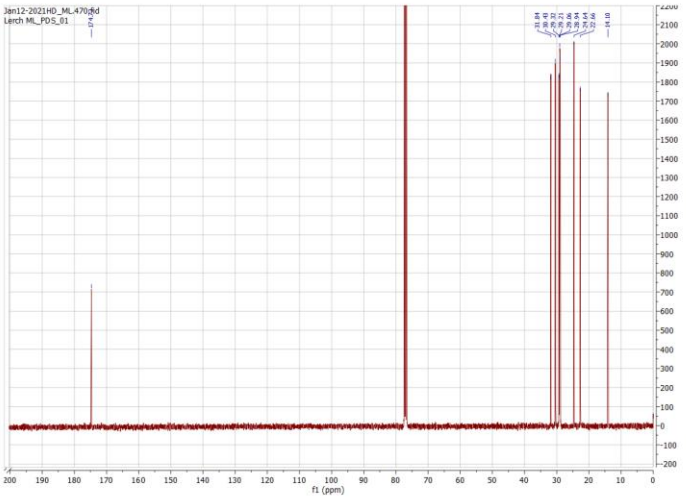

Figure S33. ^{13}C-NMR of perdecanoic acid. The sample was dissolved in chloroform-*d*. TCM was used as reference for the ^{13}C-NMR spectrum.

6 | References

[1] L. Krause, R. Herbst-Irmer, G. M. Sheldrick, D. Stalke, J. Appl. Crystallogr. 2015, 48, 3–10.

[2] G. M. Sheldrick, Acta Crystallogr., Sect. A: Found. Adv. 2015, 71, 3–8.

[3] G. M. Sheldrick, Acta Crystallogr., Sect. C: Struct. Chem. 2015, 71, 3–8.

[4] C. R. Groom, I. J. Bruno, M. P. Lightfoot, S. C. Ward, Acta Crystallogr., Sect. B: Struct. Sci., Cryst. Eng. Mater. 2016, 72, 171–179.

[5] P. Müller, Crystallogr. Rev. 2009, 15, 57–83.

[6] A. Thorn, B. Dittrich, G. M. Sheldrick, Acta Crystallogr., Sect. A: Found. Crystallogr. 2012, 68, 448–451.

[7] L. J. Farrugia, J. Appl. Crystallogr. 2012, 45, 849–854.

[8] a) Proc. R. Soc. Lond. A. 1929, 123, 714–733; b) J. C. Slater, Phys. Rev. 1951, 81, 385–390; c) S. H. Vosko, L. Wilk, M. Nusair, Can. J. Phys. 1980, 58, 1200–1211; d) Becke, Phys. Rev. [Sect.] A. 1988, 38, 3098–3100; e) Lee, Yang, Parr, Phys. Rev. [Sect.] B. 1988, 37, 785–789; f) A. D. Becke, J. Chem. Phys. 1993, 98, 5648–5652; g) M. Reiher, O. Salomon, B. Artur Hess, Theor. Chem. Acc. 2001, 107, 48–55; h) S. Grimme, J. Antony, S. Ehrlich, H. Krieg, J. Chem. Phys. 2010, 132, 154104; i) S. Grimme, S. Ehrlich, L. Goerigk, J. Comput. Chem. 2011, 32, 1456–1465; j) K. Eichkorn, F. Weigend, O. Treutler, R. Ahlrichs, Theor. Chem. Acc. 1997, 97, 119–124; k) F. Weigend, R. Ahlrichs, Phys. Chem. Chem. Phys. 2005, 7, 3297–3305; l) F. Weigend, M. Häser, H. Patzelt, R. Ahlrichs, Chem. Phys. Lett. 1998, 294, 143–152.

[9] a) A. Schäfer, A. Klamt, D. Sattel, J. C. W. Lohrenz, F. Eckert, Phys. Chem. Chem. Phys. 2000, 2, 2187–2193; b) A. Klamt, G. Schüürmann, J. Chem. Soc., Perkin Trans. 2. 1993, 799–805.

[10] a) S. G. Balasubramani, G. P. Chen, S. Coriani, M. Diedenhofen, M. S. Frank, Y. J. Franzke, F. Furche, R. Grotjahn, M. E. Harding, C. Hättig, A. Hellweg, B. Helmich-Paris, C. Holzer, U. Huniar, M. Kaupp, A. Marefat Khah, S. Karbalaei Khani, T. Müller, F. Mack, B. D. Nguyen, S. M. Parker, E. Perlt, D. Rappoport, K. Reiter, S. Roy, M. Rückert, G. Schmitz, M. Sierka, E. Tapavicza, D. P. Tew, C. van Wüllen, V. K. Voora, F. Weigend, A. Wodyński, J. M. Yu, J. Chem. Phys. 2020, 152, 184107; b) TURBOMOLE V7.5 2020, a development of University of Karlsruhe and Forschungszentrum Karlsruhe GmbH, **1989-2007**, *TURBOMOLE GmbH*, since **2007**; *available from https://www.turbomole.org.*

[11] a) J. P. Perdew, M. Ernzerhof, K. Burke, J. Chem. Phys. 1996, 105, 9982–9985; b) Perdew, Wang, Phys. Rev. B: Condens. Matter Mater. Phys. 1992, 45, 13244–13249; c) Perdew, Burke, Ernzerhof, Phys. Rev. Lett. 1996, 77, 3865–3868; d) A. Schäfer, H. Horn, R. Ahlrichs, J. Chem. Phys. 1992, 97, 2571–2577.

[12] a) R. Ahlrichs, M. Bär, M. Häser, H. Horn, C. Kölmel, Chem. Phys. Lett. 1989, 162, 165–169; b) P. Deglmann, F. Furche, R. Ahlrichs, Chem. Phys. Lett. 2002, 362, 511–518; c) P. Deglmann, F. Furche, J. Chem. Phys. 2002, 117, 9535–9538; c) P. Deglmann, F. Furche, J. Chem. Phys. 2002, 117, 9535–9538; d) TURBOMOLE V7.3 2018, a development of University of Karlsruhe and Forschungszentrum Karlsruhe GmbH, **1989-2007**, *TURBOMOLE GmbH*, since **2007**; *available from http://www.turbomole.com.*

5 | Literaturliste

[001] S. Herres-Pawlis, P. Kluefers, *Bioanorganische Chemie*: Metalloproteine, Methoden und Konzepte, Wiley VCH Verlag GmbH & Co. KGaA, Weinheim, **2017**.

[002] N. Abbaspour, R. Hurrell, R. Kelishadi, *Journal of Research in Medical Sciences : The Official Journal of Isfahan University of Medical Sciences* **2014**, *19*, 164-174.

[003] M. Bost, S. Houdart, M. Oberli, E. Kalonji, J.-F. Huneau, I. Margaritis, *J. Trace Elem. Med. Biol. : organ of the Society for Minerals and Trace Elements (GMS)* **2016**, *35*, 107-115.

[004] C. Elschenbroich, F. Hensel, H. Hopf, W. Kaim, B. Schwederski, *Bioanorganishe Chemie*: Zur Funktion chemischer Elemente in Lebensprozessen, Vieweg+Teubner Verlag, Wiesbaden, **1991**.

[005] J. Liu, S. Chakraborty, P. Hosseinzadeh, Y. Yu, S. Tian, I. Petrik, A. Bhagi, Y. Lu, *Chem. Rev.* **2014**, *114*, 4366-4469.

[006] R. H. Holm, P. Kennepohl, E. I. Solomon, *Chem. Rev.* **1996**, *96*, 2239-2314.

[007] W. Kaim, J. Rall, *Angew. Chem. Int. Ed.* **1996**, *35*, 43-60.

[008] X. Huang, J. T. Groves, *Chem. Rev.* **2018**, *118*, 2491-2553.

[009] I. A. Koval, P. Gamez, C. Belle, K. Selmeczi, J. Reedijk, *Chem. Soc. Rev.* **2006**, *35*, 814-840.

[010] I. Persson, *Pure Appl. Chem.* **2010**, *82*, 1901-1917.

[011] P. M. Colman, H. C. Freeman, J. M. Guss, M. Murata, V. A. Norris, J. A. M. Ramshaw, M. P. Venkatappa, *Nature* **1978**, *272*, 319-324.

[012] H. B. Gray, B. G. Malmström, R. J. Williams, *J. Biol. Inorg. Chem.* **2000**, *5*, 551-559.

[013] J. P. Klinman, *Chem. Rev.* **1996**, *96*, 2541-2562.

[014] C. E. Elwell, N. L. Gagnon, B. D. Neisen, D. Dhar, A. D. Spaeth, G. M. Yee, W. B. Tolman, *Chem. Rev.* **2017**, *117*, 2059-2107.

[015] K. A. Magnus, B. Hazes, H. Ton-That, C. Bonaventura, J. Bonaventura, W. G. Hol, *Proteins.* **1994**, *19*, 302-309.

[016] C. Elschenbroich, F. Hensel, H. Hopf, R. B. Jordan, *Mechanismen anorganischer und metallorganischer Reaktionen,* Vieweg+Teubner Verlag, Wiesbaden, **1994**.

[017] A. Volbeda, W. G. Hol, *J. Mol. Biol.* **1989**, *209*, 249-279.

[018] A. Volbeda, W. G. Hol, *J. Mol. Biol.* **1989**, *206*, 531-546.

[019] Z. Gai, A. Matsuno, K. Kato, S. Kato, M. R. I. Khan, T. Shimizu, T. Yoshioka, Y. Kato, H. Kishimura, G. Kanno, Y. Miyabe, T. Terada, Y. Tanaka, M. Yao, *Structure.* **2015**, *23*, 2204-2212.

[020] H. Decker, T. Schweikardt, F. Tuczek, *Angew. Chem. Int. Ed.* **2006**, *45*, 4546-4550.

[021] M. Rolff, J. Schottenheim, H. Decker, F. Tuczek, *Chem. Soc. Rev.* **2011**, *40*, 4077-4098.

[022] M. Momenteau, C. A. Reed, *Chem. Rev.* **1994**, *94*, 659-698.

[023] C. E. Mortimer, U. Müller, J. Beck, *Chemie*: Das Basiswissen der Chemie : 410 Abbildungen, 545 Formelbilder, Georg Thieme Verlag, Stuttgart, New York, **2015**.

[024] I. Garcia-Bosch, K. D. Karlin, in *PATAI'S Chemistry of Functional Groups*, (Ed. Z. Rappoport), John Wiley & Sons, Ltd, Chichester, UK, **2009**, pp. 1-52.

[025] K. D. Karlin, S. Itoh, Eds, *Copper-Oxygen Chemistry,* John Wiley & Sons, Inc, Hoboken, NJ, USA, **2011**.

[026] L. M. Mirica, X. Ottenwaelder, T. D. P. Stack, *Chem. Rev.* **2004**, *104*, 1013-1045.

[027] C. Würtele, O. Sander, V. Lutz, T. Waitz, F. Tuczek, S. Schindler, *J. Am. Chem. Soc.* **2009**, *131*, 7544-7545.

[028] E. A. Lewis, W. B. Tolman, *Chem. Rev.* **2004**, *104*, 1047-1076.

[029] C. Citek, S. Herres-Pawlis, T. D. P. Stack, *Acc. Chem. Res.* **2015**, *48*, 2424-2433.

[030] T. N. Sorrell, *Tetrahedron* **1989**, *45*, 3-68.

[031] W. Keown, J. B. Gary, T. D. P. Stack, *J. Biol. Inorg. Chem.* **2017**, *22*, 289-305.

[032] L. Q. Hatcher, K. D. Karlin, *J. Biol. Inorg. Chem.* **2004**, *9*, 669-683.

[033] S. Schindler, *Eur. J. Inorg. Chem.* **2000**, *2000*, 2311-2326.

[034] R. R. Jacobson, Z. Tyeklar, A. Farooq, K. D. Karlin, S. Liu, J. Zubieta, *J. Am. Chem. Soc.* **1988**, *110*, 3690-3692.

[035] C. Würtele, E. Gaoutchenova, K. Harms, M. C. Holthausen, J. Sundermeyer, S. Schindler, *Angew. Chem. Int. Ed.* **2006**, *45*, 3867-3869.
[036] C. Würtele, E. Gaoutchenova, K. Harms, M. C. Holthausen, J. Sundermeyer, S. Schindler, *Angew. Chem.* **2006**, *118*, 3951-3954.
[037] T. Hoppe, S. Schaub, J. Becker, C. Würtele, S. Schindler, *Angew. Chem. Int. Ed.* **2013**, *52*, 870-873.
[038] K. Komiyama, H. Furutachi, S. Nagatomo, A. Hashimoto, H. Hayashi, S. Fujinami, M. Suzuki, T. Kitagawa, *BCSJ* **2004**, *77*, 59-72.
[039] M. J. Baldwin, D. E. Root, J. E. Pate, K. Fujisawa, N. Kitajima, E. I. Solomon, *J. Am. Chem. Soc.* **1992**, *114*, 10421-10431.
[040] S. Mahapatra, V. G. Young, S. Kaderli, A. D. Zuberbühler, W. B. Tolman, *Angew. Chem. Int. Ed.* **1997**, *36*, 130-133.
[041] S. Mahapatra, J. A. Halfen, W. B. Tolman, *J. Am. Chem. Soc.* **1996**, *118*, 11575-11586.
[042] C. J. Cramer, W. B. Tolman, *Acc. Chem. Res.* **2007**, *40*, 601-608.
[043] N. Kindermann, E. Bill, S. Dechert, S. Demeshko, E. J. Reijerse, F. Meyer, *Angew. Chem. Int. Ed.* **2015**, *54*, 1738-1743.
[044] K. D. Karlin, N. Wei, B. Jung, S. Kaderli, P. Niklaus, A. D. Zuberbuehler, *J. Am. Chem. Soc.* **1993**, *115*, 9506-9514.
[045] M. Schatz, M. Becker, F. Thaler, F. Hampel, S. Schindler, R. R. Jacobson, Z. Tyeklár, N. N. Murthy, P. Ghosh, Q. Chen, J. Zubieta, K. D. Karlin, *Inorg. Chem.* **2001**, *40*, 2312-2322.
[046] M. Bhadra, W. J. Transue, H. Lim, R. E. Cowley, J. Y. C. Lee, M. A. Siegler, P. Josephs, G. Henkel, M. Lerch, S. Schindler, A. Neuba, K. O. Hodgson, B. Hedman, E. I. Solomon, K. D. Karlin, *J. Am. Chem. Soc.* **2021**, *143*, 3707-3713.
[047] N. Kitajima, K. Fujisawa, Y. Moro-oko, K. Toriumi, *J. Am. Chem. Soc.* **1989**, *111*, 8975-8976.
[048] K. Fujisawa, M. Tanaka, Y. Moro-oko, N. Kitajima, *J. Am. Chem. Soc.* **1994**, *116*, 12079-12080.
[049] T. N. Sorrell, W. E. Allen, P. S. White, *Inorg. Chem.* **1995**, *34*, 952-960.
[050] S. Itoh, S. Fukuzumi, *Acc. Chem. Res.* **2007**, *40*, 592-600.
[051] L. M. Mirica, M. Vance, D. J. Rudd, B. Hedman, K. O. Hodgson, E. I. Solomon, T. D. P. Stack, *Science* **2005**, *308*, 1890-1892.
[052] N. W. Aboelella, S. V. Kryatov, B. F. Gherman, W. W. Brennessel, V. G. Young, R. Sarangi, E. V. Rybak-Akimova, K. O. Hodgson, B. Hedman, E. I. Solomon, C. J. Cramer, W. B. Tolman, *J. Am. Chem. Soc.* **2004**, *126*, 16896-16911.
[053] S. Itoh, H. Nakao, L. M. Berreau, T. Kondo, M. Komatsu, S. Fukuzumi, *J. Am. Chem. Soc.* **1998**, *120*, 2890-2899.
[054] M. Becker, F. W. Heinemann, F. Knoch, W. Donaubauer, G. Liehr, S. Schindler, G. Golub, H. Cohen, D. Meyerstein, *Eur. J. Inorg. Chem.* **2000**, *2000*, 719-726.
[055] W. E. Lynch, D. M. Kurtz, S. Wang, R. A. Scott, *J. Am. Chem. Soc.* **1994**, *116*, 11030-11038.
[056] J. E. Bol, W. L. Driessen, R. Y. N. Ho, B. Maase, L. Que, J. Reedijk, *Angew. Chem.* **1997**, *109*, 1022-1025.
[057] G. J. Karahalis, A. Thangavel, B. Chica, J. Bacsa, R. B. Dyer, C. C. Scarborough, *Inorg. Chem.* **2016**, *55*, 1102-1107.
[058] A. Franke, C. Fertinger, R. van Eldik, *Angew. Chem. Int. Ed.* **2008**, *47*, 5238-5242.
[059] M. F. Perutz, *Trends Biochem. Sci.* **1989**, *14*, 42-44.
[060] S. E. Phillips, B. P. Schoenborn, *Nature* **1981**, *292*, 81-82.
[061] D. Sawyer, *Oxygen chemistry,* Oxford University Press, New York, **1991**.
[062] M. Hayyan, M. A. Hashim, I. M. AlNashef, *Chem. Rev.* **2016**, *116*, 3029-3085.
[063] J. F. Turrens, *The Journal of Physiology* **2003**, *552*, 335-344.
[064] J. Reedijk, *Bioinorg. Catal.,* Taylor & Francis Group, Milton, **1999**.
[065] M. A. Holmes, R. E. Stenkamp, *J. Mol. Biol.* **1991**, *220*, 723-737.
[066] K. Zhang, E. A. Stern, F. Ellis, J. Sanders-Loehr, A. K. Shiemke, *Biochem.* **1988**, *27*, 7470-7479.
[067] M. Y. Okamura, I. M. Klotz, C. E. Johnson, M. R. Winter, R. J. Williams, *Biochem.* **1969**, *8*, 1951-1958.
[068] A. K. Shiemke, T. M. Loehr, J. Sanders-Loehr, *J. Am. Chem. Soc.* **1986**, *108*, 2437-2443.

[069] A. K. Shiemke, T. M. Loehr, J. Sanders-Loehr, *J. Am. Chem. Soc.* **1984**, *106*, 4951-4956.
[070] J. S. Pap, M. A. Cranswick, E. Balogh-Hergovich, G. Baráth, M. Giorgi, G. T. Rohde, J. Kaizer, G. Speier, L. Que, *Eur. J. Inorg. Chem.* **2013**, *2013*, 3858-3866.
[071] B. J. Wallar, J. D. Lipscomb, *Chem. Rev.* **1996**, *96*, 2625-2658.
[072] C. E. Tinberg, S. J. Lippard, *Acc. Chem. Res.* **2011**, *44*, 280-288.
[073] K. E. Liu, A. M. Valentine, D. Wang, B. H. Huynh, D. E. Edmondson, A. Salifoglou, S. J. Lippard, *J. Am. Chem. Soc.* **1995**, *117*, 10174-10185.
[074] L. Shu, Y. Liu, J. D. Lipscomb, L. Que, *J. Biol. Inorg. Chem.* **1996**, *1*, 297-304.
[075] R. Banerjee, Y. Proshlyakov, J. D. Lipscomb, D. A. Proshlyakov, *Nature* **2015**, *518*, 431-434.
[076] A. C. Rosenzweig, C. A. Frederick, S. J. Lippard, P. Nordlund, *Nature* **1993**, *366*, 537-543.
[077] S. K. Lee, J. C. Nesheim, J. D. Lipscomb, *Int. J. STD AIDS* **1993**, *268*, 21569-21577.
[078] L. Shu, J. C. Nesheim, K. Kauffmann, E. Münck, J. D. Lipscomb, L. Que, *Science* **1997**, *275*, 515-518.
[079] D. J. Rudd, M. H. Sazinsky, S. J. Lippard, B. Hedman, K. O. Hodgson, *Inorg. Chem.* **2005**, *44*, 4546-4554.
[080] A. C. Rosenzweig, P. Nordlund, P. M. Takahara, C. A. Frederick, S. J. Lippard, *Chem. & Biol.* **1995**, *2*, 409-418.
[081] J. G. DeWitt, J. G. Bentsen, A. C. Rosenzweig, B. Hedman, J. Green, S. Pilkington, G. C. Papaefthymiou, H. Dalton, K. O. Hodgson, S. J. Lippard, *J. Am. Chem. Soc.* **1991**, *113*, 9219-9235.
[082] N. Elango, R. Radhakrishnan, W. A. Froland, B. J. Wallar, C. A. Earhart, J. D. Lipscomb, D. H. Ohlendorf, *Prot. Sci.* **1997**, *6*, 556-568.
[083] K. E. Liu, D. Wang, B. H. Huynh, D. E. Edmondson, A. Salifoglou, S. J. Lippard, *J. Am. Chem. Soc.* **1994**, *116*, 7465-7466.
[084] C. Krebs, J. M. Bollinger, S. J. Booker, *Curr. Opin. Chem. Biol.* **2011**, *15*, 291-303.
[085] D. Das, B. E. Eser, J. Han, A. Sciore, E. N. G. Marsh, *Angew. Chem. Int. Ed.* **2011**, *50*, 7148-7152.
[086] M. E. Pandelia, N. Li, H. Nørgaard, D. M. Warui, L. J. Rajakovich, W. Chang, S. J. Booker, C. Krebs, J. M. Bollinger, *J. Am. Chem. Soc.* **2013**, *135*, 15801-15812.
[087] K. Garbett, D. W. Darnall, I. M. Klotz, R. Williams, *Arch. Biochem. Biophys.* **1969**, *135*, 419-434.
[088] D. M. Kurtz, D. F. Shriver, I. M. Klotz, *J. Am. Chem. Soc.* **1976**, *98*, 5033-5035.
[089] M. A. Holmes, I. Le Trong, S. Turley, L. C. Sieker, R. E. Stenkamp, *J. Mol. Biol.* **1991**, *218*, 583-593.
[090] R. E. Stenkamp, *Chem. Rev.* **1994**, *94*, 715-726.
[091] D. T. Logan, X.-D. Su, A. Åberg, K. Regnström, J. Hajdu, H. Eklund, P. Nordlund, *Structure* **1996**, *4*, 1053-1064.
[092] J. Baldwin, C. Krebs, L. Saleh, M. Stelling, B. H. Huynh, J. M. Bollinger, P. Riggs-Gelasco, *Biochem.* **2003**, *42*, 13269-13279.
[093] L. M. K. Dassama, A. Silakov, C. M. Krest, J. C. Calixto, C. Krebs, J. M. Bollinger, M. T. Green, *J. Am. Chem. Soc.* **2013**, *135*, 16758-16761.
[094] Y.-S. Yang, J. Baldwin, B. A. Ley, J. M. Bollinger, E. I. Solomon, *J. Am. Chem. Soc.* **2000**, *122*, 8495-8510.
[095] P. Moënne-Loccoz, J. Baldwin, B. A. Ley, T. M. Loehr, J. M. Bollinger, *Biochem.* **1998**, *37*, 14659-14663.
[096] J. M. Bollinger, S. Chen, S. E. Parkin, L. M. Mangravite, B. A. Ley, D. E. Edmondson, B. H. Huynh, *J. Am. Chem. Soc.* **1997**, *119*, 5976-5977.
[097] P. J. Riggs-Gelasco, L. Shu, S. Chen, D. Burdi, B. H. Huynh, L. Que, J. Stubbe, *J. Am. Chem. Soc.* **1998**, *120*, 849-860.
[098] P. Nordlund, B. M. Sjöberg, H. Eklund, *Nature* **1990**, *345*, 593-598.
[099] T. M. Makris, V. van Vu, K. K. Meier, A. J. Komor, B. S. Rivard, E. Münck, L. Que, J. D. Lipscomb, *J. Am. Chem. Soc.* **2015**, *137*, 1608-1617.
[100] C. J. Knoot, E. G. Kovaleva, J. D. Lipscomb, *J. Biol. Inorg. Chem.* **2016**, *21*, 589-603.

[101] A. J. Jasniewski, A. J. Komor, J. D. Lipscomb, L. Que, *J. Am. Chem. Soc.* **2017**, *139*, 10472-10485.
[102] A. Trehoux, J.-P. Mahy, F. Avenier, *Coord. Chem. Rev.* **2016**, *322*, 142-158.
[103] A. J. Jasniewski, L. Que, *Chem. Rev.* **2018**, *118*, 2554-2592.
[104] A. Schirmer, M. A. Rude, X. Li, E. Popova, S. B. del Cardayre, *Science* **2010**, *329*, 559-562.
[105] N. Li, W. Chang, D. M. Warui, S. J. Booker, C. Krebs, J. M. Bollinger, *Biochem.* **2012**, *51*, 7908-7916.
[106] B. Khara, N. Menon, C. Levy, D. Mansell, D. Das, E. N. G. Marsh, D. Leys, N. S. Scrutton, *ChemBioChem* **2013**, *14*, 1204-1208.
[107] D. Das, B. E. Eser, J. Han, A. Sciore, E. N. G. Marsh, *Angew. Chem.* **2011**, *123*, 7286-7290.
[108] C. Jia, M. Li, J. Li, J. Zhang, H. Zhang, P. Cao, X. Pan, X. Lu, W. Chang, *Protein Cell.* **2015**, *6*, 55-67.
[109] L. J. Rajakovich, H. Nørgaard, D. M. Warui, W. Chang, N. Li, S. J. Booker, C. Krebs, J. M. Bollinger, M.-E. Pandelia, *J. Am. Chem. Soc.* **2015**, *137*, 11695-11709.
[110] N. Li, H. Nørgaard, D. M. Warui, S. J. Booker, C. Krebs, J. M. Bollinger, *J. Am. Chem. Soc.* **2011**, *133*, 6158-6161.
[111] K. G. Aukema, T. M. Makris, S. A. Stoian, J. E. Richman, E. Münck, J. D. Lipscomb, L. P. Wackett, *ACS Catal.* **2013**, *3*, 2228-2238.
[112] S. V. Kryatov, S. Taktak, I. V. Korendovych, E. V. Rybak-Akimova, J. Kaizer, S. Torelli, X. Shan, S. Mandal, V. L. MacMurdo, A. Mairata i Payeras, L. Que, *Inorg. Chem.* **2005**, *44*, 85-99.
[113] M. A. Cranswick, K. K. Meier, X. Shan, A. Stubna, J. Kaizer, M. P. Mehn, E. Münck, L. Que, *Inorg. Chem.* **2012**, *51*, 10417-10426.
[114] A. T. Fiedler, X. Shan, M. P. Mehn, J. Kaizer, S. Torelli, J. R. Frisch, M. Kodera, L. Que, *J. Phys. Chem. A* **2008**, *112*, 13037-13044.
[115] T. Ookubo, H. Sugimoto, T. Nagayama, H. Masuda, T. Sato, K. Tanaka, Y. Maeda, H. Ōkawa, Y. Hayashi, A. Uehara, M. Suzuki, *J. Am. Chem. Soc.* **1996**, *118*, 701-702.
[116] Y. Dong, S. Menage, B. A. Brennan, T. E. Elgren, H. G. Jang, L. L. Pearce, L. Que, *J. Am. Chem. Soc.* **1993**, *115*, 1851-1859.
[117] Y. Hayashi, T. Kayatani, H. Sugimoto, M. Suzuki, K. Inomata, A. Uehara, Y. Mizutani, T. Kitagawa, Y. Maeda, *J. Am. Chem. Soc.* **1995**, *117*, 11220-11229.
[118] J. R. Frisch, V. van Vu, M. Martinho, E. Münck, L. Que, *Inorg. Chem.* **2009**, *48*, 8325-8336.
[119] T. C. Brunold, N. Tamura, N. Kitajima, Y. Moro-oka, E. I. Solomon, *J. Am. Chem. Soc.* **1998**, *120*, 5674-5690.
[120] K. Kim, S. J. Lippard, *J. Am. Chem. Soc.* **1996**, *118*, 4914-4915.
[121] J. S. Pap, A. Draksharapu, M. Giorgi, W. R. Browne, J. Kaizer, G. Speier, *Chem. Commun.* **2014**, *50*, 1326-1329.
[122] N. Kitajima, N. Tamura, H. Amagai, H. Fukui, Y. Moro-oka, Y. Mizutani, T. Kitagawa, R. Mathur, K. Heerwegh, *J. Am. Chem. Soc.* **1994**, *116*, 9071-9085.
[123] M. Sekino, H. Furutachi, R. Tojo, A. Hishi, H. Kajikawa, T. Suzuki, K. Suzuki, S. Fujinami, S. Akine, Y. Sakata, T. Ohta, S. Hayami, M. Suzuki, *Chem. Commun.* **2017**, *53*, 8838-8841.
[124] H. Arii, S. Nagatomo, T. Kitagawa, T. Miwa, K. Jitsukawa, H. Einaga, H. Masuda, *J. Inorg. Biochem.* **2000**, *82*, 153-162.
[125] A. Miska, J. Norbury, M. Lerch, S. Schindler, *Chem. Eng. Technol.* **2017**, *40*, 1522-1526.
[126] A. Miska, D. Schurr, G. Rinke, R. Dittmeyer, S. Schindler, *Chem. Eng. Sci.* **2018**, *190*, 459-465.
[127] Y. Dong, S. Yan, V. G. Young, L. Que, *Angew. Chem. Int. Ed.* **1996**, *35*, 618-620.
[128] Y. Dong, S. Yan, V. G. Young, L. Que, *Angew. Chem.* **1996**, *108*, 673-676.
[129] X. Zhang, H. Furutachi, S. Fujinami, S. Nagatomo, Y. Maeda, Y. Watanabe, T. Kitagawa, M. Suzuki, *J. Am. Chem. Soc.* **2005**, *127*, 826-827.
[130] Y. Dong, Y. Zang, L. Shu, E. C. Wilkinson, L. Que, K. Kauffmann, E. Münck, *J. Am. Chem. Soc.* **1997**, *119*, 12683-12684.
[131] L. Westerheide, F. K. Müller, R. Than, B. Krebs, J. Dietrich, S. Schindler, *Inorg. Chem.* **2001**, *40*, 1951-1961.

[132] A. L. Feig, M. Becker, S. Schindler, R. van Eldik, S. J. Lippard, *Inorg. Chem.* **1996**, *35*, 2590-2601.
[133] A. L. Feig, S. J. Lippard, *J. Am. Chem. Soc.* **1994**, *116*, 8410-8411.
[134] S. V. Kryatov, E. V. Rybak-Akimova, S. Schindler, *Chem. Rev.* **2005**, *105*, 2175-2226.
[135] M. Costas, M. P. Mehn, M. P. Jensen, L. Que, *Chem. Rev.* **2004**, *104*, 939-986.
[136] E. Y. Tshuva, S. J. Lippard, *Chem. Rev.* **2004**, *104*, 987-1012.
[137] S. Menage, B. A. Brennan, C. Juarez-Garcia, E. Munck, L. Que, *J. Am. Chem. Soc.* **1990**, *112*, 6423-6425.
[138] Y. Nishida, M. Nasu, T. Akamatsu, *Zeitschrift für Naturforschung B* **1992**, *47*, 115-120.
[139] B. A. Brennan, Q. Chen, C. Juarez-Garcia, A. True, C. O'connor, L. Que, *Inorg. Chem.* **1991**, *30,* 1937-1943.
[140] F. Avenier, C. Herrero, W. Leibl, A. Desbois, R. Guillot, J.-P. Mahy, A. Aukauloo, *Angew. Chem. Int. Ed.* **2013**, *52*, 3634-3637.
[141] U. K. Bagha, J. K. Satpathy, G. Mukherjee, C. V. Sastri, S. P. de Visser, *Org. Biomol. Chem.* **2021**, *19*, 1879-1899.
[142] B. Kripli, F. V. Csendes, P. Török, G. Speier, J. Kaizer, *Chem. Eur. J.* **2019**, *25*, 14290-14294.
[143] V. McKee, M. Zvagulis, J. V. Dagdigian, M. G. Patch, C. A. Reed, *J. Am. Chem. Soc.* **1984**, *106*, 4765-4772.
[144] L. Que, in *Active Oxygen in Biochemistry*, (Eds. J. S. Valentine, C. S. Foote, A. Greenberg, J. F. Liebman), Springer Netherlands, Dordrecht, **1995**, pp. 232-275.

6 | Publikationsliste

[1] **Crystallographic Characterization of Trilostane and Derivatives**

M. Jopp, J. Becker, **M. Lerch**, A. Miska, H. Hausmann, R. Neiger, S. Schindler, *ChemistrySelect*, **2017**, *2*, 2251- 2256.

[2] **Dioxygen Activation: Potential Future Technical Applications in Reactive Bubbly Flows**

A. Miska, J. Norbury, **M. Lerch**, S. Schindler, *Chem. Eng. Technol.*, **2017**, *40*, 1522-1526.

[3] **Kinetic Investigation of the Reaction of Dioxygen with the Copper(I) Complex [Cu(Pim^{iPr2})(CH$_3$CN)]CF$_3$SO$_3$ {Pim^{iPr2} = Tris[2-(1,4-diisopropylimidazolyl)]phosphine}**

M. Lerch, M. Weitzer, T.-D. J. Stumpf, L. Laurini, A. Hoffmann, J. Becker, A. Miska, R. Göttlich, S. Herres-Pawlis, S. Schindler, *Eur. J. Inorg. Chem.*, **2020**, 3143-3150.

[4] **A Thioether-Ligated Cupric Superoxide Model with H Atom Abstraction Reactivity**

M. Bhadra, W. J. Transue, H. Lim, R. E. Cowley, J. Y. C. Lee, M. A. Siegler, P. Josephs, G. Henkel, **M. Lerch**, S. Schindler, A. Neuba, K. O. Hodgson, B. Hedman, E. I. Solomon, K. D. Karlin, *J. Am. Chem. Soc.,* **2021**, *143*, 3707−3713.

[5] **A Mechanistic Study on the Reaction of Non-Heme Diiron(III)-Peroxido Complexes with Benzoyl Chloride**

M. Lerch, A. J. Achazi, D. Mollenhauer, J. Becker, S. Schindler, *Eur. J. Inorg. Chem.*, **2021**, 4122-4132.